Photonic Devices and Subsystems for Future WDM PON and Radio over Fiber Technologies

XU, Lin

A Thesis Submitted in Partial Fulfillment of the Requirements for the Degree of Doctor of Philosophy in Electronic Engineering

The Chinese University of Hong Kong
April 2010

Abstract of thesis entitled:

Photonic Devices and Subsystems for Future WDM PON and Radio over Fiber Technologies

Submitted by XU, Lin

for the degree of Doctor of Philosophy in Electronic Engineering

at The Chinese University of Hong Kong in March 2010

Abstract

Internet traffic has undergone tremendous growth in the past decades and has already penetrated into the daily lives of the general population. Demand for new high bandwidth services is beginning to drive the deployment of optical fiber-based access networks to solve the so-called last mile bottleneck around the world. Passive optical networks (PON) are attractive because there are no active components in the transmission line, thus reducing operational and deployment costs. Time-division-multiplexing (TDM) used in currently deployed PON, in which the bandwidth is shared among the users by time domain multiplexing, does not fully utilize the bandwidth potential of optical fibers and will not be able to satisfy the bandwidth demand in access networks in the near future. Among the advanced multiplexing techniques, wavelength-division-multiplexing (WDM) PON is a good candidate technology for providing sustained bitrates beyond 10 Gb/s in access networks. However, reduction of costs in WDM PON remains a key challenge for their practical deployment.

In this thesis, we describe our research on photonic devices and subsystems for future access networks. Since optical network units (ONUs) are the most cost-sensitive parts, we first investigate the use of advanced modulation format in colorless ONU structure. We implement a scheme which uses dark return-to-zero (DRZ) for downstream transmission and remodulation of it using a differential-phase-shift-keying (DPSK) for upstream both at 10 Gb/s. We also

experimentally demonstrate silicon microring based optical frequency discriminators for use in demodulating DPSK and differential-quadrature-phase-shift-keying (DQPSK) signals. We show that the scheme is robust to variations in bit-rates in contrast with conventional Mach-Zehnder delay interferometer scheme.

In order to reduce the complexity and costs of ONU transceiver, we propose a scheme based on a nonreciprocal optical modulator and a linear loop mirror for receiving downstream and sending upstream data. We show that the nonreciprocity of traveling wave electrodes can selectively impress signal modulation onto the reflected upstream signals only. Monolithic integrated transceivers may thus remodulate downstream signals for upstream data transmission without needing integrated optical circulators. The proposed ONU is thus compatible with monolithic integration.

Besides colorless ONUs, we investigate potentially low cost, high speed vertical-cavity-surface-emitting lasers (VCSELs) for use in future access networks. VCSELs are attractive because they may meet the stringent size, power dissipation and cost constraints of access network components. We carry out experiments to demonstrate that up to 20 Gb/s direct modulation of long wavelength VCSEL is possible and evaluate their performance as high-speed transceivers.

Wired and wireless hybrid optical access networks are also investigated. Radio-over-fiber is one low-cost approach to deliver broadband wireless services, in which radio signals at the carrier frequency are delivered over optical networks from a central office to remote antenna base stations. Generation of high frequency carrier and radio frequency fading are the main research challenges. We propose and demonstrate frequency upconversion based on frequency doubling and quadrupling. Novel wired and wireless hybrid subsystems that mitigate millimeter-wave signal distortion are also demonstrated.

摘要

互聯網流量在過去數十年發生了巨大的增長，並已滲透到人們的日常生活。新的高帶寬服務的需求已開始推動在世界各地部署光纖接入網絡以解決最後一公里的瓶頸。無源光網絡極具吸引力，因為在傳輸線中沒有有源部件，從而降低了運營和部署成本。目前已部署的無源光網絡使用時分復用，用戶通過時域复用共享帶寬，但該技術不能充分利用光纖潛在的帶寬，不能滿足將來接入網絡對帶寬的需求。在先進的復用技術中，波分復用無源光網絡是一個很好的候選技術，它能為接入網絡提供超過 10 Gb / s持續的比特率。然而降低波分複用無源光網絡的成本仍然是其實際部署的一個主要挑戰。

在這篇論文中，我們主要研究未來接入網絡的光子器件和系統。在波分複用無源光網絡中，光網絡單元是最具成本敏感的部分，我們首先研究利用先進調製格式來實現波長獨立的光網絡單元。我們研究了利用反歸零調製格式進行下行傳輸然後對其用差分相位鍵控調製格式再調製以用於上行傳輸， 均以10 Gb/s比特率。我們亦研究了硅波導微環諧振腔以用於解調差分相位信號。實驗表明該結構較傳統的馬赫澤德型延遲干涉儀適應更寬範圍比特率信號的解調。

為了減少收發器的複雜性和成本，我們提出在波分複用無源光網絡中基於非相互光相位調製器和非線性光學環路鏡接收下行和發送上行數據。實驗表明，非相互性的行波電極可以選擇性地對上行信號進行相位調製。因此單片集成收發器可以對下行信號進行在調製以用於上行數據傳輸，而無需集成光環型器。擬議的光網絡單元因此兼容低成本單片集成。

另外我們亦研究了潛在低成本的高速垂直腔表面發射激光器作爲光網絡單元的上行傳輸的

光源。該激光器極具吸引力，因為它體積小，功耗和成本低，滿足接入網絡對組件的苛刻要求。實驗證明了高達 20 Gb/s 的直接調製長波長垂直腔表面發射激光器的可能性并測試了它們作爲收發器的表現。

我們對綜合有線和無線接入網絡也進行了研究。利用光纖傳輸微波是一種低成本提供寬帶無線服務的方式，其中載有無線電信號的高頻載波通過光網絡從中央基站被輸送到遠程基站。高頻信號的產生以及光纖傳輸中由于色散導緻的信號衰減是該系統的主要研究問題。我們提出並論證倍頻信號及減小高頻信號衰減的若干方法。

Acknowledgement

First of all, I owe my deepest gratitude to my supervisor, Prof. Hon Tsang, whose unflinching encouragement, patient guidance and support in various ways from the initial to the final level enabled me to develop an understanding of the subject. His truly scientist intuition has made him as a constant oasis of ideas and passions in science, which exceptionally inspire and enrich my growth. This thesis would not have been possible without him.

I gratefully thank Prof. Chester Shu, Prof. K. T. Chan, Prof. L. K. Chen, and Prof. G. K. Chang for their valuable advices.

Many thanks go in particularly to Prof. C. W. Chow and Dr. Emily P. S. Chan for their helpful discussion and experimental guide.

I also would like to acknowledge Prof. R. V. Penty for hosting my 4 months visit at Cambridge University which was a great experience for me.

I gratefully acknowledge Ms Barbara L. C. Ho for her technical assistance. Many thanks go to Dr. Li Chao, Chen Xia and Wong Chiyan for science discussion and the pleasure working together in the laboratory.

Words fail me to express my appreciation to my beloved parents who deserve special mention for their inseparable dedication and love. Appreciation also gives to my wife whose support and persistent confidence in me, has taken the load off my shoulder.

Last but not least, I offer my regards and blessings to all of those who supported me in any respect during the completion of the thesis.

XU Lin

28 February 2010

Table of Contents

Chapter 1

Introduction

The root of modern fiber optics goes to the year 1966 when Charles Kao of Standard Telecommunication Laboratories (UK) proposed fibers with low loss of 20 dB/km at which level communications would be feasible. Over the last two decades the world has seen a great transformation in telecommunications and its impacts on the human civilization in digital information transmission and storage, media, and entertainment. This is in many ways due to the advances in computer networking and the emergence of global Internet, which were made possible by the various advances in the high-speed, high-capacity broadband telecommunications technologies [1]. Nowadays, most of the backbone infrastructures are connected by optical fibers, due to its ultra-high bandwidth (>50 THz), low propagation loss (<0.2 dB/km), low manufacturing cost, small size, light weight and immunity to electromagnetic interference (EMI).

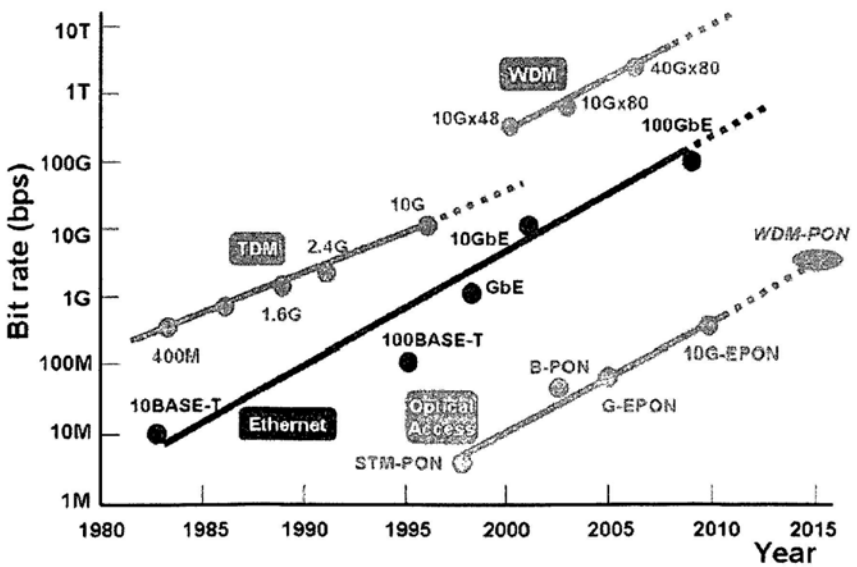

Fig.1.1 Transmission speeds of core and access systems [2]

Figure 1.1 shows the transmission speeds of core and access systems over time. The transmission speeds of core networks are being dramatically accelerated with the use of time-division multiplexing (TDM) and wavelength-division multiplexing (WDM) technologies; the total transmission capacity of WDM can reach up to 3 Tbits/s (40 Gbits/s_80 wavelengths). The tremendous growth of Internet traffic has accentuated the aggravating lag of access network capacity. The transmission speed of optical access has increased by around 100 times in the past decade as traffic patterns in access networks have evolved from voice- and text-oriented services to video- and image-based services. How ever, the "last mile" still remains the bottleneck between high-capacity local area networks (LANs) and the backbone network.

In this chapter, research challenges of access networks are described in section 1.1 including existing PON, trend to WDM PON, and challenges of WDM PON. The thesis outline is described in section 1.2.

1.1 Research Challenges of Access Networks

The conventional access network infrastructures, namely the twisted-pair telephony networks and the coaxial cable CATV networks, are having a hard time to keep up with traffic demands. Digital subscriber line techniques (ADSL, VDSL, etc.) and cable modem techniques are evolving into higher speeds, but at the cost of a shorter reach. It is commonly know that the conventional access networks have very limited bandwidth-distance products. For example, the transmission distance is only 100 m at the datarate of 100 Mb/s, and highly complicated transmission technologies are required [3]. The unique properties of optical single-mode fiber, being its low loss and extremely wide inherent bandwidth, make it the ideal candidate to meet the capacity challenges for now and the foreseeable future [4].

The access market is extremely cost-sensitive; the components used in backbone system which can be shared among thousands of users are still far too expensive for the access networks. A passive optical network (PON) is a point-to-multipoint, fiber to the premises network architecture in which unpowered optical splitters are used to enable a single optical fiber to serve multiple premises, typically at a split of 32-128. A PON consists of an optical line terminal (OLT) at the service provider's central office (CO) and a number of optical network units (ONUs) near end users. A PON configuration reduces the amount of fiber and central office equipment required compared with point to point architectures. Thus, PONs are highly recognized as the most promising candidates for next generation access systems because of low cost, simple maintenance and operation, and high-bandwidth provision [5].

1.1.1 Existing PON

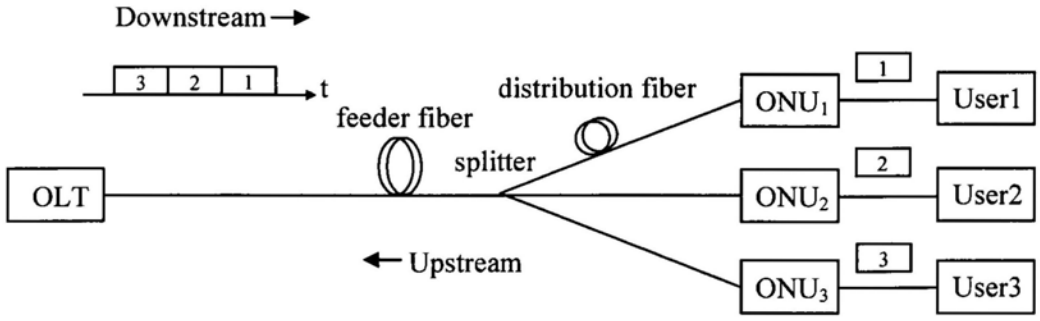

Fig. 1.2 TDM PON sketch

TDM PON is based on bandwidth sharing among multiple users in time domain. A typical TDM PON structure is shown in Fig. 1.2. The OLT and the ONU are deployed as the two ends of the

passive optical distribution network which consists of feeder and distribution fibers. Each ONU selects the packets destined to it from downstream light and discards the packets addressed to other ONUs. In the upstream, each ONU transmits during the time slots that are allocated by the OLT.

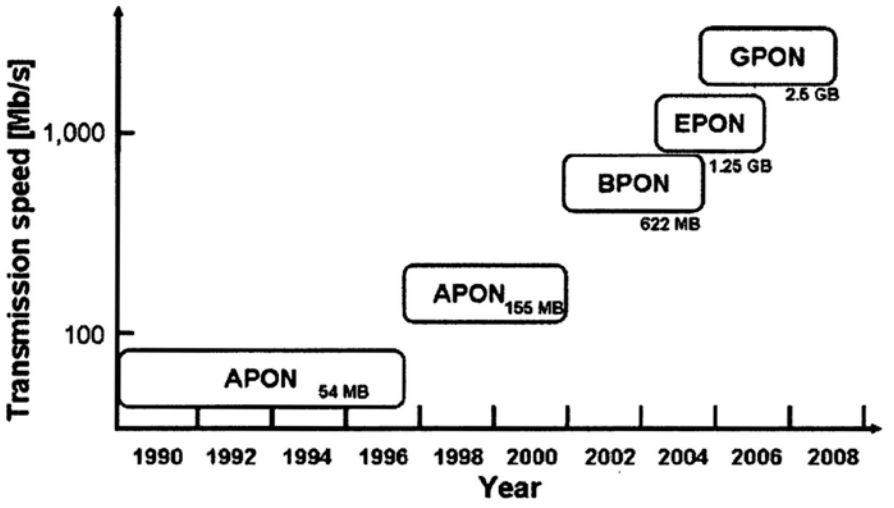

Fig. 1.3 History of TDM-PON developments [4]

The development history of TDM-PONs is illustrated in Fig. 1.3. The first TDM-PONs to be deployed was referred to as APON since it was based on the asynchronous-transfer-mode (ATM) communication protocol. It used a shared transmission data rate of 54 Mb/s and was mainly designed for compatibility with existing voice and phone services [6]. With the emergence of the Internet, the shared data rate was upgraded to 155 Mb/s in the latter half of the 1990s [7]. As bandwidth demand continued to grow due to the increasing popularity of the Internet and WWW, the downstream bandwidth was upgraded again to 622 Mb/s [8]. To reflect this increase in bandwidth, the acronym APON was replaced by broadband PON (BPON).

With the growing popularity of the Ethernet protocol in access networks and the increase in Internet data traffic, the IEEE developed a TDM-PON standard based on the Ethernet protocol referred to as Ethernet PON (EPON). The EPON standard was designed to better handle packet-based data traffic compared to the A/BPON standard that was optimized for voice traffic. The EPON standard also increased the shared transmission data rate to 1.25 Gb/s in both the downstream and upstream directions [9]. One of the goals of this standard was to also reduce the cost of the transmission equipment by relaxing many of the specifications that were developed for the full service access network (FSAN)-BPON standard. The EPON standard is being actively deployed in Japan and is also been considered in some other Asian countries.

Recently, there has been a growing consensus that the most efficient way to reduce capital investment and operational costs is to develop a common network platform capable of delivering the converged services of data, voice, and video. This offering is commonly referred to as triple-play service. Since it is questionable whether the existing standards such as BPON or EPON can deliver enough bandwidth or provide the required quality of service (QoS), the FSAN body has recently developed another standard called Gigabit PON (GPON). This standard uses 2.5 Gb/s for the downstream-transmission channel and 1.25 Gb/s for the upstream [10].

The passive optical networks currently being deployed in Asia and North America rely on TDM to share the fiber bandwidth amongst multiple users in the access network. Thus, despite nominal line-rates of about 1Gb/s, the dedicated speed of G-PON for individual users can be only ~78 Mb/s in 32-split PON because of bandwidth sharing [4]. Although TDM-PONs enable significant bandwidth boost as compared to copper-based access networks, with demand for access network bandwidth growing at an annual rate of 42% [4] and expected continued growth because of new bandwidth consuming services based on high definition video (HDTV), online gaming and peer

to peer networks, etc., it is widely predicted that TDM-PON will not cope with the bandwidth demand in access networks beyond the 15 year timeframe.

1.1.2 Trend to WDM-PON

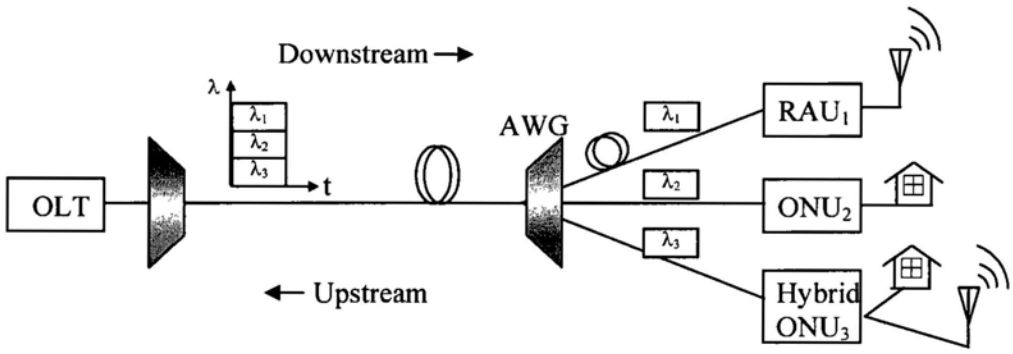

Fig. 1.4 Wired and wireless hybrid WDM PON sketch

The increasing demand for bandwidth moves WDM techniques closer to end users. The use of WDM PON can eliminate the time-sharing issues in TDM PON. The only difference in the outside-fiber plant is replacing the optical-power splitter in a TDM PON with an arrayed waveguide grating (AWG) to demultiplex the downstream wavelengths and multiplex the upstream wavelengths. A typical WDM PON structure is shown in Fig.1.4. On the left, the OLT, which resides at the CO, has an array of transmitters and receivers. Each transmitter–receiver pair is set at the wavelength band of the port of the multiplexing device, in this case, an AWG, to which the pair is connected. A feeder fiber connects this AWG at OLT to another AWG in the distribution network. Each port of the second AWG is connected to a different ONU. Each ONU has a passive splitter that is connected, on one end, to a transmitter and, on the other end, to a

receiver. The transmitter needs to be set at a particular wavelength of the AWG port that it is connected to. The distribution network can include several AWGs that are cascaded to increase flexibility, as in [11].

WDM PON has the advantages such as reduced optical path loss, point-to-point connectivity, protocol agnosticism, bit-rate transparency, scalability (the number of channels that can be easily upgraded), and flexibility (several types of tributary channels transmitted at different wavelengths that can coexist on the same link) [12,13]. Typically, the main services include direct residential access, dedicated access for business, and radio access networks. To make full use of the huge bandwidth offered by optical fiber and flexibility features presented via wireless, the convergence of radio-over- fiber (RoF)-based optical-wireless networks and WDM PON are regarded as the most promising solution to increase the capacity, coverage, bandwidth, and mobility in environments such as conference centers, airports, hotels, and shopping malls and ultimately to homes and small offices [14]. Today, WDM PON is a non-standard type of PON. The multiple wavelengths of a WDM-PON can be used to separate ONUs into several virtual PONs co-existing on the same physical infrastructure. Alternatively the wavelengths can be used collectively through statistical multiplexing to provide efficient wavelength utilization and lower delays experienced by the ONUs.

Compared to TDM PONs, WDM PONs can provide a much higher dedicated bandwidth but would require dedicated hardware for each user, which would result in higher cost. On the other hand, WDM-PONs allow for increased PON transmission lengths, which may offer significant cost savings in future access networks. These cost savings can be realized by reducing the number of COs between the metro network and the end customer [15, 16]. The consolidation would also enhance the QoS by reducing the number of hops experienced by the data signals [16]. Although extended ranges are also technically possible using TDM PONs, they may require relatively

expensive optical amplification and dispersion compensation techniques to overcome the inherent inefficiencies of this approach.

1.1.3 Challenges for future access networks

One way to provide upstream transmission is having a wavelength-tunable transmitter at ONU. The wavelength-tunable scheme is expected to meet the stringent power budget and high-speed operation at 10 Gb/s, because a coherent light is used. However, the biggest issue is to realize a tunable Tx cost effectively to provide broadband access services with a reasonable fee. The high cost of wavelength sensitive components and wavelength stable transmitters make WDM PON not yet practical today. In Chapter 4, we propose VCSELs as a low cost solution. Besides, an alternative way is using spectrum sliced [17] broadband light source instead of tunable laser diode. However, the broadband light source is not coherent, thus, can only be modulated at a low data rate. In addition, broadening the sliced bandwidth also increases the fiber dispersion penalty.

One main technical issue is how to realize colorless ONU which is not wavelength specific to decrease the costs of operation, administration, and maintenance functions, as well as the production cost since mass production becomes possible with just one specification. There have been three main proposals for the colorless ONUs: a seeded reflective semiconductor optical amplifier (RSOA) [18]; an incoherently injection locked Fabry-Perot laser diode (FPLD) [19]; and a light loop back scheme using an external modulator [20]. The first two approaches suffer from limited data rate (typically under 2.5 Gb/s) [21] and limited transmission distance. RSOA has the problem of temperature dependant gain [22]. FP-LD also has the problem of the sensitivity of injection-locking to wavelength/temperature changes, which may require the introduction of precise temperature controllers. The third approach suffers from limited power

budget unless amplifiers are added, and also high cost of using conventional lithium niobate based modulators.

Due to the limited modulation bandwidth of the colorless light sources described above, advanced modulation formats such as DRZ, DPSK, DQPSK investigated in Chapter 2 enable the operation of colorless ONU. However, we still need to improve the power budget.

ONU located in individual homes is the most cost sensitive part in WDM PON because it can not be shared among multiple uses compared to OLT. As a result, reducing the cost and complexity of ONU is crucial. Previous ONU structures [23, 24] either need an optical circulator or isolator for carrier reuse. However, optical circulator and isolator are expensive and not applicable for silicon integration. In Chapter 3, a novel low cost, silicon integratable structure based on non-reciprocal modulation is proposed.

To make full use of the huge bandwidth offered by fiber and the mobile feature presented via a wireless scheme, the integration of wireless and optical networks is a potential solution for increasing the capacity and mobility as well as decreasing the costs in the access network. Generating mm-wave frequencies using electrical devices is challenging due to the electronic bottleneck. The most promising solution is to use optical means.

One major issue is mm-wave generation. Traditionally, there are three approaches for the generation of mm-wave signals with intensity modulation: direct intensity modulation, external modulation, and remote heterodyning. Although direct modulation [25] is by far the simplest, it is not suitable for mm-wave generation due to the limited modulation bandwidth of the laser. The configuration of external modulation is simple, but it has some disadvantages that limit its implementation at mm-wave because of high cost for electric high frequency driving signals and

low dispersion tolerance. For optical heterodyning technique, several optical signals are simultaneously transmitted and are heterodyned in the receiver. However, it requires either a precisely biased electrooptic modulator or a complex laser to reduce the severe phase noise, which greatly adds to the cost and complexity of the system [26].

Another major issue of hybrid optical wired and wireless access network is limited by the fiber transmission distance of mm-wave signals, which is mainly due to the fading and time-shifting effects induced by fiber chromatic dispersion [27], and thus makes it merely suitable for integrating with those conventional PONs with coverage around tens of kilometer in radius. Such short-reach access system will lead to higher cost in terms of network deployment and management, and is expected to be upgraded urgently toward a next-generation access scenario with longer reach and less number of COs in the metro area, which is highly expected to simplify the entire network infrastructure by consolidating both metro and access networks [28, 29]. Basically, delivering mm-wave and baseband signals at different wavelengths and then mixing them remotely, so called remote local oscillator delivery schemes, is regarded as effective alternatives to mitigate the dispersion effect in hybrid mm-wave optical-wireless links [30-32], and is a promising deployment strategy for long-reach access networks. These schemes, however, usually require costly mm-wave-band electrical mixing at each hybrid ONU for the remote signal upconversion.

The generation and transmission of optical mm-wave are crucial in ROF systems. In Chapter 5, low cost approaches for mm-wave generation and mitigation of RF signal distortion are investigated.

1.2 Outline of This Thesis

This thesis focuses on the novel components and subsystem for use in future WDM PON and Radio over Fiber optical access networks. In Chapter 1, an introduction to existing, future PON and research challenges of optical access networks are presented. The continuing growth of interest in optical communication reflects the growing demand for communication in nowadays' information age. WDM-PON is considered the best solution for next generation access networks, but reducing the cost is still a challenge.

In Chapter 2, we investigate advanced optical modulation formats which have become key to the design of modern WDM fiber systems. DRZ was first proposed for use as payload in optical packet switching [33] since there is always a constant power in every bit of DRZ. To achieve colorless ONU (also investinged in Chapter 3), we investigate the combination of DRZ/DPSK for orthogonal modulation. To increase the capacity of transmission, a spectral efficient modulation is desirable for WDM system. DPSK and DQPSK are becoming attractive because they can reduce the nonlinear effect while transmission and improve the receiver sensitivity. Further more, DQPSK doubles the spectral efficiency when compared with binary formats. However, demodulation of these advanced formats usually needs complicated receiver which may increase the ONU cost. We demonstrate integrated silicon devices for DPSK and DQPSK demodulation which may meet the stringent cost constraints of access network components.

A common technical issue in WDM PON is colorless ONU. The ONUs should be colorless (in other words, ONU is not wavelength specific) to decrease the costs of operation, administration, and maintenance functions, as well as the production cost, since mass production becomes

possible with just one specification. In Chapter 3, we propose a novel architecture for colorless ONU transceiver, which can be compatible with low cost monolithic integration of high speed electro-optic modulators in silicon based on non-reciprocal modulation.

VCSELs based on the GaAs substrate have been extensively studied and some 980, 850, and 780 nm devices have been commercialized into various lightwave systems since 1992. In 2005, the first monolithic VCSEL arrays for 1550 nm have been developed showing maximum output powers beyond 30 mW [34]. Long wavelengths VCSELs are attracting increasing interest for metro optical access networks because they can be highly cost effective light sources which may meet the stringent cost constraints of access network components. In Chapter 4, we show the testing results of high speed modulation, advanced format generation and applications in access networks using long wavelength VCSELs.

The integration of optical wired and wireless hybrid access networks is desirable in near future. The generation and transmission of mm-wave signal are crucial in RoF systems, and chromatic dispersion can cause signal distortions to the optical mm-wave signals. High frequency RF signal generation using low frequency RF components are attractive because of the expensive cost of high frequency RF components. Chapter 5 describes RF generation using frequency doubling and quadrupling approaches, taking use of silicon microring as a filter. The scheme can potentially be integrated on a silicon chip. We also demonstrate several approaches to mitigate RF fading and achieve high speed wireline and wireless services based on hybrid RAU/ONU. The scheme can potentially lead to low cost, long reach hybrid access networks.

In Chapter 6, a summary and conclusion of the research work are presented along with future work in the area of silicon modulator and integration.

REFERENCES

[1] Chinlon Lin, "Book: Broadband optical access networks and fiber-to-the-home", 2006

[2] K. Iwatsuki and J. Kani, "Applications and Technical Issues of Wavelength-Division Multiplexing Passive Optical Networks With Colorless Optical Network Units [Invited]", vol. 1, no. 4, J. OPT. COMMUN. NETW., pp. c17-c24, 2009

[3] T. Koonen, "Fiber to the home/fiber to the premises: What, where, and when?", Proceedings of The IEEE, vol. 94, no. 5, pp. 911-934, 2006

[4] C. H. Lee, W. V. Sorin, and B. Y. Kim, "Fiber to the Home Using a PON Infrastructure," Journal of Lightwave Technology, vol. 24, no. 12, pp. 4568-4583, 2006.

[5] L. G. Kazovsky, W.-T. Shaw, D. Gutierrez, N. Cheng, and S.-W. Wong, "Next-generation optical access networks," J. Lightwave Technol., vol. 25, no. 11, pp. 3428–3442, 2007.

[6] C. Engineer, "Fiber in the loop: An evolution in service and systems," in Proc. SPIE Fiber Opt. Subscriber Loop, vol. 1363, pp. 19–29, 1990

[7] G. Van der Plas et al., "Demonstration of ATM-based passive optical network in the FTTH trial on the Bermuda," in Proc. GLOBECOM, vol. 99, pp. 988–992, 1995

[8] ITU-T, "Broadband optical access systems based on passive optical networks," Recommendation, G. 983.1, 1998.

[9] IEEE, "Physical medium dependent (PMD) sublayer and medium, type 1000 BASE-PX10 and 1000 BASE-PX20 (long wavelength passive optical network)," IEEE Recommendation 802.3 ah, 2002.

[10] ITU-T, "Broadband optical access systems based on passive optical networks," Recommendation G. 984.2, 2003.

[11] G. Maier, M. Martinelli, A. Pattavina, and E. Salvadori, "Design and cost performance of the multistage WDM-PON access networks," *J. Lightw. Technol.*, vol. 18, no. 2, pp. 125–143, 2000.

[12] A. Banerjee, Y. Park, F. Clarke, H. Song, S. Yang, G. Kramer, K. Kim, and B. Mukherjee, "Wavelength-division-multiplexed passive optical network (WDM-PON) technologies for broadband access: a review," *J. Opt. Netw.*, vol. 4, no. 11, pp. 737–758, 2005.

[13] S. J. Park, C. H. Lee, K. T. Jeong, H. J. Park, J. G. Ahn, and K. H. Song, "Fiber-to-the-home services based on wavelengthdivision- multiplexing passive optical network," *J. Lightwave Technol.*, vol. 22, no. 11, pp. 2582–2591, 2004.

[14] G.-K. Chang, Z. Jia, J. Yu, and A. Chowdhury, "Super broadband optical wireless access technologies," in *Optical Fiber Communication Conf. and Expo. and The Nat. Fiber Optic Engineers Conf.*, San Diego, CA, OSA Technical Digest (CD), Washington, DC: Optical Society of America, paper OThD1, 2008

[15] S.-M. Lee, S.-G. Mun, and C.-H. Lee, "Demonstration of long-reach DWDM-PON based on wavelength locked Fabry–Pérot laser diodes," presented at the 10th OptoElectronics and Commun. Conf., Seoul, Korea, Paper PD 1, 2005.

[16] S. Hornung, D. Payne, and R. Davey, "New architecture for an all optical network," presented at the Optical Fiber Commun. Conf. (OFC), Anaheim, CA, paper OTuH7, 2005.

[17] K. Akimoto, J. Kani, M. Teshima, and K. Iwatsuki, "Gigabit WDM-PON system using spectrum-slicing technologies," presented at 29th European Conf. on Optical Communication (ECOC 2003), Rimini, Italy, paper Th2.4.6, 2003.

[18] W. Lee, M. Y. Park, S. H. Cho, J. Lee, C. Kim, G. Jeong, B. W. Kim, "Bidirectional WDM-PON based on gain-saturated reflective semiconductor optical amplifiers," IEEE Photon. Technol. Lett., vol. 17, no. 11, pp. 2460-2462, 2005

[19] S. Park, C. Lee, K. Jeong, H. Park, J. Ahn, and K. Song, "Fiber-to-the-Home Services Based on Wavelength-Division-Multiplexing Passive Optical Network," J. Lightwave Technol., vol. 22, no. 11, pp. 2582-2591, 2004

[20] J. Kani, M. Teshima, K. Akimoto, N. Takachio, H. Suzuki, K. Iwatsuki, M. Ishii, "A WDM-based optical access network for wide area gigabit access servises" IEEE Commun. Mag., vol. 41, no. 2, pp. s43-s48, 2003

[21] Wooram Lee; Mahn Yong Park; Seung Hyun Cho; Jihyun Lee; Kim, C.; Geon Jeong; Byoung Whi Kim, "Bidirectional WDM-PON based on gain-saturated reflective semiconductor optical amplifiers", " IEEE Photonic Technol. Lett., vol. 17, no. 11, pp. 2460 – 2462, 2005

[22] K. Y. Cho, Y. Takushima, K. R. Oh and Y. C. Chung, "Operating Wavelength Range of 1.25-Gb/s WDM PON Implemented by using Uncooled RSOA's ," paper OTuH3, OFC/NFOEC 2008

[23] N. J. Frigo, P. P. Iannone, P. D. Magill, T. E. Darcie, M. M. Downs, B. N. Desai, U. Koren, T. L. Koch, C. Dragone, H. M. Presby, and G. E. Bodeep, "A wavelength-division multiplexed passive optical network with cost-shared components," IEEE Photon. Technol. Lett., vol. 6, no. 11, pp. 1365–1367, 1994.

[24] L. Xu and H. K. Tsang, "WDM-PON using differential-phase-shift-keying remodulation of dark return-to-zero downstream channel for upstream", IEEE Photon. Technol. Lett., vol. 20 no. 10, pp. 833-835, 2008

[25] K. E. Razavi and P. A. Davies, "Millimetre wave generation by filtering the FM–IM spectra of a directly modulated DFB laser," in IEEE MTT-S Int. Microw. Symp. Tech. D*ig.*, vol. 3, pp. 1707–1708, 1997.

[26] L. A. Johansson and A. J. Seeds, "Millimetre-wave radio-over-fibre transmission using an optical injection phase-lock loop source," in Proc. Microw. Photon., pp. 129–132, 2000.

[27] Z. Jia, J. Yu, G. Ellinas, and G. K. Chang, "Key Enabling Technologies for Optical–Wireless Networks: Optical Millimeter-Wave Generation, Wavelength Reuse, and Architecture," J. Lightwave Technol., vol. 25, no. 11, pp. 3452–3471, 2007.

[28] S. M. Lee, S. G. Mun, M. H. Kim, and C. H. Lee, "Demonstration of a Long-Reach DWDM-PON for Consolidation of Metro and Access Networks," J. Lightwave Technol., vol. 25, no. 1, pp. 271–276, 2007.

[29] G. Talli and P. D. Townsend, "Hybrid DWDM-TDM long-reach PON for next-generation optical access," J. Lightwave Technol., vol. 24, no. 7, pp. 2827–2834, 2006.

[30] C. Lim, A. Nirmalathas, D. Novak, R. Waterhouse, and G. Yoffe, "Millimeter-Wave Broad-Band Fiber-Wireless System Incorporating Baseband Data Transmission over Fiber and Remote LO Delivery," J. Lightwave Technol., vol. 18, no. 10, pp. 1355–1363, 2000.

[31] T. Ismail, C. P. Liu and A. J. Seeds, "Millimetre-wave Gigabit/s Wireless-over-Fibre Transmission Using Low Cost Uncooled Devices with Remote Local Oscillator Delivery," Proc. OFC/NFOEC 2007, paper OWN3, 2007

[32] S. A. Malyshev and A. L. Chizh, "p-i-n Photodiodes for Frequency Mixing in Radio-Over-Fiber Systems," J. Lightwave Technol., vol. 25, no. 11, pp. 3236–3243, 2007

[33] C. W. Chow and H. K. Tsang "Polarization independent DPSK demodulation using a birefringent fiber loop" IEEE Photonic Technol. Lett., vol. 17, no. 6, pp. 1313-1315, 2005

[34] A. Ortsiefer, M., Baydar, S., Windhorn, K., Ro¨nneberg, E., Rosskopf, J., Shau, R., Grau, M., Bo¨hm, G., and Amann, M.-C.: 'Long-wavelength monolithic VCSEL arrays with high optical output power', Electron. Lett.., vol. 41, no. 14, pp. 807–808, 2005

Chapter 2
Advanced Modulation Formats

Advanced optical modulation formats have become a key to the design of modern WDM fiber systems. To address the technical problems in colorless ONU, advanced modulation formats are a good candidate. Dark return-to-zero (DRZ) has been proposed and demonstrated in [1] to have a high tolerance to chromatic dispersion (CD) and optical bandwidth limitation. Its feature of carrying power in both "one" and "zero" bits can help realize functions such as multibit per symbol. Previous work in optical packet switching [2] shows DRZ is particularly suited for use with DPSK due to the RZ like nature of the demodulated DPSK resulting in little cross talk to the DPSK label. A high ER of both the payload and label improves the receiver margin when compared with conventional orthogonal labeling.

In this chapter, we generate DRZ for downstream transmission and remodulate it with DPSK for upstream in section 2.1. In section 2.2 and 2.3, we demonstrate DPSK and DQPSK demodulation based on silicon microring.

2.1 Dark Return to Zero (DRZ) Modulation Format

Previous work on optical packet labeling investigated the combination of half-bit-delayed dark return-to-zero (HBDDRZ) payload with an orthogonally modulated DPSK label [2]. The DRZ/DPSK orthogonal modulation was found to be better than the simple use of RZ/DPSK

orthogonal modulation because the RZ-like nature of the demodulated DPSK and the high extinction ratio (ER) of both the payload and label improves the receiver margin. The earlier implementation for optical packet labeling however employed a precise time control to provide the required half bit delay. Here, we investigate the same combination of DRZ/DPSK modulation formats for use in a WDM-PON. We implement a scheme which uses DRZ modulation format for downstream transmission and re-modulation of the downstream signal using a DPSK modulation format for the upstream both at 10 Gb/s using a single transmission fiber. We further show that a precise control of time delay is not needed if the pulsewidth of the DRZ signal is sufficiently short, and this may facilitate the use of low cost ONU transceivers based on an integrated splitter and a phase modulator as shown in Fig. 2.1.

2.1.1 Principle of DRZ Generation

The principle of DRZ generation is based on frequency shift [3]. When a pump and a probe signals are launched into a nonlinear element, the input pump signal will induce transient nonlinear phase shift to the probe signal via cross phase modulation. As a result, the optical spectrum of the probe signal will be broadened. If the central wavelength of the optical bandpass filter (OBF) is blue shifted with respect to the central wavelength of the probe beam as show in Fig.2.1, the converted signal recovers much faster compared to the case that the central wavelengths of the filter and the probe beam coincide.

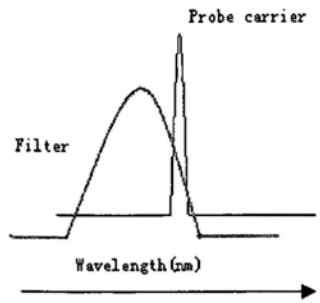

Fig. 2.1 Schematic of the input probe light and the filter characteristic against wavelength

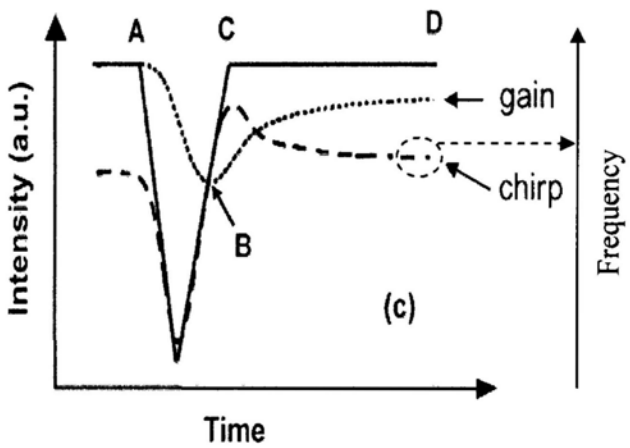

Fig. 2.2 Transmittance through the OBF as a function of time. Dotted and dashed lines are the semiconductor optical amplifier (SOA) gain and chirp, respectively [16]

Fig.2.2 describes the working principle of offset filtering. When a pulse goes into SOA with a CW light, the pulse induces a chirp to the CW light because of the change of the index. At rising part, there is a red chirp, and at falling part, there is a blue chirp. When the pulse appears at point A, the SOA carriers deplete and the gain drops, reaching its minimum at point B. The SOA gain saturates during timeslot A–B. Furthermore, in time slot A–B, the

wavelength of the probe light moves to a longer wavelength (red chirp) and thus receives more attenuation by the filter. As a result, the transmittance of the probe light through the filter is reduced. At point B, the chirp becomes zero, and the SOA starts to recover from this point onwards, the wavelength of the probe light is blue shifted, leading to an increased transmittance. If the OBF is properly selected (the slope of the OBF is especially essential), the enhancement of transmittance due to the blue chirp can compensate the gain saturation. Thus, the transmittance at point C is equal to the transmittance at point A. From points C to D, the wavelength of the probe light slowly moves back to the probe carrier wavelength, leading to a decreased transmittance. However, the SOA gain starts to recover, leading to an increased amplification of the probe light. These two effects take place on the same timescale and cancel each other out. As a result, the net intensity at the filter output is constant. This means that the system effectively recovers much faster than the SOA gain.

2.1.2 Experimental Assessment of DRZ in Access Networks

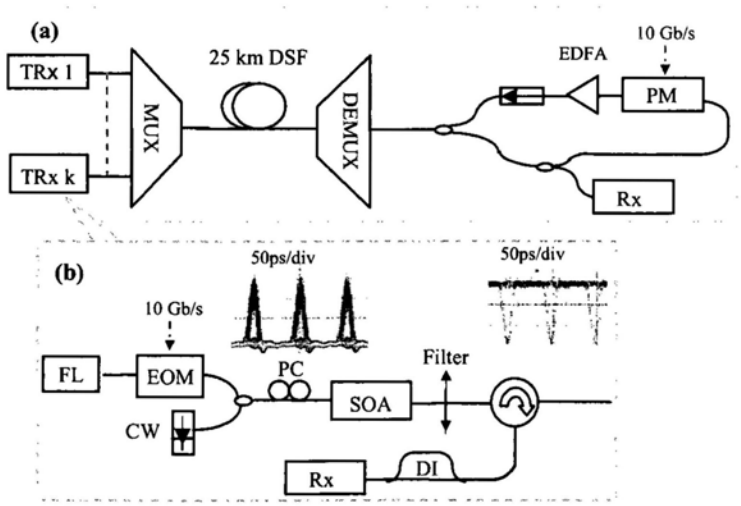

Fig.2.3. (a)System setup of colorless PON using DRZ downstream (b)DRZ generation unit. Inset left: Eye-diagram of 10 Gb/s RZ signal at input of SOA. Inset right: Eye-diagram of 10 Gb/s DRZ signal at output of SOA TRx: Transceiver FL: Fiber laser PM: Phase modulator DI: Delay interferometer DSF: Dispersion shift fiber Rx: receiver

We evaluated the proposed DRZ/DPSK modulation formats for the downstream/upstream channels experimentally using the testbed depicted schematically in Fig.2.3. In the proposed orthogonal re-modulation scheme, the downstream data is carried by a dark RZ signal at bitrate R and period $T = 1/R$. If Δt is the full-width- half-maximum (FWHM) of the dark RZ pulse, there is a time interval of about $T - \Delta t$ between one bit and the following bit that has only a small variation in optical power from its maximum value. The use of this time interval for phase encoding of the upstream channel ensures the integrity for the upstream data without any compromise on the ER of the downstream channel as is needed with conventional on-off keying of the downstream channel [4]. A phase modulated DPSK signal at bit-rate R can be added to the dark pulse sequence in the time interval $T - \Delta t$. Previous work employing the DRZ/DPSK modulation formats of optical labeling in packet switching used a half-bit-time-delay between the DRZ and DPSK signals to minimize the crosstalk between the channels [2]. In order to minimize costs of the ONU transceiver, we propose the use of short pulse DRZ ($<<$ half bit period) so that no precise optical delay is needed at the ONU before the signal is re-modulated with the DPSK upstream channel. The WDM-PON architecture considered (Fig.2.3(a)) uses DRZ modulation format in the downstream channel

and DPSK modulation format in the upstream channel. Each transceiver at the OLT generates the downstream DRZ signal and receives the upstream orthogonally remodulated DPSK signals for the corresponding subscriber. Note that due to the EDFA (tailored for ultra short pulse amplification) used in this proof-of-principle demonstration, Rayleigh back scattering had little effect on the upstream detection. However, EDFA may not be necessary if a second fiber was used for upstream transmission only. Fig.2.3(b) shows the setup for generating downstream DRZ signal using a single mode-locked fiber laser. The fiber laser generated 10-GHz RZ pulses which had a full-width- half-maximum pulsewidth of about 1.5 ps. An optical modulator was used to modulate the downstream data at a rate of 10 Gb/s. The data was generated from a pseudo-random binary sequence (PRBS) pattern generator with a pattern length of 2^{31}-1. The modulated optical signal was coupled into a SOA and the average input power at the SOA was -4 dBm. A CW light from a tunable laser at 1547 nm was also coupled into the SOA with an input power of -3 dBm. The CW signal was chirped by the picoseconds pulse from the fiber laser. An optical filter selected the blue sideband of the spectrum of the probe light [3]. In this experiment, the SOA (Kamelian) was pumped with 250 mA of current. The filter had a 3-dB bandwidth of 0.5 nm and was detuned by 0.4 nm from the center wavelength of the CW laser. The generated DRZ has a FWHM pulse width of about 10 ps and the extinction ratio of 8 dB as shown in Fig.2.3(b) right inset. The maximum extinction ratio depends on the filter's spectrum profile. It was then fed into a span of 25-km dispersion-shifted fiber with input power of 4.8 dBm. At the ONU, a portion of the received downstream signal power is tapped off for reception, while the remaining power was re-modulated by the local 10-Gb/s upstream data via a phase modulator. Here we use the

10-Gb/s PRBS data with a length of 2^{31}-1 directly encoding onto the payload by the phase modulator instead of DPSK pre-coding. The upstream DPSK signal can be detected by the receiver at the OLT. It consisted of a DI with a one bit delay in one arm (100 ps) for demodulating the 10-Gb/s DPSK label and allow detection by a PIN PD.

2.1.3 Experimental Results

The DI is actually performing an exclusive OR logic operation. Any difference from the bit period will degrade BER because it will reduce the eye-width and introduce errors when timing jitter is present. The DPSK eye was optimized by adjusting the wavelength. The bit error rates were measured both at OLT and ONU for upstream and downstream signals, both of which have negligible power penalty.

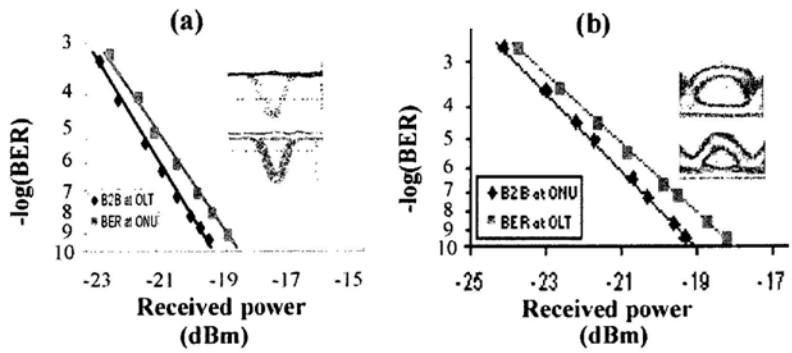

Fig. 2.4 Back-to-back and after transmission experimental BER measurements for (a) downstream DRZ (b) upstream DPSK

Fig.2.4 shows the bit-error rate (BER) measurements for both downstream DRZ signal and upstream DPSK signal of the experiment. The power penalty for downstream and upstream is

0.5 dB and 1 dB separately. The power penalty may be caused by pulsewidth broadening and cross talk between downstream and upstream signals. The corresponding eye-diagrams are shown in the inset of Fig.2.4. The ultra-short pulsewidth DRZ payload is particularly suited for use with DPSK labeling because of the RZ-like nature of the demodulated DPSK signal. The phase modulator for upstream remodulation can be integrated with the splitter and receiver in silicon, potentially allowing low cost transceivers to be used at the ONU [4].

2.1.4 Discussion of Possible Integrated Structure

The scheme shown in Fig.2.3 for preliminary demonstration may seem to be expensive as one way to generate DRZ practically. In our proposal sketched in Fig.2.5, we need only a single DI at the OLT instead of setting individual DIs at each ONU [5]. The costs of the fiber laser can be shared by all the channels. Longer reach and lower received power levels can be achieved by using an EDFA before the PIN at the OLT. Eventually it needs a scheme based on integrated distributed fiber bragg laser (DFBs), modulators and AWG as shown in Fig.2.5 which may be made cost effective to allow the deployment of high bitrate WDM-PON.

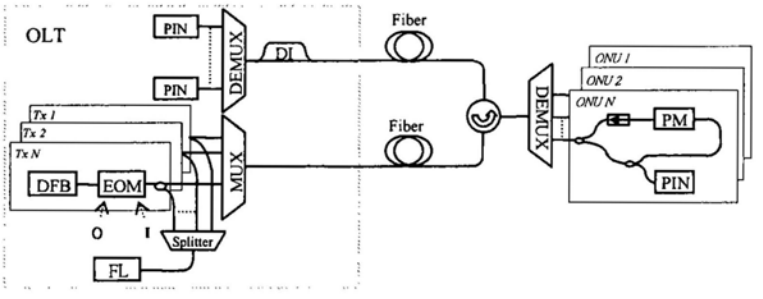

Fig. 2.5 Schematic diagram of proposed WDM-PON. EOM: electronic optic modulator O: output of EOM I: input of EOM FL: fiber laser Tx: transceiver OLT: optical line terminal ONU: optical network unit PM: phase modulator

Traveling wave electro-optical modulators can achieve highly efficient modulation at high data speeds by having the electrical signal copropagating with the optical signal at a well-matched group velocity. However if the optical signal were to travel in the opposite direction to the electrical modulation, the electrical–optical modulation becomes inefficient and may even be nulled out at particular frequencies which will be investigated in Chapter 3. When external light is injected, the carrier number decreases and the laser diode (LD) frequency shifts toward to a longer wavelength (red shift) [6]. The RZ pulses from fiber laser modulated by electro-optic modulator (EOM) can achieve frequency shift in the DFB, and the output light of DFB will be selected by the AWG channel which is blueside detuned and generate short pulse DRZ [3]. The proposed transceiver/receiver may therefore be suitable for monolithic integration, which will help in meeting the low cost targets. The inventory cost of our proposal (eg. 32 DFBs, AWG, one fiber laser and splitter) may be cheaper than putting 32 DFBs at OLT and another 32 DFBs at ONU side. On the other side, our proposals may have ~30-dB power budget for 25-km round-trip transmission which needs a preamplification at OLT for upstream light detection. Moreover our proposal simplifies the wavelength management for ONU. Since no precise time control for remodulation, ONUs are much simplified. However, the use of short pulse DRZ may limit the transmission length unless DCF or DSF is used. Although phase modulator can be integrated with splitters at ONU, the isolator is still difficult to be integrated. Possible solutions will be addressed in Chapter 3.

2.2 DPSK Demodulation using Silicon Microring

Differential-phase-shift keying (DPSK) is becoming one of the favored formats in the deployment of next-generation optical communication systems because of its robustness to fiber nonlinearities and polarization-mode dispersion [7, 8]. One approach for demodulating the DPSK signal is based on a Mach–Zehnder delay interferometer (MZDI) [9], in which the one-bit delay between the Mach–Zehnder arms of the MZDI convert the phase modulation to intensity modulation. A photodiode (PD) can be placed after the MZDI for direct detection of the DPSK signal. Direct detection can also be performed by using injection locking of a semiconductor laser [10], in which a slave laser is injection locked by the DPSK signal. DPSK signal using a birefringent fiber loop (BFL) was also demonstrated in [11]. The BFL introduces a differential group delay (DGD) between its fast and slow optical axes, which replace the two separate arms of the MZDI. In addition, Fiber Bragg gratings (FBG) have also been used for DPSK demodulation [12].

Microring based devices have attracted a great deal of attention in recent years [13]. Zhang et al. [14, 15] recently reported simulation results showing that microring based DPSK demodulator could offer improved performance in DPSK demodulation. Here we study experimentally the use of integrated microring resonator structures to demodulate DPSK signals, and compare their performance with conventional MZDI for DPSK demodulation. Compared to conventional approaches, microring structures require a relatively small chip area and are easy to integrate with other devices such as silicon photodetectors [16, 17]. Here,

we experimentally verified that 10-Gb/s DPSK signal may be demodulated using an integrated race-track microring as shown in Fig.2.6. We also showed the scheme can operate over a wide range of bit rates.

2.2.1 Device Design and Principle

The double-waveguide microring resonator, shown in Fig.2.6, operates as a filter to demodulate the DPSK signal. The output at port T behaves as a notch filter to produce the alternate mark inversion (AMI) signal while port D behaves as a band-pass filter which outputs a duobinary signal. The transfer function of the microring resonator can be described by [18]:

$$\frac{E_{out}}{E_{in}} = \frac{(1-t^2)\sqrt{a\exp(i\phi)}}{1-t^2 a\exp(i\phi)} \qquad (2.1)$$

where t and a denote the transmission coefficient and loss respectively, and ϕ is the phase change in one round trip. Here the microring resonator performs the function of an optical discriminator filter [19]. The duobinary and AMI may both be detected and then combined electrically to obtain balanced detection of DPSK signal with 3-dB power penalty improvement. In this paper, however, we only employed a single photodetector that measured the AMI signal and the duobinary signal separately.

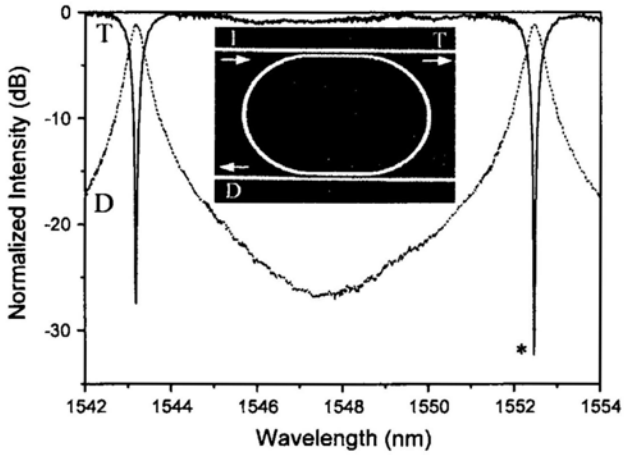

Fig.2.6 Measured TE-polarized transmission and drop-port spectra of the fabricated silicon microring resonator. Inset: top-view of the devise. I: input port, T: transmission port, D: drop port.

The microring resonator was fabricated at IMEC on silicon-on-insulator (SOI) wafer with a 0.22-μm thick top silicon layer and a 2-μm thick buried oxide (BOX) layer. The waveguides were 500 nm wide and the device layout was defined by 193-nm-deep-UV photolithography, and transferred onto the device layer by dry etching. The entire device was clad with a 0.75-μm-thick high density plasma (HDP) oxide. Light was coupled into and out of the microring resonator via a tapered waveguide grating coupler [20]. The spectra of TE-polarized through port and drop port, measured using a narrow linewidth tunable laser, are shown in Fig.2.6 (the notch depth appears larger than in Fig.2.7 inset because of the higher spectral resolution from scanning the tunable laser). The quality factor (Q) is defined as

$$Q = \frac{\lambda}{\Delta\lambda} \qquad (2.2)$$

$\Delta\lambda$ is 3-dB bandwidth of the spectrum. The Q for the "*" resonance is ~ 4,000. However the effective Q is around 20000 as measured from Fig.2.7 right inset. Fig.2.6 inset shows the top-view scanning electron micrograph of the fabricated microring device. The racetrack microring arc radius is 8 μm, and the straight interaction length is 6 μm. The fabricated air-gap spacing g between the ring and the waveguide is about 200 nm.

2.2.2 Experiment and Results

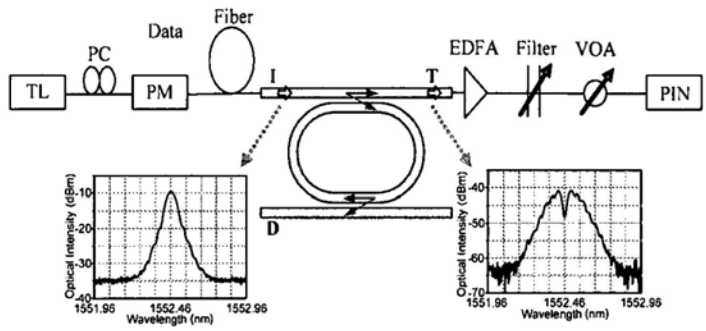

Fig. 2.7 DPSK demodulation experimental setup. TL: tunable laser PC: polarization controller PM: phase modulator VOA: variable optical attenuator PIN: photo detector

The experimental setup is shown in Fig.2.7. A CW light at the wavelength of 1552.46 nm was generated by a tunable laser (HP 8168F) with 0.001 nm tuning step and was tuned exactly at the resonance wavelength ("*") as shown in Fig.2.6. It was then phase modulated with the data generated from a PRBS pattern generator with a pattern length of 2^{31}-1 at 10-Gb/s data rate. The generated DPSK signal was coupled into a microring resonator through input port I and then coupled out from output port T. The through port T extracted the AMI format from

the DPSK spectrum for detection. The left and right diagrams in Fig.2.7 show the DPSK signal spectrum before and after demodulation respectively with a nominal 0.01 nm 3-dB bandwidth spectral resolution optical spectrum analyzer. When Q factor is higher, the notch filter profile of the demodulator becomes narrower and leaves more power in the AMI port which leads to a more opened eyediagram. However, the Duobinary signal is cut by the narrowed bandpass filtering which causes pattern dependence in the Duobinary data which may decrease the eye opening. Thus there is a trade off between the two demodulated channels. The microring exhibits better tolerance to frequency offset between the resonant filter wavelength and the optical carrier [14]. A larger power penalty is present at very high bit-rates due to the Duobinary signal suffering from pattern dependence [15].

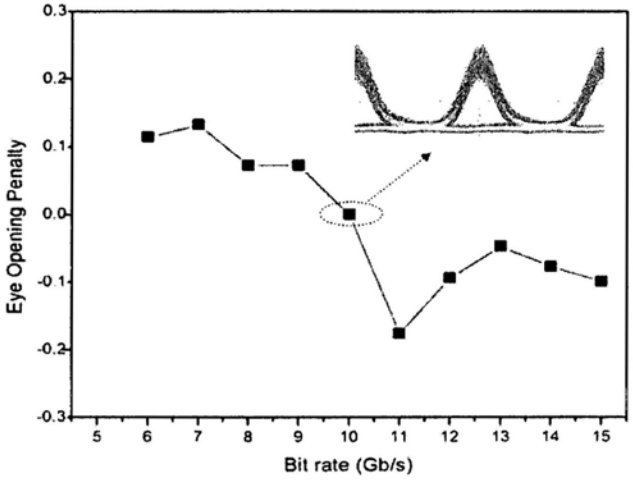

Fig.2.8 Tolerance of microring resonator based DPSK demodulator to varied signal bit-rate.

Fig.2.8 shows the demodulation performance at different signal bit-rates for the back-to-back case. The inset picture shows a clean and open demodulated eye diagram at 10 Gb/s. The eye-opening penalty was measured relative to the eye-opening at 10 Gb/s. It is noted that the

microring resonator demodulation scheme exhibits better tolerance to a wide data rate range as the penalty fluctuation was less than 0.2 dB at bit rates ranging from 6 Gb/s to 15 Gb/s. We also studied the performance of the microring resonator when the DPSK signal was distorted by dispersion. The DPSK signal was launched into a span of 11.6-km non-zero dispersion-shift-fiber (NZ-DSF) and demodulated by the microring resonator. The overall performance of the DPSK detection was compared for both the back-to-back and after dispersion from fiber transmission cases. Comparison was also made with the performance from a conventional MZDI. The measured BER curves for the different cases are plotted in Fig. 2.9. The demodulation performances for the drop port and through port were quite close. Error-free was achieved for both back-to-back and after fiber dispersion transmission. Compared to the conventional MZDI scheme, we observed that the microring-based scheme had about 2.5-dB power penalty improvement for both the back to back case and the fiber transmission case. The observed improvement is due to the non-optimized path difference in the MZDI: the MZDI used in the experiments had a path length difference which was longer than optimum for 10-GHz demodulation and the frequency offset at 10 GHz introduced a measured excess power penalty of about 3 dB from the optimum data rate [23]. Thus although these experimental results do not show any inherent improvement in receiver sensitivity from the microring demodulator, they do illustrate the practical advantages (of not having any requirement for a precise time delay control as in the MZDI) of this approach.

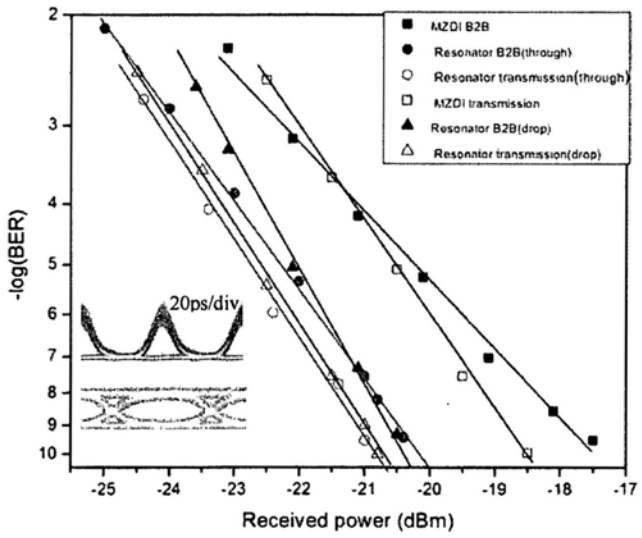

Fig.2.9 10 Gb/s BER measurements for microring resonator based and conventional MZDI based DPSK demodulator with/without 11.6-km NZ-DSF. Inset up: Back to back eyediagram of resonator through port. Inset down: Back to back eyediagram of resonator drop port

2.2.3 Summary

We have experimentally verified that a silicon microring resonator offers a practical improved performance for demodulation of a DPSK signal compared to a conventional MZDI. The microring resonator also offers advantages of easy integration and operation over a wide range of bit rates from 6 Gb/s to 15 Gb/s. This scheme has the potential for integrating DPSK demodulator, ASE filter, and WDM demultiplexer functionality in a single element which may facilitate integrated receivers/transceivers in optical access networks [21, 22]. Experimental measurements of the performance of the demodulation of a DPSK signal validated the potential of using the microring resonator for balanced detection using the AMI and duobinary outputs of the dual waveguide microresonator filter. The ease of use and ultra small size of the microring resonator make them highly attractive for DPSK demodulation.

2.3 DQPSK Demodulation using Silicon Microring

Differential quadrature phase-shift keying (DQPSK) doubles the spectral efficiency when compared with binary formats such as OOK or DPSK. The most common approach for DQPSK demodulation employs a MZDI for demodulation of each quadrature [24], followed by balanced detection. Optical frequency discriminator with direct detection is also an alternative approach [25]. DPSK demodulation based on a frequency discriminator implemented with a silicon microring resonator was recently demonstrated [26] to operate over a wider range of bit rates than the conventional MZDI approach. Zhang, et al [27] recently analyzed the performance of DQPSK demodulation using microring resonators. Compared to the MZDI approach, microring structures occupy a much smaller chip area and are thus easy to stabilize thermally and can be integrated with other devices such as waveguide photodetectors.

2.3.1 Device Design

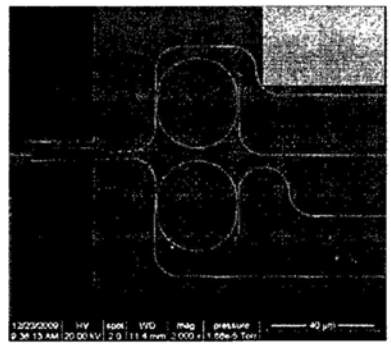

Fig. 2.10 Top view of silicon microring based DQPSK demodulator

The integrated microring resonators were fabricated at IMEC with the same condtions as in section 2.2.1. Fig.2.10 shows the top-view scanning electron micrograph of the fabricated microring device. The racetrack microring arc radius is 15 μm, and the straight interaction length is 8 μm. The fabricated air-gap spacing g between the ring and the waveguide is about 200 nm.

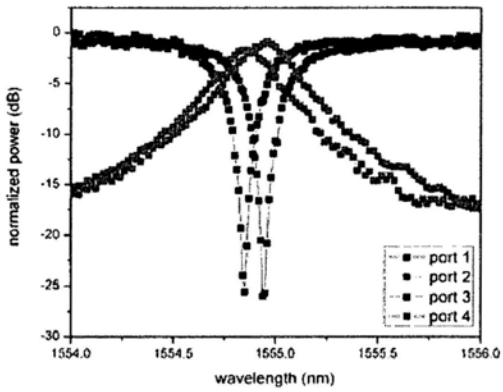

Fig. 2.11 Measured TE-polarized through-port and drop-port spectra of the fabricated silicon microring resonators.

The spectra of TE-polarized light at the through port and drop port, measured using a narrow linewidth tuneable laser with 0.01 nm spectral resolution, are shown in Fig.2.11. It is found that the transmitted power at the on-resonance wavelength drops by more than 25 dB with respect to that of the off-resonance wavelengths. The quality factor (Q) for both resonators were measured to be about 6500. Input and output coupling to the microresonators were via integrated fiber grating couplers [28] coupling to single mode optical fibers orientated at about 10 degrees off-vertical.

2.3.2 Experiment and Results

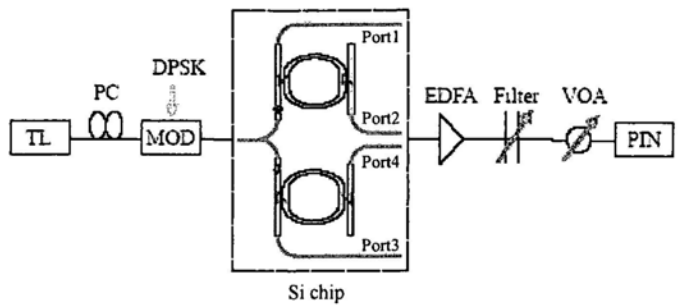

Fig. 2.12 Experimental set up of DQPSK demodulation. TL: tunable laser; MOD: modulator; VOA: variable optical attenuator; PIN: Pin diode

The experimental setup is shown in Fig.2.12. A CW light at the wavelength of 1554.85/1554.94 nm was generated by a tunable laser (HP 8168F) with 0.001-nm tuning step and was tuned exactly to the resonance of one resonator. It was then phase modulated with the data generated from a PRBS pattern generator with a pattern length of 2^{31}-1 at 10-Gb/s data rate. The generated DPSK signal was coupled into a microring resonator through input port of 1x2 MMI and then coupled out from output port 1/port 3, which extracted the AMI format from the DPSK spectrum for detection.

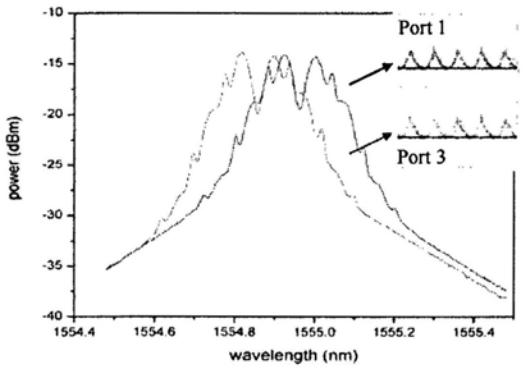

Fig. 2.13 Spectra after filtering and respective eye diagrams

Fig.2.13 shows spectra after demodulation measured with a nominal 0.01 nm 3-dB bandwidth spectral resolution optical spectrum analyzer. The inset pictures show clean and open demodulated eye diagrams at 10 Gb/s. Wavelength detuning against the resonance wavelength was investigated for port 1 shown in Fig.2.14. Here a negative detuning is defined as tuning the signal towards shorter wavelength while positive detuning means tuning towards longer wavelength.

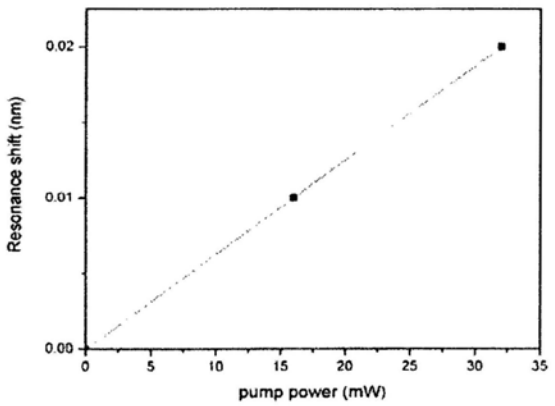

Fig. 2.14 Resonance shift against injected pump power

Precise tuning of the two microrings may be carried out using electrical wire heaters. However for this proof-of principle experiment, we used the local heating from the absorption of 980 nm wavelength light to tune the resonator's refractive index. The absorption of light produces free carriers (reduces the refractive index) and local heating (increases the refractive index). It is observed that the thermo-optic effect is the larger effect since the resonant wavelength shifts to longer wavelength as shown in Fig.2.14. It is thus possible to tune the separation between the two resonances and carrier to match the required $\pm\frac{1}{4}\pi$ for DQPSK demodulation .

2.3.3 Summary

In this section, we report the performance of a pair of integrated silicon microring resonators for 20 Gb/s DQPSK demodulation. The testing of the frequency discriminator employed 10 Gb/s DPSK for each quadrature channel for proof-of-principle, and we show that tuning of the resonator frequency to match the requirements of DQPSK demodulation may be achieved by localized optical heating of each resonator.

REFERENCES

[1] M. Ogusu, K. Ide, and S. Ohshima, "0.8-b/s/Hz WDM of 40-Gb/s inverse-RZ signals without using polarization-division-multiplexing and pre-filtering techniques," in OECC 2004, Paper 13C2-2, pp. 58 59, 2004

[2] C. W. Chow, C. H. Kwok, H. K. Tsang, Chinlon Lin, "Optical label switching of DRZ/DPSK orthogonal signal generated by photonic-crystal fiber", OPTICS LETTERS, vol. 31, no. 17, pp. 2535-2537, 2006

[3] Liu Y, "Error-free 320-Gb/s all-optical wavelength conversion using a single semiconductor optical amplifier" JOURNAL OF LIGHTWAVE TECHNOLOGY, vol. 25, no. 1, pp. 103-108, 2007

[4] F.A.Kish, "Large scale photonic integrated circuits for long-haul transmission and switching" Journal of Optical Networking, vol. 6, no. 2, pp. 102-111, 2007

[5] W. Hung, C. K. Chan, L. K. Chen, et al. "An Optical Network Unit for WDM Access Networks With Downstream DPSK and Upstream Remodulated OOK Data Using Injection-Locked FP Laser" IEEE Photonic Technol. Lett., vol. 15, no. 10, pp. 1476-1478, 2003

[6] KYO INOUE, "Wavelength Conversion for Frequency-Modulated Light Using Optical Modulation to Oscillation Frequency of a DFB Laser Diode" JOURNAL OF LIGHTWAVE TECHNOLOGY, vol. 8, no. 6, pp. 906-911, 1990

[7] M. Rohde, C. Caspar, N. Heimes, M. Konitzer, E. J. Bachus, N. Hanik, "Robustness of DPSK direct detection transmission format in standard fiber WDM system," Electron. Lett., vol. 36, no. 17, pp. 1483 1484, 2000.

[8] C. Xie, L. Moller,H. Haunstein, and S. Hunsche, "Comparison of system tolerance to polarization mode dispersion between different modulation formats," IEEE Photon. Technol. Lett., vol. 15, no. 2, pp. 1168 1170, 2003.

[9] E. A. Swanson, J. C. Livas, and R. S. Bondurant, "High sensitivity optically preamplified direct detection DPSK receiver with active delay-line stabilization," IEEE Photon. Technol. Lett., vol. 6, no. 2, pp. 263 265, 1994.

[10] Y. Awaji, T. Kuri, W. Chujo, M. Naganuma, K. Kitayama, "Differential-phase-to-intensity conversion (DPIC) based on injection locking of a semiconductor laser," Opt. Lett., vol. 26, no.20, pp. 1538 1540, 2001

[11] C. W. Chow and H. K. Tsang, "Polarization-Independent DPSK Demodulation Using a Birefringent Fiber Loop," IEEE Photon. Technol. Lett., vol. 17, no.6, pp. 1313-1315, 2005

[12] T. Y. Kim, M. Hanawa S. J. Kim, S. Hann Y. H. Kim W. T. Han C. S. Park, "Optical DPSK demodulator based on pi-phase-shifted fiber bragg grating with an optically tunable phase shifter," IEEE Photon. Technol. Lett., vol.18, no.17, pp. 1834-1836, 2006

[13] J. Niehusmann, A. Vorckel, P. H. Bolivar, T. Wahlbrink, W. Henschel, H. Kurz "Ultrahigh-quality-factor silicon-on-insulator microring resonator," Opt. Lett., vol.29, no.24, pp. 2861-2863, 2004.

[14] L. Zhang, Y. C. Li, M. P. Song, R.G. Beausoleil, A. E. Willner. "Data quality dependencies in microring-based DPSK transmitter and receiver," Opt. Express, vol. 16, No.8, pp. 5739-5745, 2008.

[15] L. Zhang, J. Y. Yang, M. P. Song, Y. C. Li, B. Zhang, R. G. Beausoleil, and A. E. Willner "Microring-based modulation and demodulation of DPSK signal," Opt. Express, Vol.15, No.18, pp.11564-11569, 2007.

[16] Y. Liu, C. W. Chow, W. Y. Cheung and H. K. Tsang: "In-line Channel Power Monitor based on Helium Ion Implantation in Silicon-on-Insulator Waveguides," IEEE Photon. Technol. Lett., Vol.18, No.17, pp.1882 - 1884, 2006

[17] M. W. Geis, S. J. Spector, M. E. Grein, R. T. Schulein, J. U. Yoon, D. M. Lennon, C. M. Wynn, S. T. Palmacci, F. Gan, F. X. Kärtner, and T. M. Lyszczarz , "All silicon infrared photodiodes: photo response and effects of processing temperature," Opt. Express, Vol.15, No. 25, pp.16886-16895, 2007

[18] Y. Chen and S. Blair, "Nonlinear phase shift of cascaded microring resonators," J. Opt. Soc. Am. B, Vol.20, No.10, pp.2125-2132, 2003

[19] I. Lyubomirsky and C. Chien, "DPSK demodulator based on optical discriminator filter," IEEE Photon. Technol. Lett., Vol.17, No. 2, pp.492-494, 2005

[20] D. Taillaert, P. Bienstman, and R. Baets, "Compact efficient broadband grating coupler for silicon-on-insulator waveguides," Opt. Lett., Vol.29, No. 23, pp.2749-2751, 2004.

[21] L. Xu and H. K. Tsang, "WDM-PON Using Differential-Phase- Shift-Keying Remodulation of Dark Return-to-Zero Downstream Channel for Upstream" IEEE Photon. Technol. Lett., Vol. 20, No.10, pp.833-835, 2008

[22] L. Xu and H. K. Tsang, "Colorless WDM-PON Optical Network Unit (ONU) Based on Integrated Nonreciprocal Optical Phase Modulator and Optical Loop Mirror" IEEE Photon. Technol. Lett., Vol. 20, No.10, pp.863-865, 2008

[23] H. Kim and P. J. Winzer, "Robustness to Laser Frequency Offset in direct-detection DPSK and DQPSK Systems," J. of Lightwave Technol. Vol.21, No. 9, pp.1887-1891, 2003

[24] Y. K. Lizé, M. Faucher, É. Jarry, P. Ouellette, É. Villeneuve, A.Wetter, and F. Séguin, "Phase-tunable low-loss, S-, C-, and L-band DPSK and DQPSK demodulator," IEEE Photon. Technol. Lett., vol. 19, no. 3, pp.1886 1888, 2007.

[25] C. C. Chien, Y. H. Wang, I Lyubomirsky, and Y. K.. Lizé, "Experimental Demonstration of Optical DQPSK Receiver Based on Frequency Discriminator Demodulator", J. Lightw. Technol. vol. 27, no. 19, pp. 4228- 4232, 2009

[26] L. Xu, C Li, C. Y. Wong, and H. K. Tsang, "Optical Differential-Phase-Shift-Keying Demodulation Using a Silicon Microring Resonator", IEEE Photon. Technol. Lett., vol. 21, no. 5, 2009

[27] L. Zhang, J. Y. Yang, Y. C. Li, M. P. Song, R. G. Beausoleil, and A. E. Willner, "Monolithic modulator and demodulator of differential quadrature phase-shift keying signals based on silicon microrings", Optics Lett., vol. 33, no. 13, pp. 1428-1430, 2008

[28] D. Taillaert, F. V. Laere, M. Ayre, W. Rogaerts, D. V. Thourhout, P. Bienstman and R. Baets, "Grating couplers for coupling between optical fiber and nanophotonic waveguide", Jap. J. Appl. Phys., vol. 45, pp. 6071-6077, 2006.

Chapter 3

Non-reciprocal Modulations

As stated in Chapter 1 that reduction of costs in WDM PON is a key challenge for their practical deployment in the highly cost-sensitive ONUs located in individual homes. It is essential that wavelength independent upstream transmitters be developed in order to have cost effective inventory management for equipment to be deployed at the customer premises. One way to ensure that costs are minimized is to use a colorless ONU, which allows the same physical unit to be used irrespective of the downstream wavelength. There have been three main proposals for the colorless ONUs: There have been three main proposals for the colorless ONUs: a seeded reflective semiconductor optical amplifier (RSOA) [1]; an incoherently injection locked Fabry-Perot laser diode (FPLD) [2]; and a light loop back scheme using an external modulator [3]. The first two approaches suffer from limited data rate (under 2.5 Gb/s) [4], limited transmission distance. RSOA has the problem of temperature dependant gain [5]. FP-LD also has the problem of the sensitivity of injection-locking to wavelength/temperature changes, which may require the introduction of precise temperature controllers. The third approach suffers from limited power budget unless amplifiers are added.

In another scenario of optical access networks employing wavelength re-use with external modulator [6], we consider a scheme which uses differential-phase-shift-keying (DPSK) modulation format for downstream data and non return-to-zero (NRZ) for transmission of the

upstream data using non-reciprocal amplitude modulator known as DPSK/ASK, both at 10 Gb/s using a single transmission fiber. The scheme provides higher extinction ratio (ER) for both upstream and downstream channels, easier generation of downstream signal compared to previous approach of NRZ downstream and DPSK upstream (ASK/DPSK) using non-reciprocal phase modulator [7] and is also more suitable for long reach PON which aims at building a high split passive optical network PON architecture with high capacity and extended reach (over 80 km) to merge optical access and metro networks into a single system [8].

In this chapter, we propose a novel architecture for ONU transceiver, which can be compatible with low cost monolithic integration of high speed electro-optic modulators in silicon [9] without needing the optical circulator nor second transmission fiber that was in earlier implementations of carrier re-use [10]. Instead, for the downstream detection and upstream re-modulation at the ONU, we propose a transceiver which can monolithically integrate a waveguide modulator, a partially reflecting linear optical loop mirror [11] and an optical receiver A commercial electro-optic amplitude modulator and an optical fiber loop mirror are used in the experiment to verify the proposed network architecture. We also have some studies on the performance for ASK downstream/DPSK upstream and DPSK downstream /ASK upstream.

3.1 Non-reciprocal Travelling Wave Modulators

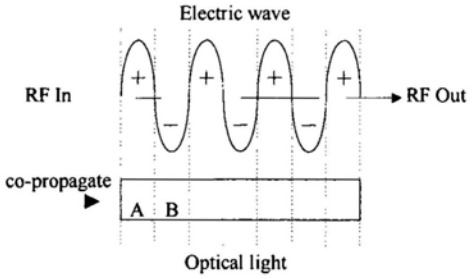

Fig. 3.1 Illustration of the traveling wave modulation

Traveling wave electro-optic modulators can achieve highly efficient modulation at high speed data rate by having the electrical signal co-propagate with the optical signal at a matched group velocity. However if the optical signal were to travel in the opposite direction to the electrical modulation, the electro–optic modulation becomes inefficient and may even be nulled out at particular frequencies [12]. Typically, at frequencies above 2 GHz, the counter-propagating frequency response is about 15 to 40 dB below the co-propagating response [13]. Fig.3.1 illustrates the working principle of traveling wave modulator. If the electric wave co-propagates with the optical light, optical light slot A would overlap with the positive slope while slot B would overlap with the negative slope of the electric wave all the way along the waveguide. In this case the modulation efficiency is high since it allows long interaction length. However if the two counter-propagates in the waveguide, either optical light slot A nor slot B would experience a number of positive and negative slopes which eventually compensate each other. Also mismatch between the electric-wave phase velocity and the optical group velocity limits the effective interaction length leading low modulation

efficiency [14]. The frequency response, the magnitude and the position of nulls in the counter-propagating case depend on both device design and drive conditions. For example, we measured the frequency response of a commercial electro-optic amplitude modulator and phase modulator by detecting the received optical intensity modulation with an electrical spectrum analyzer for both forward and backward transmission as shown in Fig.3.2 and Fig.3.3. The inset diagrams are the related measurement setups respectively. The electrical drive signal is launched into one of the electrode ports, and then it propagates through the active section where electrooptical interaction takes place and finally it reaches the other electrode port, which is terminated in 50-Ohm impedance. If the electrode impedance is not perfectly matched, the propagating electrical wave undergoes multiple reflections at the electrode ports which show the oscillations as observed.

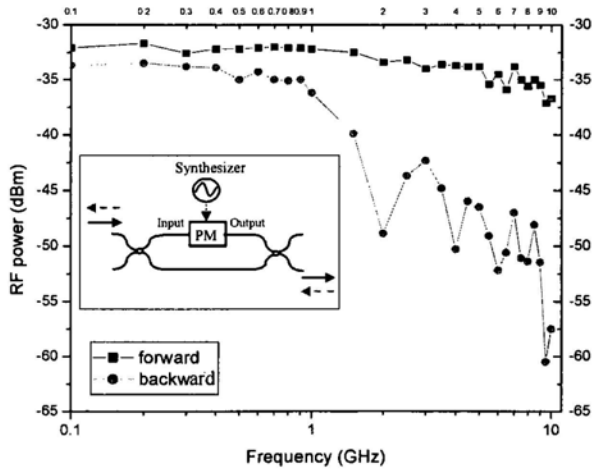

Fig. 3.2 Frequency response of electro-optic amplitude modulator

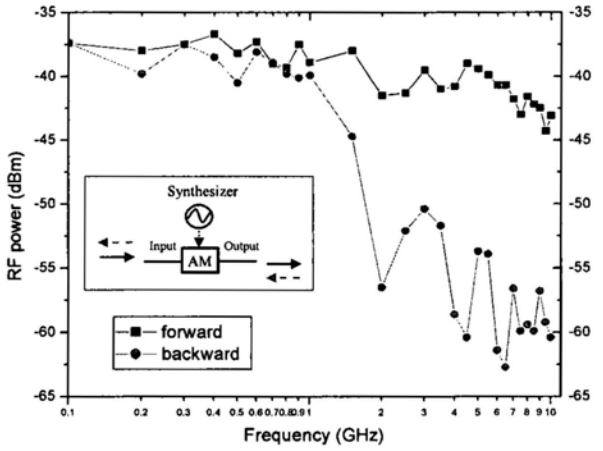

Fig. 3.3 Frequency response of electro-optic phase modulator

The RF drive power was 20 dBm and the amplitude modulator was biased at 90 degrees on the negative slope. From the diagram we can see that the relative response difference between forward and backward signals is above 10 dB at frequencies over 2 GHz. Here we propose to exploit this non-reciprocal feature of high speed traveling wave electro-optic modulators for selective efficient re-modulation of the reflected signal. The advantage of the proposed architecture is that it does not need optical circulators or isolators, which are difficult to implement as an integrated component. The proposed ONU transceiver may therefore be suitable for monolithic integration, which will help in meeting the low cost targets for ONU.

3.2 Optical Loop Mirror

The partially reflecting optical loop mirror's operation relies on the phase difference inherent in a waveguide coupler with power-coupling ratio α : (1- α) and the two output ports joined

together in a loop. For a 3-dB coupler, the device operates as a 100% mirror but by using different split ratios in the coupler the reflectivity can be varied [11].

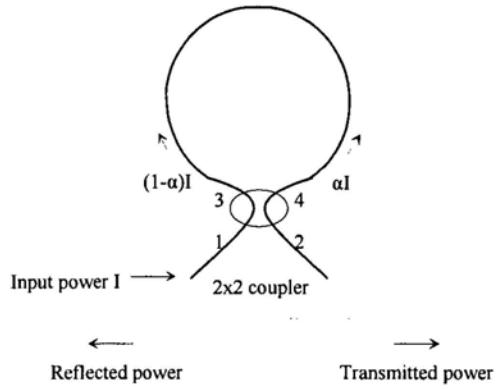

Fig.3.4 Typical optical loop mirror configuration

The schematic of a typical fiber loop mirror configuration is shown in Fig.3.4. It consists of a 2 x 2 coupler with a power coupling ratio of α, a fiber loop connected with the two arms of the coupler as shown. Input signal pulses are launched into arm 1 of the 2 x 2 coupler and divided into arms 3 and 4 with respective intensity. The pulses travel in two counter-propagating directions. In the coupler after propagating the loop, the two signal components interfere with the relative phase difference between clockwise and counterclockwise signals. Equation (3.1) gives the linear power transmittance defined by the ratio of power output from arm 2 to the input power launched into arm 1 [11].

$$T = 1 - 4\alpha(1-\alpha) \qquad (3.1)$$

Although here we use a fiber based partially reflecting loop mirror with separately packaged electro-optic modulators and photodiodes, all three components are compatible with monolithic integration on silicon and are thus can potentially meet the low cost targets for colorless ONU transceivers. Polarization control is not necessary for integrated version.

3.3 Transmission Performance of ASK Downstream and DPSK Upstream Remodulation

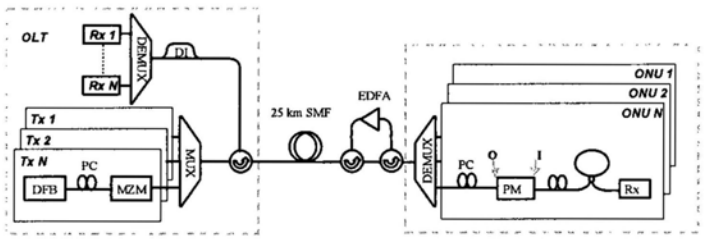

Fig. 3.5 Nonreciprocal phase modulator based colorless ONU. PM: phase modulator. O: output port of PM. I: input port of PM. SMF: single mode fiber. PC: polarization controller (not needed in integrated version) OLT: optical line terminal. ONU: optical network unit. TL: tunable laser. Rx: receiver

We used a discrete packaged optical phase modulator and an optical fiber loop mirror to verify the proposed ONU transceiver architecture. To demonstrate the proposed scheme as shown in Fig.3.5, we evaluated the performance of the downstream and upstream channels at ~10 Gb/s. The upstream DPSK signal was produced by modulating the received NRZ

downstream optical signal at the ONU. A low ER NRZ modulation for the downstream channel with ER of 2.7 dB was produced by a mis-biased Mach Zehnder modulator (70 degrees on the negative slope) at the OLT transmitter. The data was generated from a pseudo-random binary sequence (PRBS) pattern generator with a pattern length of 2^{31}-1. The downstream signal (1550 nm) was fed into a span of 25-km single mode fiber (SMF) with input power of 2 dBm. The optical fiber cannot be fully dispersion compensated in practice since the distance varies for different ONUs, thus no dispersion compensation was used in the experiment. At the ONU, the downstream signal was received via the output port of the phase modulator (O→I) and partially passed through the optical loop mirror to the photodetector which received the downstream data. The fiber loop mirror with splitting ratio of 3:7 reflected about 60% of the downstream signal for use in the upstream data transmission and transmitted about 40% of the downstream signal for detection. The reflected downstream light, in going from the input port to the output port of the phase modulator (I→O) was efficiently re-modulated by the local ~10-Gb/s upstream DPSK data. We also used a ~10-Gb/s PRBS data with a length of 2^{31}-1 for the DPSK upstream data modulation. The upstream DPSK signal then was demodulated by the shared delay interferometer (DI) and detected by the receiver in the OLT at the central office (CO). The DPSK demodulator consisted of a Mach Zehnder delay interferometer (DI) with one bit delay in one arm (100 ps) for demodulating the ~10-Gb/s DPSK and allow detection by a P-i-N photodiode. The received DPSK eye at the OLT may conveniently be optimized by adjusting the wavelength of the tunable laser in the OLT transceiver. It is worth to note that the modulation frequency have to be carefully adjusted in order to set the response of counter-propagating frequency to the null point. The

polarization controllers at both sides of the phase modulator need to be well adjusted and the bandwidth of modulator is crucial. Due to the upstream signal being amplified before re-transmission, influence of Rayleigh back scattering was minimized. However, some power fluctuation was observed, possibly due to a small amount of coherent backscattering (from unintended reflections) and this will need to be solved for practical use. The bit error rates were measured both at OLT and ONU for upstream and downstream signals as shown in Fig.3.6 which was the best case we observed.

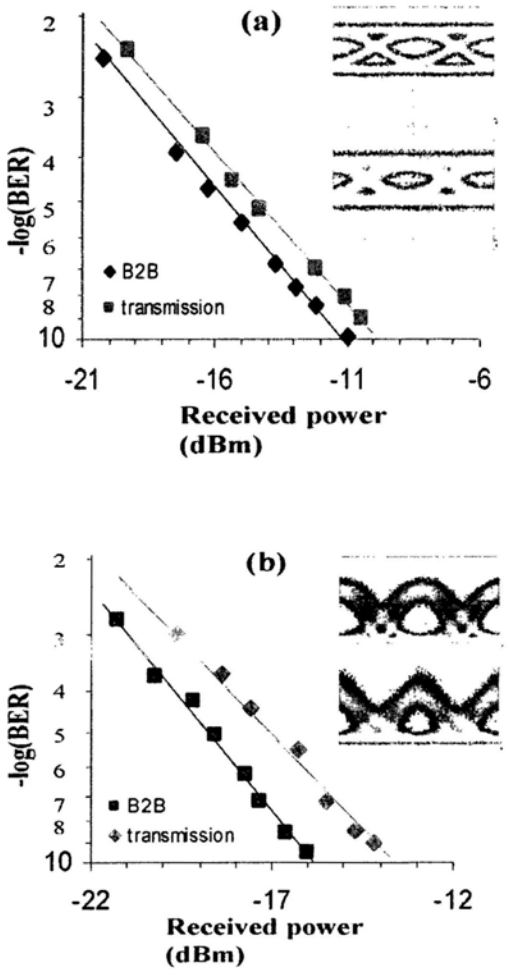

Fig. 3.6 BER measurement of (a) downstream NRZ and (b) upstream DPSK. Inset top and bottom are eyediagrams of back-to-back and after transmission respectively.

The downstream and upstream signals have approximately 1 dB and 2.5 dB power penalty separately after 25-km transmission at ~10 Gb/s. The upstream power penalty may be induced by consecutive 1s or 0s of the ~10-Gb/s signal used in the experiment. However, 8b/10b encoding may be introduced that there are not more than five 1s or 0s in a row [15]. Error free operation was obtained for both the downstream and upstream transmission. In the experiment, the extinction ratio employed for the downstream NRZ signal is critical to the bit-error-rate and eye opening of the upstream DPSK signal. An error floor at a BER of about 10^{-9} was observed when the ER of the ASK payload was equal below 1 dB. However the use of ER above 4 dB in the payload gives a lower power penalty (2 dB compared to back-to-back signal using ER=11.6 dB) but increased the power penalty of the label to 3.6 dB at a BER of 10^{-9} [16]. For the symmetric 10 Gb/s ASK/ DPSK orthogonal modulation, 2.8 dB ER is an optimized trade-off in power penalty for label and payload. The dark return-to-zero (DRZ) /DPSK orthogonal modulation was found to be better than the simple use of RZ/DPSK orthogonal modulation because the RZ-like nature of the demodulated DPSK and the high ER of both the payload and label improves the receiver margin. We may use DRZ investigated in Chapter 2 as downstream and further improve the system.

3.4 Transmission Performance of DPSK Downstream and ASK Upstream Remodulation

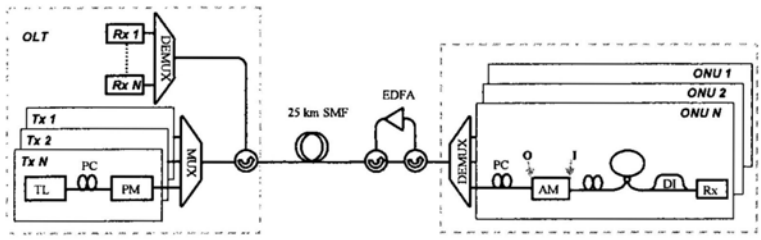

Fig. 3.7 Non-reciprocal amplitude modulator based colorless ONU. AM: amplitude modulator PM: phase modulator O: output port of AM I: input port of AM SMF: single mode fiber PIN: P-i-N detector PC: polarization controller (not needed in integrated version) OLT: optical line terminal ONU: optical network unit TL: tunable laser Rx: receiver

In order to avoid scarifying extinction ratio of downstream signal, we use the scheme as shown in Fig.3.7. We evaluated the performance of the downstream and upstream channels at ~10 Gb/s. The upstream NRZ signal was produced by modulating the received DPSK downstream optical signal at the ONU. Both the downstream and upstream signals can have high ER compared to using NRZ for downstream and DPSK for upstream. The data was generated from a PRBS pattern generator with a pattern length of 2^{31}-1. The downstream signal was fed into a span of 25-km SMF with the input power of 5 dBm. At the ONU, the downstream signal was received via the output port of the electro-optic modulator and demodulated by a Mach-Zehnder DI and then detected by a photodetector. Due to counter-propagating between electric

wave and optical light, the local ~10-Gb/s data modulation was transparent to the downstream light. The DPSK receiver consisted of an asymmetric Mach-Zehnder interferometer with one bit delay in one arm (100 ps) for demodulating the ~10 Gb/s DPSK and allowed detection by a P-i-N photodiode. In these laboratory measurements the received DPSK eye at the ONU was optimized by adjusting the wavelength of the DFB laser in the OLT transceiver. In practice when the OLT transmitter wavelength cannot be controlled by the ONU, it may be necessary to temperature tune the DI interferometer to optimize the DPSK demodulation. The fiber loop mirror [11] with 3:7 split ratios also reflected about half of the downstream light for use in the upstream data transmission. The reflected downstream light, in going from the input port to the output port of the electro-optic modulator (I→O) was efficiently re-modulated by the local ~10-Gb/s upstream data. The optical loop mirror is easy for monolithic integration on silicon chip with compact size and polarization controller for a polarization sensitive monolithic transceivers may be avoid by using a polarization diversity approach in the transceiver [17]. We also used a ~10-Gb/s PRBS data with a length of 2^{31}-1 for the NRZ upstream data. The upstream NRZ signal can be detected directly by the receiver in the OLT at the CO. The bit error rates were measured both at OLT and ONU for upstream and downstream signals as shown in Fig.3.8 which was the best case in this laboratory test. The power penalty for downstream and upstream was 1.2 dB and 1.7 dB, respectively.

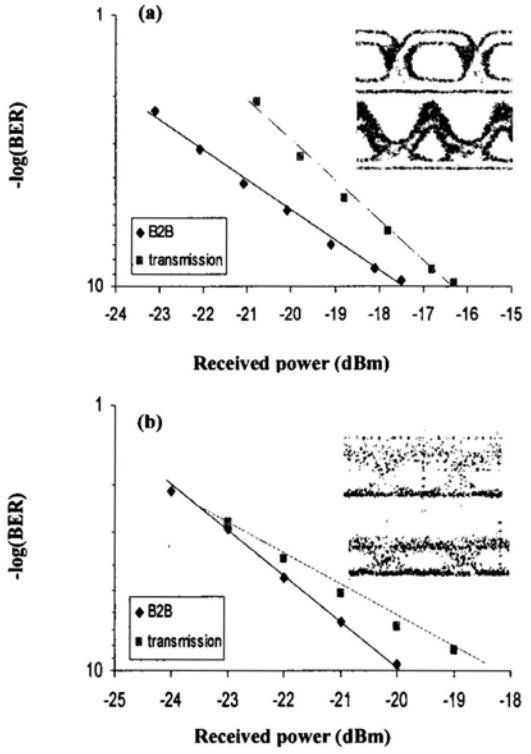

Fig. 3.8 BER measurement of (a) downstream DPSK and (b) upstream NRZ. Inset top and bottom are eyediagrams of back-to-back and after transmission respectively.

3.5 Comparison of the Above Schemes

We proposed, compared and evaluated a novel re-modulation scheme using the non-reciprocity of a traveling wave electro-optic phase/amplitude modulator. This technique allows a simple and cost effective ONU structure, which has potential for low cost implementation via the use of silicon photonics based integrated receivers and modulators. Error free transmission over a length of 25-km of standard single mode fiber was observed only in the DPSK downstream/NRZ upstream case and the power penalties for both the

DPSK downstream and NRZ upstream signals were 1.1 dB. Additional upstream power penalty may be induced by having too many consecutive 1s or 0s of the 10-GHz signal which would introduce low frequency components in the spectrum and degrade the differential modulation between forward and backward optical signals in the travelling wave modulator. However, in practice 8b/10b encoding may be used to ensure that there are not more than five 1s or 0s in a row [15].

Costs considerations may make ASK downstream and DPSK upstream scheme appear more attractive since only one DI is used to demodulate all upstream channels at OLT [7]. Since the demodulated DPSK signal is sensitive to environmental fluctuations, putting one DI at OLT (only one temperature controlled receiver at OLT) instead of putting individual DIs at ONUs can avoid the cost of having many temperature controlled components at ONUs and thus reduces the cost of the system.

However the downstream ASK signal must have a reduced ER to permit use of the downstream signal for the upstream DPSK remodulation. The received power for both DPSK and NRZ orthogonal modulation at BER of 10^{-8} for back-to-back case were measured against the NRZ ER as shown in Fig.3.9. The error floor will necessitate the use of error correction codes if DPSK is to be used with the low ER NRZ downstream signals.

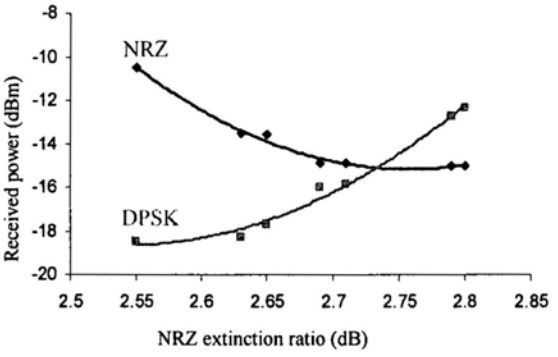

Fig. 3.9 Plot of the received power against the NRZ extinction ratio

The NRZ received power decreases while its ER increases and reaches a floor when ER goes up to 2.8 dB. The DPSK received power increases while ER of NRZ increases. A trade off between the downstream and the upstream performance should be considered carefully by optimizing the ER of NRZ. In practice, the received upstream signal has traveled twice the distance and would have lower power for detection. NRZ for 2.7-dB ER offers a good balance performance for both downstream and upstream channels. However the relatively poor receiver sensitivity may not satisfy future power budgets for optical access networks [18].

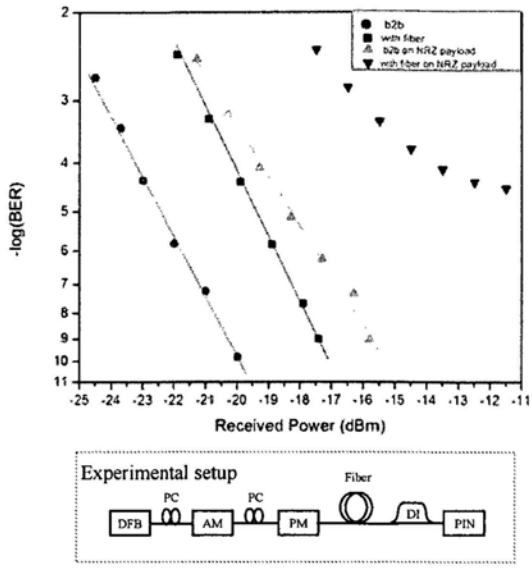

Fig. 3.10 DPSK BER measurements modulated on CW light and NRZ of 2.7dB ER respectively.

We measured the BER of the DPSK modulation for different ER optical carriers and compared the performance of the DPSK modulated signals after transmission over a fiber length of 44.2 km (33-km single mode fiber + 11.2-km dispersion-shifted fiber, total dispersion 575 ps) with the back to back case. For the high ER tests we simply used a CW optical carrier for the DPSK modulation. For the low ER transmission tests, the optical carrier consisted of a NRZ modulated signal which had 2.7-dB ER. From the results shown in Fig.3.10, the transmission over the 44.2-km fiber length introduced a 4.5-dB power penalty in the DPSK on CW optical carrier, and there is an error floor at BER of 10^{-5} after fiber transmission in the DPSK on NRZ optical carrier.

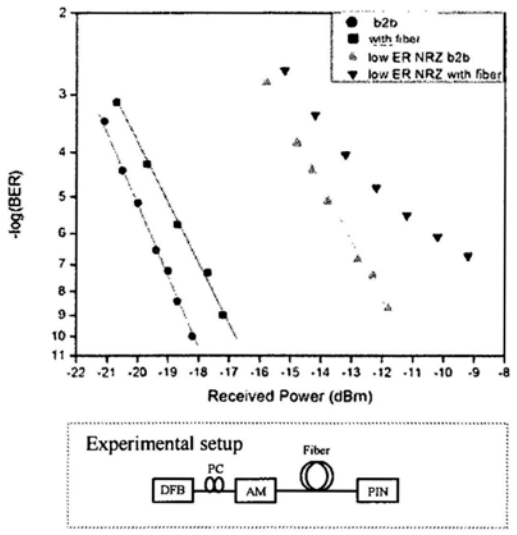

Fig. 3.11 NRZ BER measurements with conventional ER and 2.7-dB low extinction ratio.

The performance of the downstream NRZ transmission are shown in Fig.3.11 which shows the back-to-back case and after the fiber transmission (over the same fiber length) and with the maximum ER achievable (17 dB) and 2.7-dB ER respectively. There is over 6-dB power penalty between the two approaches and the low ER NRZ has an error floor at BER of 10^{-7} after fiber transmission.

The requirement for a low ER and consequent limited reach of the ASK downstream/DPSK upstream case raises the question of how much improvement can be offered by using DPSK downstream and ASK upstream as shown in Fig.3.11. The disadvantage of this approach is that each ONU will need to demodulate the DPSK downstream signal. We think that the DPSK downstream and ASK uptstream remodulation has good potential for use in WDM PON, however, practical implementation depends on a robust low cost DPSK demodulation scheme such as cost effective athermal DPSK demodulators can be used at ONU.

REFERENCES

[1] W. Lee, M. Y. Park, S. H. Cho, J. Lee, C. Kim, G. Jeong, B. W. Kim, "Bidirectional WDM-PON based on gain-saturated reflective semiconductor optical amplifiers," IEEE Photon. Technol. Lett., vol. 17, no. 11, pp. 2460-2462, 2005

[2] S. Park, C. Lee, K. Jeong, H. Park, J. Ahn, and K. Song, "Fiber-to-the-Home Services Based on Wavelength-Division-Multiplexing Passive Optical Network," J. Lightwave Technol., vol. 22, no. 11, pp. 2582-2591, 2004

[3] J. Kani, M. Teshima, K. Akimoto, N. Takachio, H. Suzuki, K. Iwatsuki, M. Ishii, "A WDM-based optical access network for wide area gigabit access servises" IEEE Commun. Mag., vol. 41, no. 2, pp. s43-s48, 2003

[4] Wooram Lee; Mahn Yong Park; Seung Hyun Cho; Jihyun Lee; Kim, C.; Geon Jeong; Byoung Whi Kim, "Bidirectional WDM-PON based on gain-saturated reflective semiconductor optical amplifiers", " IEEE Photonic Technol. Lett., vol. 17, no. 11, pp. 2460 – 2462, 2005

[5] K. Y. Cho, Y. Takushima, K. R. Oh and Y. C. Chung, "Operating Wavelength Range of 1.25-Gb/s WDM PON Implemented by using Uncooled RSOA's", paper OTuH3, OFC/NFOEC 2008

[6] N. J. Frigo, P. P. Iannone, P. D. Magill, T. E. Darcie, M. M. Downs, B. N. Desai, U. Koren, T. L. Koch, C. Dragone, H . M. Presby, and G. E. Bodeep, "A wavelength-division multiplexed passive optical network with cost-shared components," IEEE Photon. Technol. Lett., vol. 6, no. 11, pp. 1365-1367, 1994

[7] L. Xu and H. K. Tsang, "Colorless WDM-PON Optical Network Unit (ONU) Based on

Integrated Nonreciprocal Optical Phase Modulator and Optical Loop Mirror," IEEE Photon. Technol. Lett., vol. 20, no. 9-12, pp. 863-865, 2008

[8] Darren P. Shea and John E. Mitchell, "Long-Reach Optical Access Technologies," IEEE Network, vol. 21, no. 5, pp. 5-11, 2007.

[9] A. S. Liu, L. Liao, D. Rubin, H. Nguyen, B. Ciftcioglu, Y. Chetrit, N. Izhaky and M. Paniccia, "High-speed optical modulation based on carrier depletion in a silicon waveguide," Optics Express, vol. 15, no. 2, pp. 660-668, 2007

[10] W. Lee, S.H. Cho, M.Y. Park, J.H. Lee, C. Kim,G. Jeong and B.W. Kim, "Wavelength filter detuning for improved carrier reuse in loop-back WDM-PON," Electron. Lett., vol. 42, no. 10, pp. 596-597, 2006

[11] N. J. Doran and D Wood, "Nonlinear-Optical Loop Mirror," Optics Letters, vol. 13, no. 1, pp. 56-58, 1988

[12] A. Loayssa, C. Lim, A. Nirmalathas, and D. Benito, "Design and performance of the bidirectional optical single-sideband modulator," J. Lightwave Technol., vol. 21, no. 4, pp. 1071 1082, 2003

[13] G. K. Gopalakrishnan and I. L. Gheorma, "Simultaneous, bidirectional modulation of two channels in a single optical modulator," IEEE Photon. Technol. Lett., vol. 19, no. 9-12, pp. 886-888, 2007

[14] Y. Zhuang, Y. Wu, W.S.C. Chang, P. K. L. Yu, S. Mathai, M. Wu, D. Tishinin, K.Y. Liou, "Peripheral Coupled Waveguide Traveling-Wave Electroabsorption Modulator," IEEE MTT-S Digest, vol. 2, pp. 1367-1370, 2003

[15] A. X. Widmer, P. A. Franaszek, "A DC-Balanced, partitioned-block, 8b/10b,

transmission code," IBM Journal of Research and Development, vol. 27, pp. 440-451, 1983

[16] C. W. Chow, C. S. Wong and H. K. Tsang: "All-Optical ASK/DPSK Label-Swapping and Buffering Using Fabry-Perot Laser Diodes" IEEE J. Selected Topics in Quantum Electronics, vol. 10, no. 2, pp. 363-370, 2004

[17] H. Fukuda, K. Yamada, T. Tsuchizawa, T. Watanabe, H. Shinojima, S. Itabashi, "Silicon photonic circuit with polarization diversity," Optics Express, vol. 16, no. 7, pp. 4872-4880, 2008

[18] K. C. Reichmann and P. P. Iannone, "A physical layer perspective on current and next generation passive optical networks," paper CTuLL1, Cleo 2008

Chapter 4

Vertical Cavity Surface Emitting Lasers (VCSELs)

VCSELs based on the GaAs substrate have been extensively studied and some 980, 850, and 780 nm devices have been commercialized into various lightwave systems since 1992. In 2005, the first monolithic VCSEL arrays for 1550 nm have been developed showing maximum output power beyond 30 mW [1]. With the increasing bandwidth demand for both downstream and upstream data transmission, it is desirable to reduce the cost per bandwidth in order to make higher speed broadband access affordable [2, 3]. VCSELs modulated at bit-rates of up to 25 Gb/s were demonstrated at 850 nm for short reach data communications [4]. Direct modulation at 12.5 Gb/s for 1.3-μm VCSEL [5] and 10 Gb/s for 1.55-μm VCSEL [6] have been demonstrated recently. Direct modulation of 1.55-μm VCSEL over 20 Gb/s has been demonstrated in [7, 8] most recently. However, 1.55-μm wavelength is preferred over 1.3-μm because the lower fiber transmission loss helps meet the strict power budget in PON [9]. Recently, long wavelengths VCSELs are attracting increasing interest for metro optical access networks because they can be highly cost effective light sources which may meet the stringent cost constraints of access network components. The wavelength of VCSELs may be tuned to the DWDM grid, and together with their other advantages (excellent spatial mode for coupling to fibers, low threshold current for high speed transmission, potential for low cost manufacturing and packaging), VCSELs are good candidates as transceivers in ONU for WDM PON besides colorless ONU approach.

We have introduced colorless ONU in Chapter 2 and 3 for a low cost WDM PON. Conventional way of local emission is putting an array of laser diodes (such as DFBs) at ONU or OLT as transmitters which are high cost. Here we use VCSEL arrays to achieve high data rate transmission. In this chapter, we first experimentally characterize the VCSEL in 4.1, and then

investigate advanced format generation in section 4.2. In section 4.3 and 4.4 we use VCSEL as transmitter both at OLT and ONU.

.

4.1 Characteristic

4.1.1 Device Structure

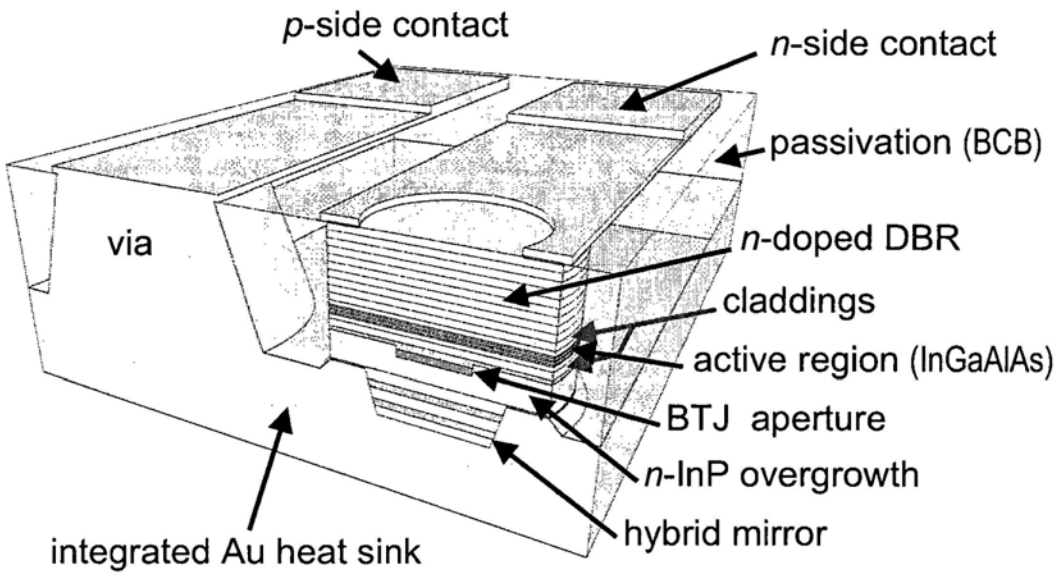

Fig.4.1 Schematic figure of the VCSEL [9]

The schematic layout of the laser chip is shown in Fig.4.1. BCB is used as low-dielectric constant passivation to enable high-speed operation. The epitaxial output mirror consists of 32 pairs of InGaAlAs and InAlAs with no fundamental absorption. To achieve high-speed operation and sufficient gain at elevated temperatures, the active region consists of 7 heavily strained InAlGaAs quantum wells of 6 nm thickness each. The strain was tailored to be 2.5% of compressive strain

(pseudomorphic) going near borderline of critical layer thickness. This should both enhance gain and differential gain and therefore enable low threshold currents and high relaxation oscillation frequencies. The mode-gain offset is optimized for high-temperature behavior. So, negative T_0 values can be obtained. This effect is caused by the different red-shift of gain and cavity-mode over temperature. Due to the BTJ, which allows the elimination of nearly all *p*-conducting material with higher electrical resistances and optical losses, a differential series resistance of 40-50 Ω has been achieved, well suited for direct modulation.

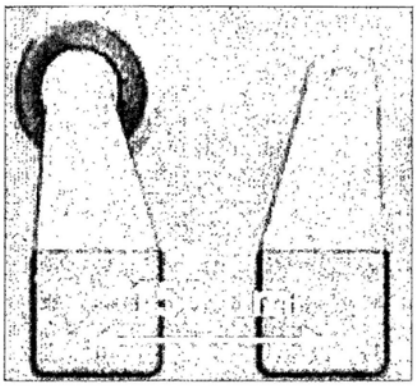

Fig.4.2 Single VCSEL chip

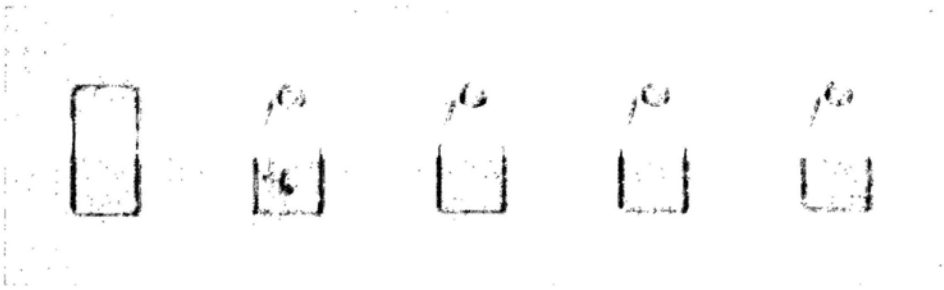

Fig.4.3 1x4 VCSEL array

Single device chip is shown in Fig. 4.2 with 150-μm pitch. 1 x 4 VCSEL arrays are shown in Fig.4.3 with 250-μm pitches which show high yield and great uniformity. As demand for

bandwidth increases, 1 x N VCSEL arrays can be used to transmit parallel datarate. One costumer can potentially use all lasers on the chip.

4.1.2 Characteristic Testing Setup

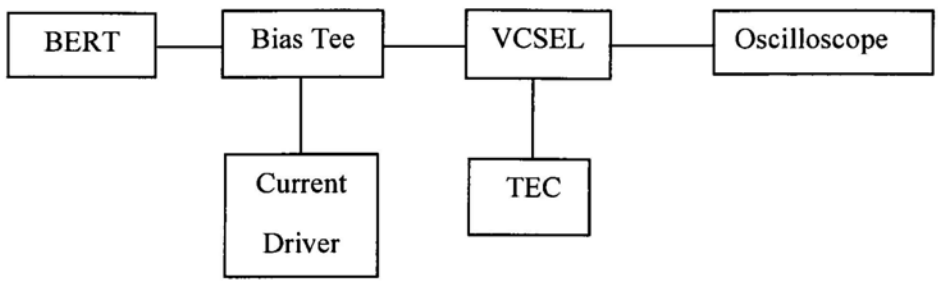

Fig.4.4 Schematic diagram of characteristic testing setup

Fig. 4.4 shows schematic diagram of large signal modulation setup. The VCSEL used in section 4.1 and 4.2 was developed improved high-speed long wavelength BJT one with superior bandwidth [9]. It had a room temperature threshold current of 1.4 mA, a differential resistance of 43.9 Ω, lasing output wavelength of ~1550 nm (laser spectrum shown in Fig. 4.5, bias current at 7 mA) and maximum output power of 2.46 mW at 20 °C. The light from the 5-μm diameter output aperture of the VCSEL was coupled into a SMF. The maximum fiber coupled power was 700 μW at 10-mA current bias. For the experiment results shown in Fig. 4.6, the VCSEL was biased at 7 mA for 10-Gb/s modulation and 12 mA for 20-Gb/s modulation respectively. The 10-Gb/s and 20-Gb/s NRZ electric driving data (2^{31}-1 PRBS) had a peak to peak voltage of 0.5 V and 1 V, respectively. The chip was mounted on a TEC set to room temperature for 10-Gb/s measurement and a temperature of 10 °C for 20-Gb/s measurement. The eyediagrams and optical spectra at 10-Gb/s and 20-Gb/s modulations are shown in Fig. 4.6. The 3-dB bandwidth was 0.1 nm measured with a 0.01-nm resolution optical spectrum analyzer. The modulated optical signal was detected by a 20-GHz photo detector and 20-GHz oscilloscope.

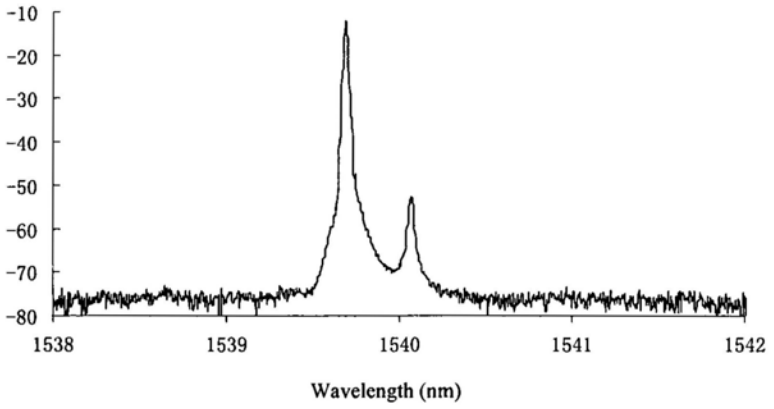

Fig. 4.5 CW VCSEL output spectrum

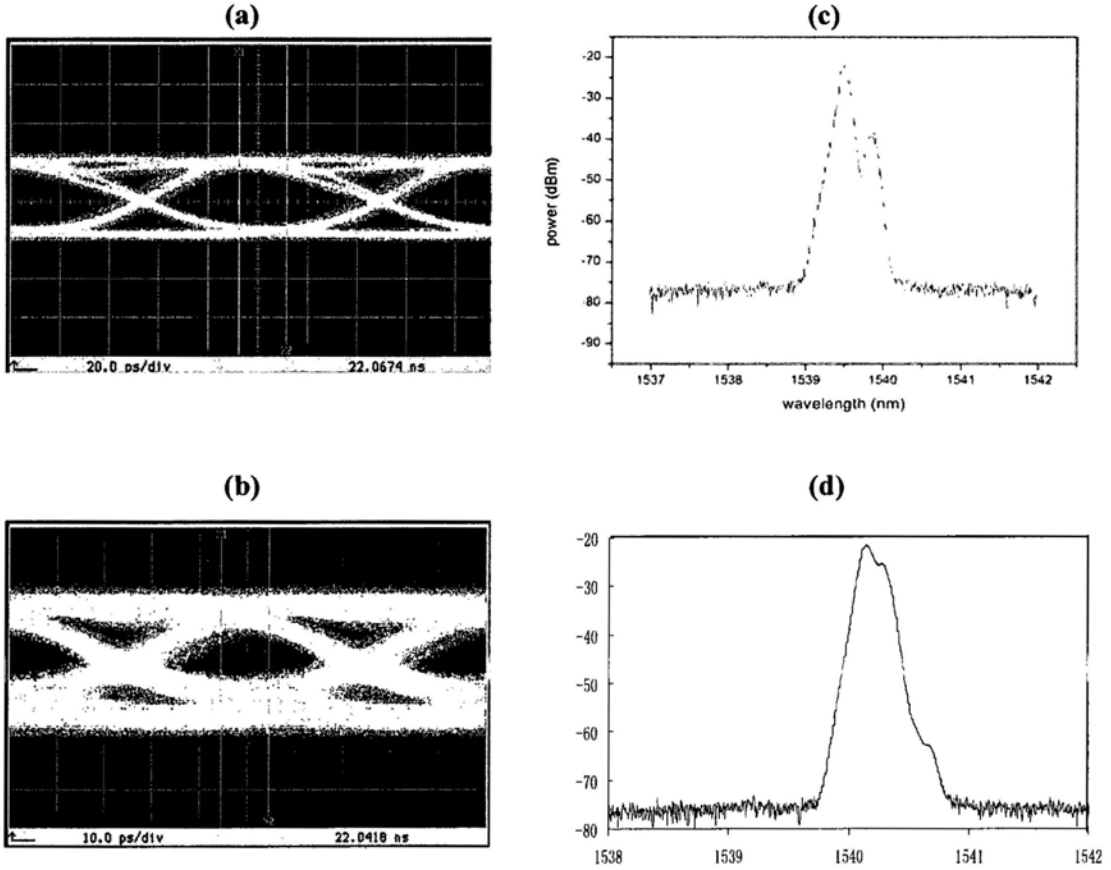

Fig. 4.6 Eyediagram of (a) 10-Gb/s modulation (b) 20-Gb/s modulation and spectrum of (c) 10-Gb/s modulation (d) 20-Gb/s modulation

Figs. 4.7 shows eye diagrams of back-to-back and transmission over a 6.5-km link of standard SMF for data-rates of 20 Gb/s. The pattern length was 2^{31}-1 PRBS for all configurations. For Fig. 4.7 (a), the bias point was set to 5.5 mA, the TEC was set to 15 °C and Vpp was 0.5 V. The achieved Q-factors were 3.03 for back to back and 2.97 for fiber transmission case, respectively. Fig. 4.7 (b) shows the same experiment at a bias point of 8 mA. The achieved Q-factors were 3.62 and 3.38 respectively. For Fig. 4.7 (c), 20 Gb/s eye diagrams with measured Q-factor of 3.99 and 3.81 can be stated at 10°C heat-sink temperature, 12-mA bias and Vpp of 1 V. This is the first preliminary experimental results so far [7]. Consequently, the performance is expected to be further improved by optimizing bias current and stabilizing the coupling efficiency.

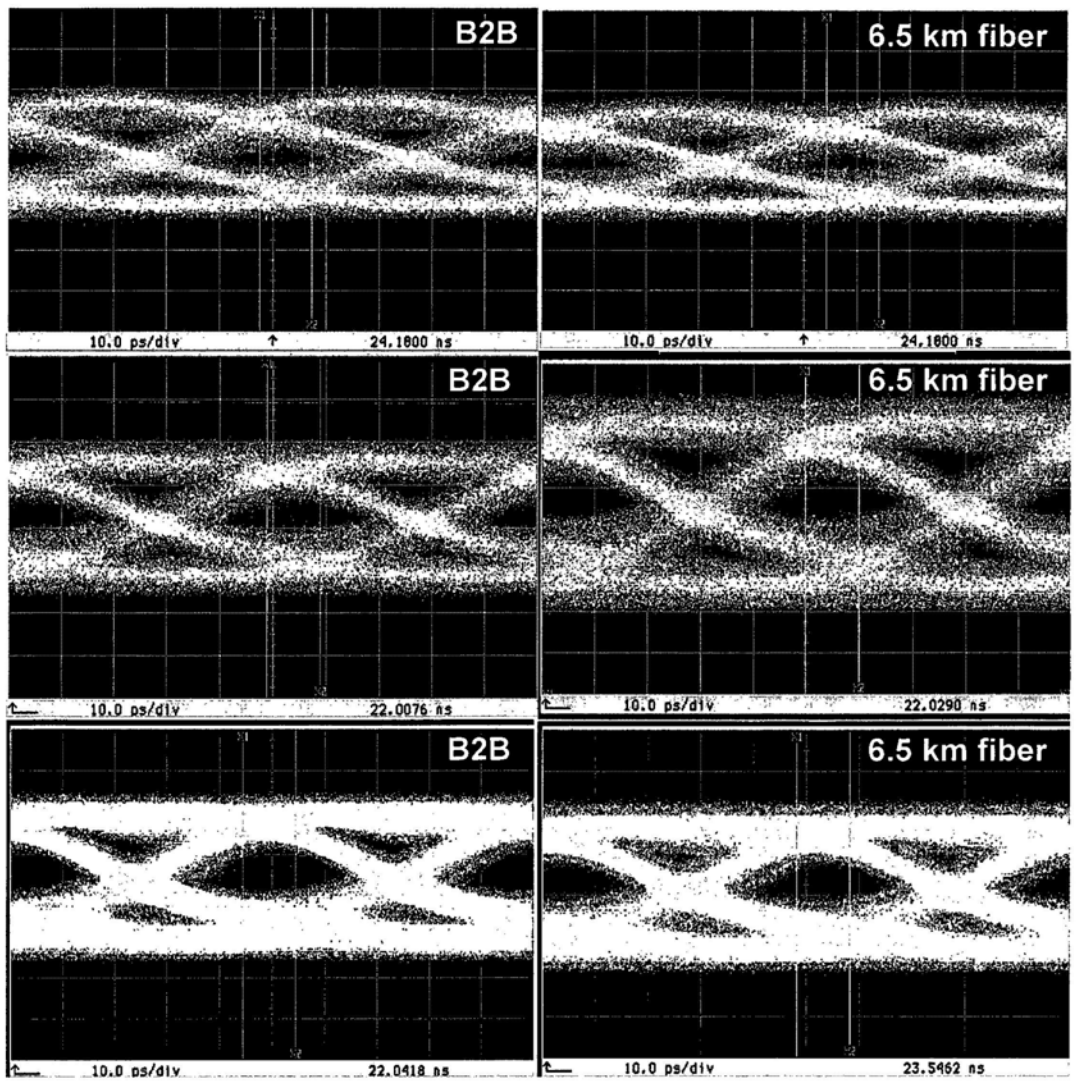

Fig. 4.7 Eyediagrams of 20-Gb/s data transmission experiment for back to back and after fiber transmission. (a) at 5.5 mA, 15 °C, 0.5 Vpp (b) at 8.0 mA, 15 °C, 0.5 Vpp (c) 12 mA, 10 °C, 1 Vpp.

Due to lack of equipment, we use VPI transmissionMaker 7.0 to simulate BER result for Fig. 4.7 (c) case as shown in Fig. 4.8. There is 0.1-dB power penalty after 6.5-km SMF transmission with the same Q factor.

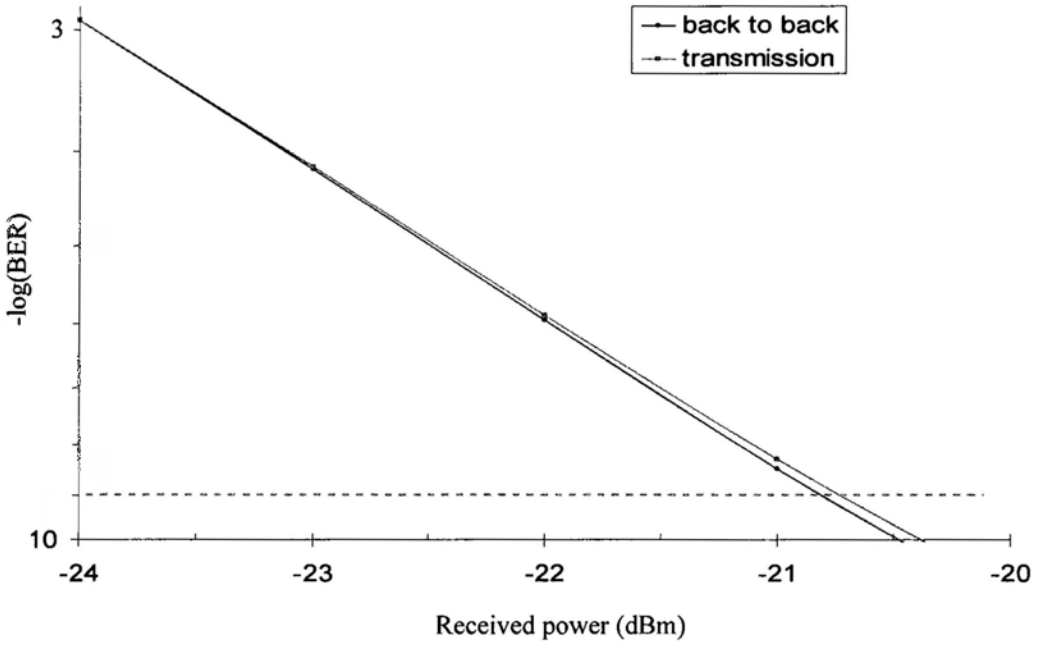

Fig. 4.8 Simulation BER for 20-Gb/s VCSEL

4.2 Advanced Modulation Format Generation

4.2.1 Dark RZ Generation

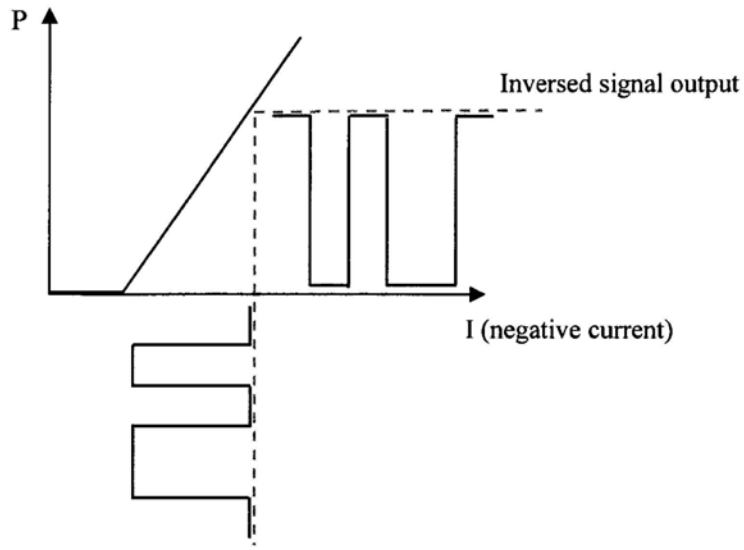

Fig. 4.9 Sketch of DRZ generation working principle

We have studied the DRZ in Chapter 2 and stated the generation difficulty. Here we use VCSEL to generate DRZ. The working principle is shown in Fig. 4.9. Since the VCSEL is negative biased, by properly setting the bias current and driving voltage, the output will be zero if driving signal is one while the output will be one if driving signal is zero. The experiment result is shown in Fig. 4.10. The generated DRZ has a small chirp at rising edge; this can be improved by pre-coding the driving signal.

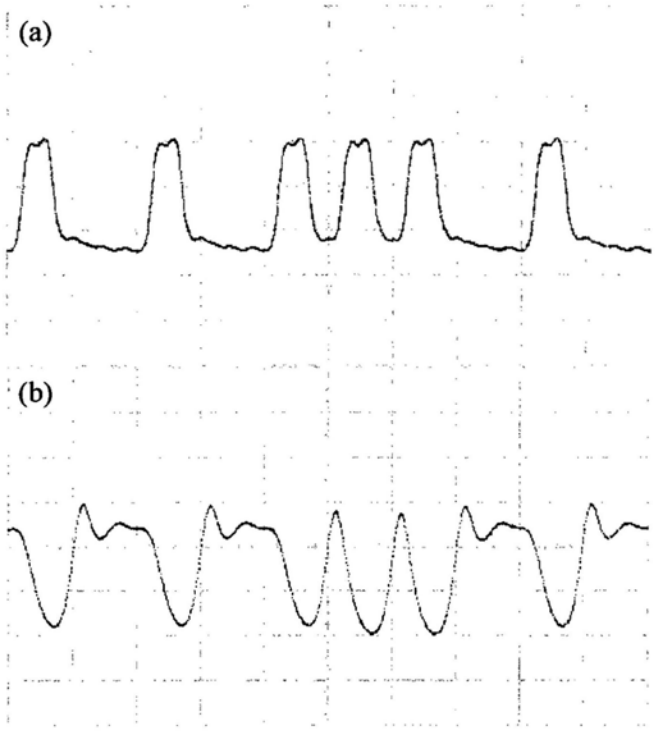

Fig. 4.10 (a) Electric RZ signal (b) generated optical DRZ signal

4.2.2 Multi-Level Modulation

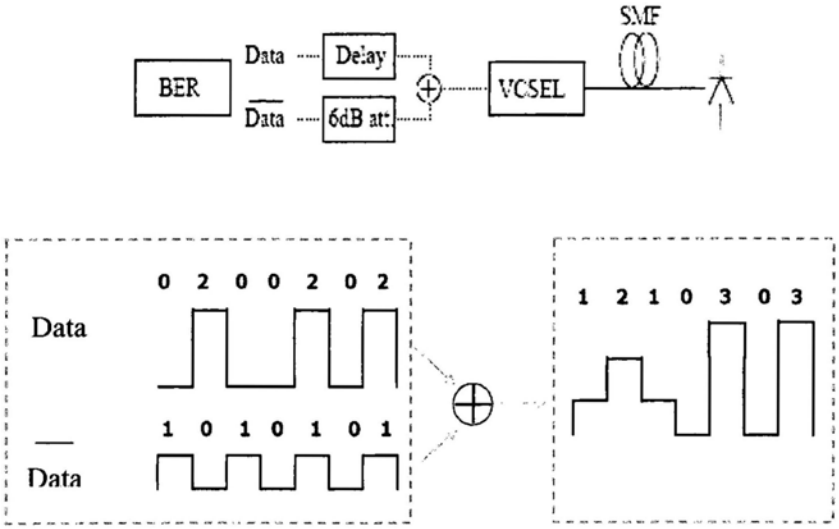

Fig. 4.11 Experimental configuration of multi-level modulation

The experimental configuration is shown in Fig.4.11 top while the electric driving signal is shown in Fig. 4.11 bottom. The data bar output was 6dB attenuated and then combined with data output. The electric delayline was adjusted to let the data period and data bar period overlap. The combined signal modulated the VCSEL directly. The light from the 5-μm diameter output aperture of the VCSEL was coupled into a SMF. In the experiment, the VCSEL was biased at 8 mA at room temperature. The 10-Gbaud/s NRZ driving data (keyed in 256 bits) had a peak to peak voltage of 0.5 V. The modulation was in the linear part of the transmission curve. The equation 4.1 shows the conversion between bitrate (I) and symbol rate (S), while N is different voltage levels.

$$I = S \cdot \log_2 N \qquad (4.1)$$

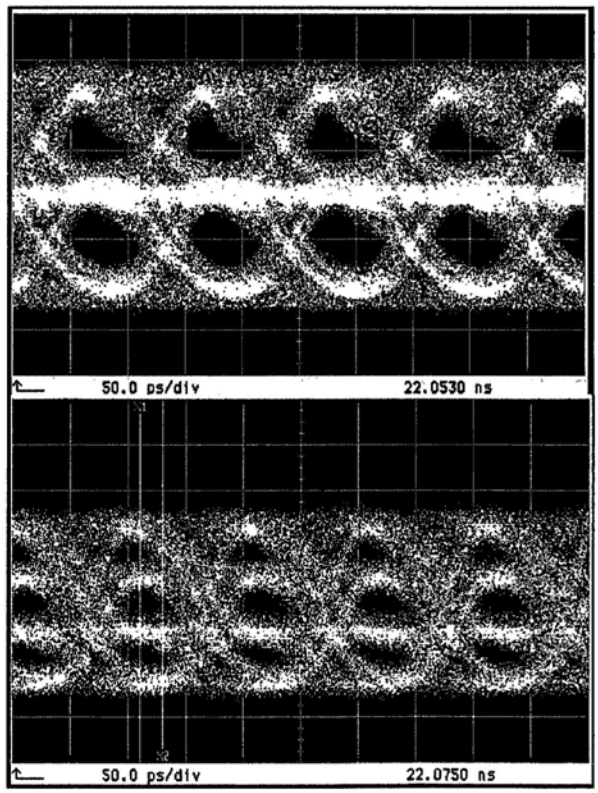

Fig. 4.12 Experimental eyediagrams at symbol rate of 10 Gbaud/s. Top: 3-Level modulation Bottom: 4-Level modulation

As shown in Fig. 4.13, we measured BER (only lower level was measured) and eyediagram of back to back case and after 6.5-km SMF transmission case at 10 °C while the other conditions are the same as stated above. A power penalty of 1 dB was observed after 6.5-km SMF propagation. This result demonstrates that multilevel modulation of VCSELs is suitable for short distance broadband connection. The RF power for each level of multi-level modulation need to be further optimized.

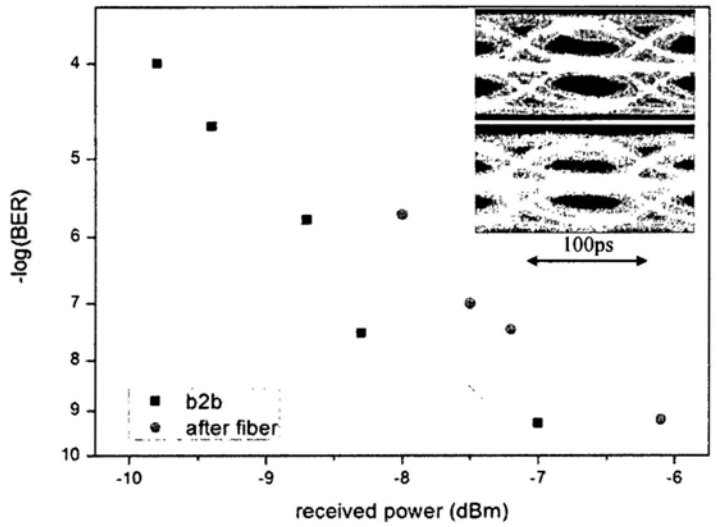

Fig.4.13 BER measurement (lower level) for 3-level modulation and eyediagrams (inset) at 10 Gbaud/s, 10 °C

4.3 VCSELs at OLT

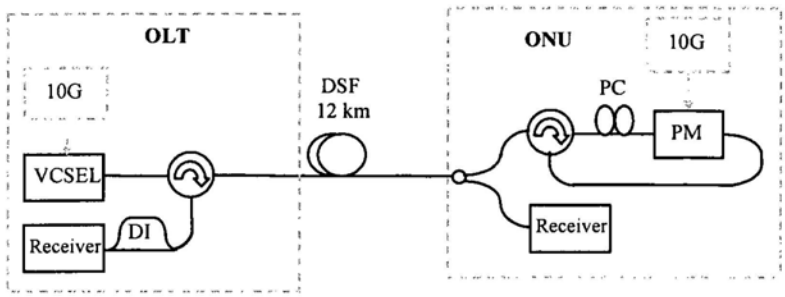

Fig. 4.14 Experimental implementation of WDM-PON using VCSEL as transmitter at OLT

One approach for implementing colorless transceivers is to use a low extinction ratio non return to zero (NRZ) modulation from a VCSEL for downstream transmission and differential phase shift keying (DPSK) remodulation of the received signal for upstream transmission as shown schematically in Fig. 4.14. The VESEL was biased at 5.2 mA. Using a driving voltage of Vpp = 400 mV, a NRZ optical signal with a low extinction ratio of 3.1 dB, suitable for DPSK remodulation, was generated .Although a discrete receiver, VCSEL array and wavelength filters were used here for implementing the transceiver at the OLT, flip-chip mounting of VCSEL array onto a silicon photonic integrated circuit containing the WDM multiplexer (MUX) and DPSK receivers has potential for implementing low cost multi-wavelength optical transceivers.

Both the downstream and upstream signals were generated from a pseudo-random binary sequence (PRBS) pattern generator with a pattern length of 2^{31}-1. The NRZ downstream signal was fed into a span of 12-km dispersion-shifted fiber (DSF, zero dispersion at 1571 nm, 1.34 ps/nm·km at 1550 nm). At the ONU part, the downstream signal was received for detection while another part was remodulated for DPSK upstream transmission. The upstream DPSK signal was

detected at OLT using a MZDI and an optical receiver. The bit error rates were measured both at OLT and ONU for upstream and downstream signals as shown in Fig.4.15. Error free transmission was observed in the upstream signal, thus demonstrating the viability of DPSK remodulation and transmission of the highly chirped downstream signal from the VCSEL.

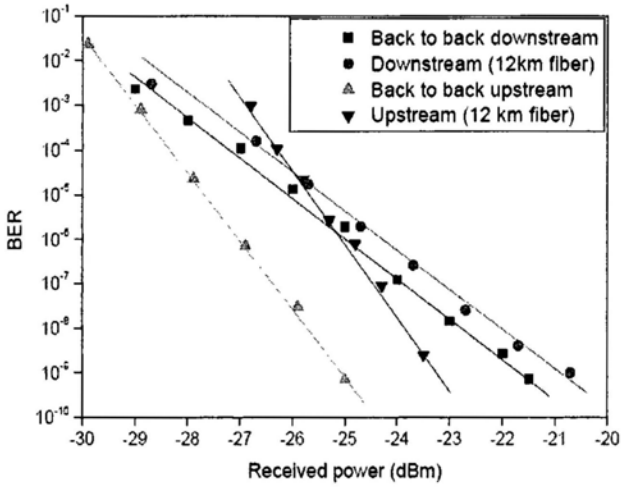

Fig. 4.15 Bit-error-rate measurements of downstream NRZ and upstream DPSK

Although this scheme achieves colorless ONU, it suffers from limited transmission distance (large chirp from direct modulation of VCSEL) and large power penalty of downstream remodulation for upstream as indicated in Chapter 3.

4.4 VCSEL at ONU

Recently, different 10 Gb/s PON solutions have been proposed [10-12] and researchers are going to further increase the data rate of PON towards 40 Gb/s and even more by using advanced modulation formats. Here, we propose a 40-Gb/s symmetric high-split-ratio PON and present the first demonstration of using a directly-modulated, uncooled 1.55-μm monolithic-integrated

VCSEL array for upstream transmitter (Tx) in the 40-Gb/s PON.

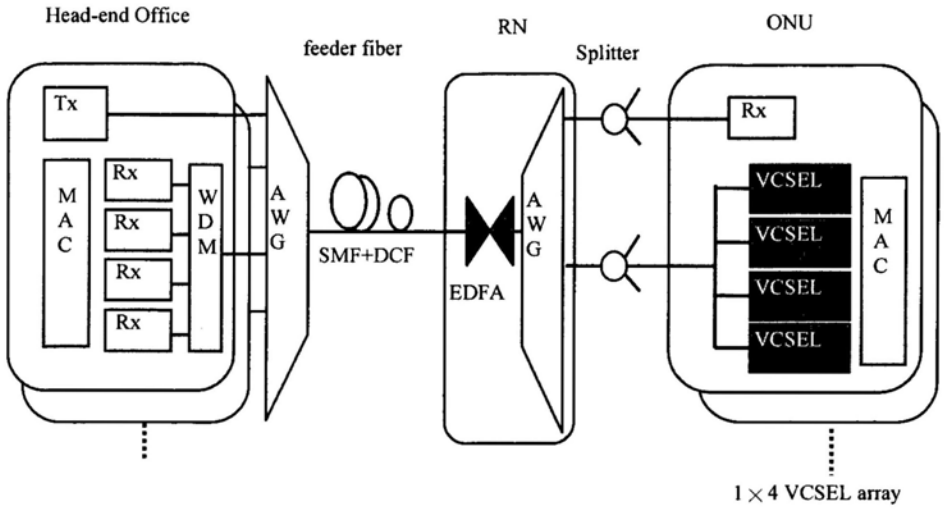

Fig. 4.16. Network architecture of a 40-Gb/s PON using directly-modulated VCSEL array as upstream transmitter. AWG: arrayed waveguide grating, WDM: wavelength division multiplexer, SMF: single mode fiber, DCF: dispersion compensating fiber, RN: remote node, EDFA: erbium-doped fiber amplifier, MAC: media access control, ONU: optical networking unit. Inset: photograph of the 1 x 4 VCSEL array.

Fig. 4.16 shows the schematic of a 40-Gb/s PON implementing directly modulated VCSEL array as the upstream Tx. WDM is used to improve the bandwidth utilization of fiber. The downstream signal is a single 40-Gb/s channel generated by external modulation. Different downstream signals are wavelength multiplexed by an AWG with 3-dB bandwidth of 100 GHz. They will be sent to the ONUs via the long reach feeder fiber, which is dispersion compensated and a remote node, which consists of optical amplifiers and an AWG. In the ONU, each laser in the VCSEL array is directly modulated at 10 Gb/s. The upstream signal is formed by wavelength multiplexing four of these channels using a WDM coupler having channel separation of ~ 25 GHz. This is to ensure the 4 x 10 Gb/s upstream signal can pass through the pass-band of the AWG. The upstream signal will then be detected by the head-end burst-mode Rxs, which are synchronized

by the MAC.

We then evaluated the transmission performance of the upstream Tx. The upstream signals were generated by directly modulating the VCSEL at 10 Gb/s, PRBS 2^{31}-1 via a coplanar radio-frequency (RF) probe each time for one channel only. The signal was then launched to the head-end direction via a variable optical attenuator (VOA), an AWG, an erbium-doped fiber amplifier (EDFA) (output saturated power of 28 dBm and noise figure of 5 dB), and then 12 km of dispersion-shifted fiber (DSF) before received by the head-end Rx, which was optically pre-amplified with an EDFA (output saturated power of 21 dBm and noise figure of 5 dB), an optical filter (3-dB bandwidth of 50 GHz) and a 10-GHz PIN. The VOA was used to emulate the achievable split-ratio of the 40-Gb/s PON. Fig. 4.17 shows the BER measurements of the 4 x 10 Gb/s upstream NRZ signals at back-to-back (B2B) and after 12-km of the transmission. There was about 2-dB power penalty at BER of 10^{-9}. We achieved error-free transmissions for the upstream signals when the VOA was set at -21 dB, corresponding to a split-ratio of 128. Typical eye diagrams at back to back and after the 12 km from the VCSEL (Ch1: 1548.3 nm) were shown in the insets. Fig. 4.18 shows the measured optical spectra (resolution bandwidth of 0.08 nm) of the four lasing outputs from the VCSEL array obtained by biasing one of the 4 lasers each time with wavelength separation of ~25 GHz. Thermal crosstalk from operating the lasers simultaneously should be small because the 0.25mm pitch is much larger than the 40μm employed earlier [1]. The side-mode is 30 dB lower than the center peak. The peaks need to be further separated to avoid the cross talk between adjacent channels.

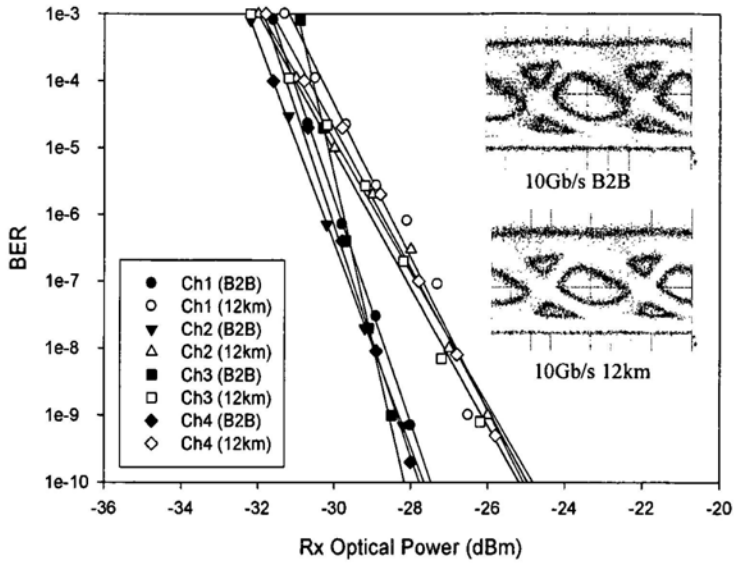

Fig. 4.17 Measured BER of the 10-Gb/s upstream signals with the corresponding eye-diagrams at back to back and 12-km transmission.

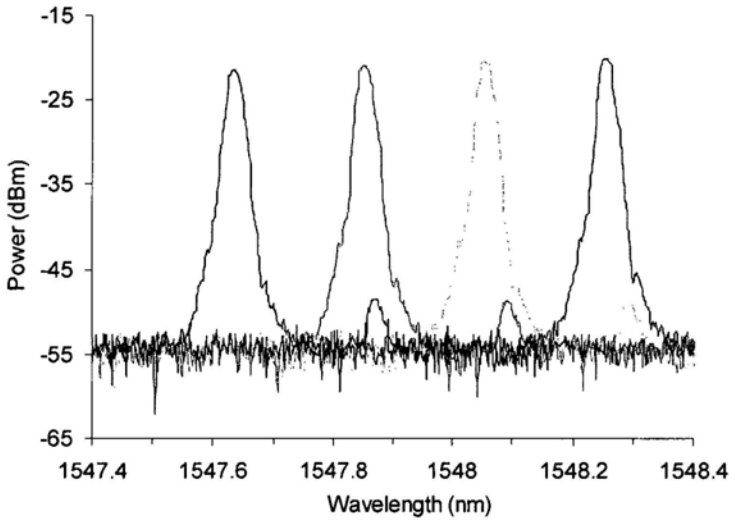

Fig. 4.18 Measured optical spectra of the four lasing outputs from the VCSEL array (wavelength separation of ~0.25 nm).

Since the ONU is cost-sensitive, we also propose using low bandwidth Rx at ONUs to receive 40 Gb/s downstream signal. Due to the unavailability of 40-Gb/s electrical NRZ pattern generator at

the laboratory, simulations using commercially available software (VPI TransmissionMakerV7.5) were performed. Fig. 4.19 shows the schematic of the downstream signal transmission of the high split-ratio PON using DRZ modulation. The DRZ was generated by a single-drive balanced Mach-Zehnder modulator (MZM), which was driven by a differentially precoded 40-Gb/s NRZ data with an amplitude of 2 V_{π}. The MZM was biased at a minimum of the transmission curve and the NRZ drive voltage switched the MZM towards the two adjacent maximums. When there is a transition from low-to-high or high-to-low in the NRZ drive voltage, the output state of the MZM is swept from a maximum, through a minimum, to an adjacent maximum, so generating a dark optical pulse. This is similar to DPSK generation, but the data is encoded onto the intensity instead of the phase of the optical carrier. The DRZ propagated through 100 km SMF (dispersion parameter: 17 ps/nm/km) and 17-km dispersion compensating fiber (DCF) (dispersion parameter: -100 ps/nm/km) and the RN. A fixed attenuator (FA) of -21 dB was used to emulate the fiber splitter. The signal was then detected by the optically pre-amplified Rx, which consisted of a VOA, an EDFA (noise figure 5 dB), an optical fiber (Gaussian-shaped, 3-dB bandwidth of 100 GHz) to filter the out-of-band amplified spontaneous emission (ASE), and a PIN photodiode (PD). An electrical 3rd order Bessel low pass filter (LPF) was used to model different bandwidth of the PD.

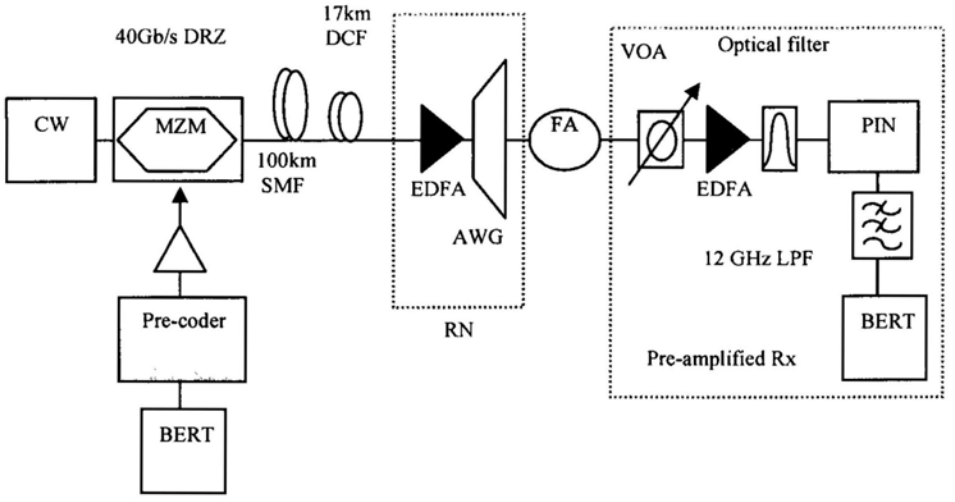

Fig. 4.19 Schematic of 40-Gb/s downstream DRZ transmission for simulations. MZM: Mach-Zehnder Modulator, AWG: arrayed waveguide grating, Rx: receiver, DSF: dispersion shifted fiber, EDFA: erbium doped fiber amplifier, VOA: variable attenuator, BERT: bit-error-rate tester, LPF: low pass filter.

Fig. 4.20 shows the Rx sensitivities of the received DRZ signals detected by using different Rx bandwidths, with the corresponding eye-diagrams at bandwidths 12, 20, 30, 40 GHz. By reducing the Rx bandwidth from 40 GHz to 12 GHz, we only sacrifice ~4 dB in the Rx sensitivity, and the costly 40 GHz Rx can be removed from the ONU. For PON applications, although the long reach feeder fiber can be dispersion compensated, the distribution/drop fibers (between OUNs and the splitter) cannot. Then we evaluated the dispersion tolerance of the 40 Gb/s DRZ signal. The residual dispersion was set with additional lengths of fibers, and the Rx bandwidth was 12 GHz. Fig. 4.21 shows that the 2-dB penalty window is at ~5-km SMF; and this is good enough for PONs. Corresponding eye-diagrams at B2B, additional SMF of 5 km and 6 km are shown in the insets.

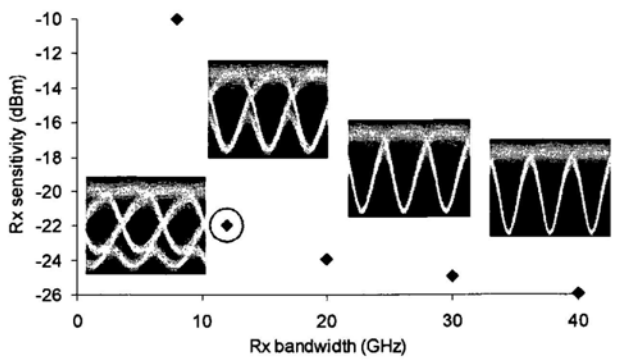

Fig. 4.20 Simulated Rx sensitivities of the DRZ signal detected by different Rx bandwidth. Inset: eye-diagrams at bandwidths 12, 20, 30, 40 GHz.

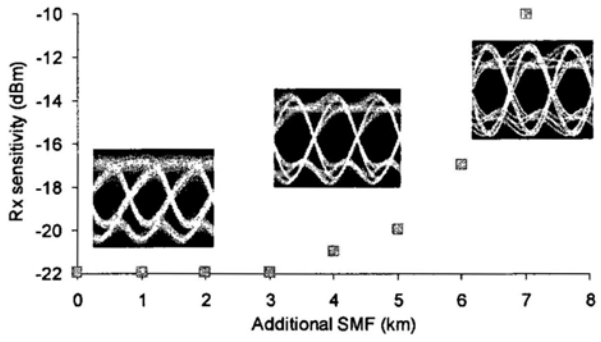

Fig. 4.21 Simulated Rx sensitivities of the received DRZ signal at different residual dispersions set by additional lengths of fibers. Inset: eye-diagrams at B2B, additional SMF of 5 km and 6 km.

In conculsion, we demonstrated a 40-Gb/s high-split-ratio PON and presented the first demonstration of using a directly-modulated, 1.55-μm VCSEL for upstream Tx in the 40-Gb/s PON. High split-ratio of 128 was achieved experimentally. Simulation results show that by using 40-Gb/s DRZ modulation as downstream signal, 12-GHz Rx can be used in the ONU. Hence, by using the proposed 4 x 10-Gb/s VCSEL array Tx and the 12-GHz Rx, expensive 40-GHz optical components can be removed from the cost-sensitive ONU for the future 40-Gb/s high-split-ratio PON. As the upstream signal in PON is bursty, and 40-Gb/s burst-mode receiver (Rx) is hard to implement, in this scheme the upstream signal can be received by using four 10-Gb/s burst-mode Rx synchronized in the media access control (MAC) layer protocol. However, the VCSEL array might not be cost effective considering its limited tuning range. This would imply that ONUs using such devices would not be colorless, thus, increasing the service provider's inventory costs in real networks. The thermal cross talk may be one problem in practical use when all channels are turned on although the threshold of the VCSELs is low. TEC may be necessary to stabilize the laser wavelength.

REFERENCES

[1] A. Ortsiefer, M., Baydar, S., Windhorn, K., Ro¨nneberg, E., Rosskopf, J., Shau, R., Grau, M., Bo¨hm, G., and Amann, M.-C.: 'Long-wavelength monolithic VCSEL arrays with high optical output power', Electron. Lett., 2005, 41, pp. 807 808

[2] W. Hofmann, E. Wong, M. Ortsiefer, N. H. Zhu and M. C. Amann, "1.55-μm VCSEL Arrays for high-bandwidth WDM-PONs" IEEE PHOTONICS TECHNOLOGY LETTERS, 20, 291-293, 2008

[3] L Xu, H. K. Tsang, W. Hofmann and M.-C. Amann "10-Gb/s Colorless Re-modulation of Signal from 1550nm Vertical Cavity Surface Emitting Laser Array in WDM PON" CI3.4, CLEO/Europe-EQEC 2009

[4] P. Westbergh, J. Gustavsson, A. Haglund, H. Sunnerud, and A. Larsson "Large aperture 850 nm VCSELs operating at bit rates up to 25 Gbit/s", Electron. Lett., vol. 44, no. 15, pp. 907-908, 2008

[5] Alberto Gatto, Anna Boletti, Pierpaolo Boffi, Christian Neumeyr, Markus Ortsiefer, Enno Rönneberg and Mario Martinelli, "1.3-mm VCSEL Transmission Performance up to 12.5 Gb/s for Metro Access Networks" IEEE Photon. Technol. Lett., vol. 21, no. 12, pp. 778-780, 2009

[6] W. Hofmann, L. Grüner-Nielsen, E. Rönneberg, G. Böhm, M. Ortsiefer, and M.-C. Amann "1.55 μm VCSEL Modulation Performance with Dispersion-Compensating Fibers" IEEE Photon. Technol. Lett., vol. 21, no. 15, pp. 1072-1074, 2009

[7] L. Xu, W. Hofmann, H. K. Tsang, R. V. Penty, I. H. White, M. C. Amann, "1.55-μm VCSEL Transmission Performance up to 20 Gb/s for Access Networks", post-deadline paper, OECC, 2009, Hong Kong

[8] W. Hofmann, M. Müller, A. Nadtochiy, C. Meltzer, A. Mutig, G. Böhm, J. Rosskopf, D. Bimberg, M-C Amann, and C. C. Hasnain, "22-Gb/s Long Wavelength VCSELs", Optics Express, vol. 17, no.20, pp. 17547-17554, 2009

[9] W. Hofmann, E. Wong, G. Böhm, M. Ortsiefer, N. H. Zhu, and M.-C. Amann, ""1.55-μm VCSEL Arrays for High-Bandwidth WDMPONs" ", IEEE Photon. Technol. Lett., vol. 20, pp. 291-293, 2008

[10] C. W. Chow, C. H. Yeh, C. H. Wang, F. Y. Shih, and S. Chi, "Signal remodulation of OFDM-QAM for long reach carrier distributed passive optical networks," IEEE Photon. Technol. Lett., vol. 21, no. 11, pp. 715-717, June 2009.

[11] M. F. Huang, J. Yu, D. Qian, N. Cvijetic, and G. K. Chang, "Lightwave centralized WDM-OFDM-PON network employing cost-effective directly modulated laser," OFC'09, Anaheim, USA, paper OMV5.

[12] P. L. Tien, Y. M. Lin, and M. C. Yuang, "A Novel OFDMA-PON architecture toward seamless broadband and wireless integration," OFC'09, Anaheim, USA, paper OMV2.

Chapter 5
Wired and Wireless Hybrid Access Networks

High data rate wireless transmission instead of installing new fiber to connect individual buildings in metropolitan areas may help to reduce cost for future deployment of broadband networks in metropolitan areas. Existing standards such as the IEEE 802.16 need high frequency carrier signals in the 10 GHz-66 GHz spectral ranges. The microwave signals may be distributed by conventional optical fiber to the antenna base-stations, thus consolidating the carrier frequency generation and data modulation at the head-end station and reducing the cost and complexity of the antenna sites. The first generations of gigabit PONs (GPON) have now been standardized and typically offer 1 2.5 Gb/s downstream and 1 Gb/s upstream. For wireless communication, it is now entering a new phase where the focus is moving from voice to high bandwidth multimedia services. Radio-over-fiber (ROF) technique is attracting much attention in the broadband wireless access networks [1]. RF over fiber is more attractive compared to intermediate frequency (IF) over fiber due to simple base station and protocol transparency. In order to support high data rate wireless communication in the future, wireless system would utilize millimeter (mm)-wave as the signal carrier. Many research efforts have been made at the 60-GHz band [2]–[7] or above [8]. Optical mm-wave generation is a key technique. In section 5.1, we present a silicon coupled microring resonator to achieve optical frequency doubling in two DWDM channels. In section 5.2, we propose and demonstrate a technique for optical mm-wave signal generation by frequency quadrupling. In section 5.3, we demonstrate mm-wave generation using FWM in silicon waveguide and microring

integrated device.

The convergence of mm-wave wireless and wired PONs in an integrated platform can be a promising technique in future access networks for providing broadband wired and wireless access services with increased mobility and reduced cost. Besides mm-wave generation, the transmission of optical mm-wave is crucial in ROF systems because chromatic dispersion can cause signal distortions. In section 5.4-5.6, we demonstrate several novel approaches to mitigate RF fading problems and thus achieve long reach PON cost effectively.

5.1 Frequency Doubling

Optical generation of microwave and mm-wave signals based on phase modulation has been investigated extensively [9, 10] and has the advantage that the optical phase modulators do not require any ultrastable DC bias. Microwave frequency doubling was achieved using an optical phase modulator followed by a FBG serving as an optical notch filter to suppress optical carrier [9], and the technique was extended to dense wavelength division multiplexed (DWDM) systems using optical interleavers [10]. Here the coupled-microring filter functioned as a high performance optical filter which removed the optical carrier, so that the two first order sidebands can then beat with each other in a photodetector at the antenna site in the ROF system. The beating of the two optical sidebands generates mm-wave at twice the frequency of the phase modulation.

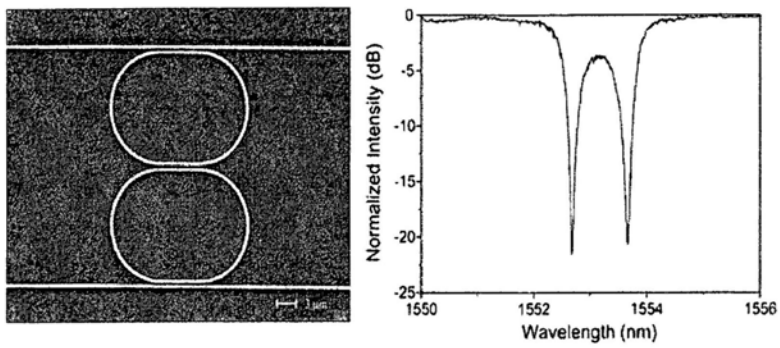

Fig. 5.1. (a) Scanning electron microscope (SEM) image of the fabricated silicon coupled-microring notch filter. (b) Measured spectrum of the device.

The coupled-microring resonator was fabricated at IMEC (http://www.imec.be) Belgium using deep-UV (193 nm) photolithography and dry etching on a silicon-on-insulator (SOI) wafer with 220-nm-thick device layer and 2-μm-thick buried oxide [11, 12]. Light was coupled in and out of the microring filter via waveguide grating couplers [13]. The racetrack microring arc radius is 8 μm, and the straight coupling length is 6 μm shown in Fig.5.1 (a). The waveguide width is about 500 nm. The fabricated air-gap spacing between the ring and the waveguide is about 200 nm. The loaded quality factor (Q) of the resonance is ~ 4,000, as shown in Fig. 5.1(b).

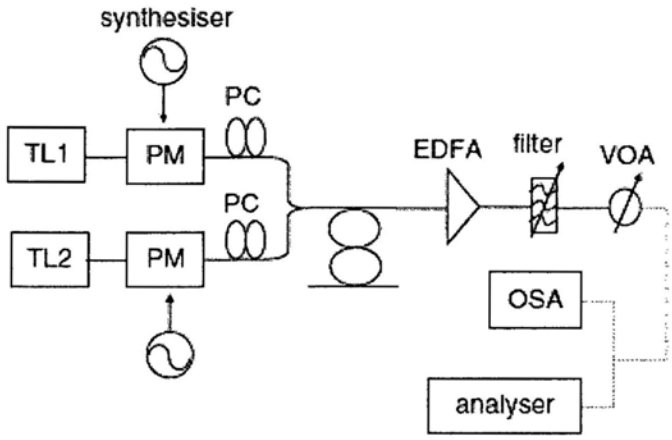

Fig.5.2. Experiment setup of multichannel frequency doubling. TL: tunable laser PC: polarization controller PM: phase modulator VOA: variable optical attenuator OSA: optical spectrum analyzer

The proposed subsystem to generate the mm-wave signal by frequency doubling is shown in Fig.5.2. Two CW optical signals at wavelengths of 1552.68 and 1553.66 nm produced by a tunable laser (Agilent 8164A) were tuned exactly to the resonance wavelengths of the coupled microring resonator. Discrete optical phase modulators may be used in this proof-of-principle demonstration, but these can eventually be integrated on the chip [14] in the ultimate design. By driving the phase modulators with 10 and 12-GHz sinusoidal signals, respectively, from a synthesizer, sidebands were produced at the respective detuning from the centre frequencies of the tunable lasers. Thus, each DWDM wavelength channel may be used to generate a different RF frequency for use in different RF cells. The coupled microring filter serves as fixed notch filters to generate the mm-wave signal by frequency doubling. The frequency separation between the two first-order sidebands is equal to twice the modulating signal frequency. Hence frequency doubling of the electrical drive signal can be simply achieved

without needing any DC bias adjustment. Frequency quadrupling could also be achieved by filtering out the optical carrier and first-order sidebands using an appropriately designed coupled microring filter.

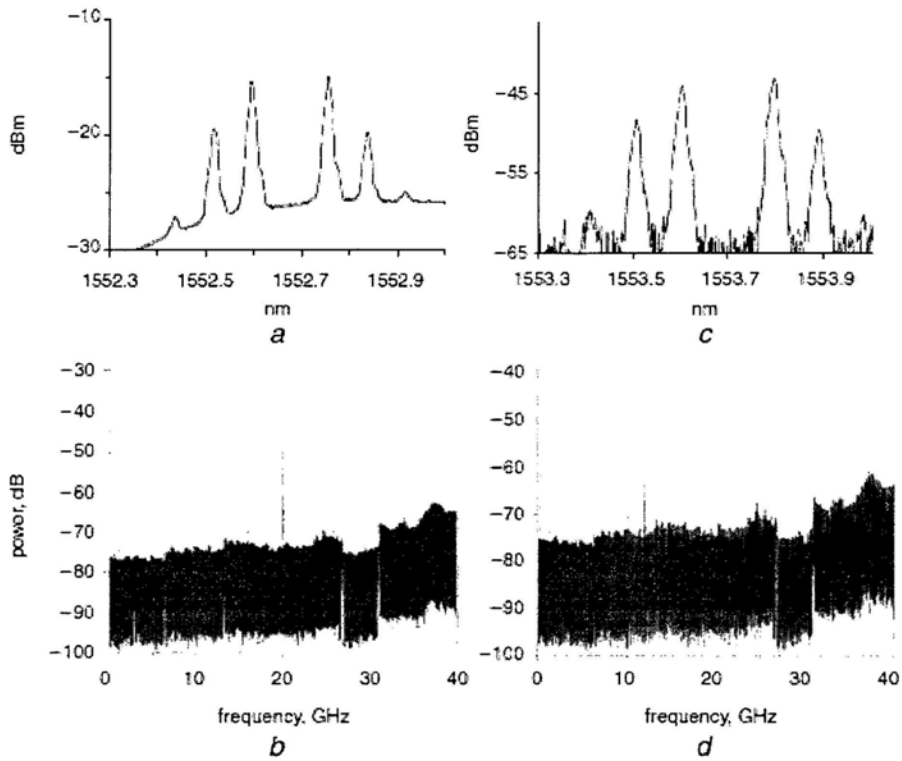

Fig.5.3. Optical spectra of (a) channel 1 (c) channel 2 and RF spectra of (b) channel 1 (d) channel 2 at the output of the microring

The output spectra after the coupled microring filter are shown in Figs.5.3a–d (a, b for channel one and c, d for channel two). The wavelength spacing between the two first-order modes were 0.16 nm (equal to 20 GHz) and 0.19 nm (equal to 24 GHz), respectively. The RF spectra of the optical signals were measured by a 32-GHz pin photodetector and HP8564E

spectrum analyzer.

We demonstrated a simple technique for DWDM frequency doubling using a phase modulator and a silicon coupled-microring. The optical carriers were removed from the output of the optical phase modulator by the cascaded microring notch filter while the remained sidebands produced frequency doubling at the photo detector. The generated signals had high-frequency stability and narrow linewidth. The scheme is potential for silicon integration and multichannel mm-wave signals generation thus significantly reduces the cost of the DWDM ROF system.

5.2 Frequency Quadrupling

The approach of using a single laser source and an external optical modulator is based on the inherent response of the optical modulator for generating high-order optical sidebands and has shown good potential for producing high-purity, high-frequency mm-wave signals. In [15-18], there have been several reports on ROF system that reduce the complexity and cost of the system. However, the local oscillator (LO) frequency is only double to produce the optical mm-wave carrier. To overcome the limitation and to produce higher frequency, an optical generation scheme that uses narrow bandwidth optical components to generate high frequency electrical signals becomes attractive. A wideband optical mm-wave generation scheme has proposed in [19] by multiple frequency doubling technique through properly adjusting DC bias on external modulator to further reduce the LO frequency and bandwidth of the external

modulator. We here show a silicon microring instead of FBG [19] which works as a notch filter.

5.2.1 Using an Intensity Modulator

By setting the DC bias of a MZM to its transmission maximum, second order sidebands are generated while the first order sidebands can be suppressed. Besides the two peaks of the second order sidebands, the output of the MZM also contains the input carrier frequency component. A high performance optical filter (a microresonator notch filter) is used to remove the optical carrier, so that the two second order sidebands can then beat together in a photodetector at the antenna site in the ROF system to generate mm-wave that has a frequency equal to four times the LO frequency.

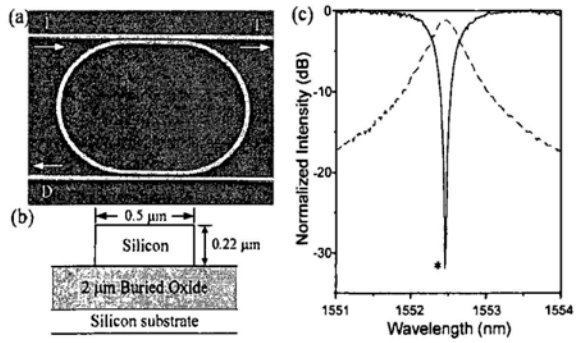

Fig.5.4 (a) Top-view scanning electron micrograph (SEM) of the fabricated waveguide coupled microring resonator. I: Input port; T: Throughput port; D: Drop port. (b) Cross-section schematics of the waveguide. (c) Measured TE-polarized throughput and drop port spectra.

Fig.5.4 shows the fabricated microring. The loaded quality factor (Q) for the resonance is ~ 4,000, as shown in Fig. 5.4(c). The racetrack microring arc radius is 8μm, and the straight interaction length is 6μm. The fabricated air-gap spacing g between the ring and the waveguide is about 200 nm.

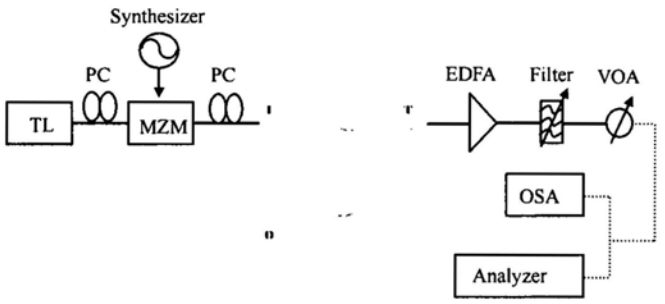

Fig.5.5 Proposed silicon-based optical mm-wave signal generator by frequency quadrupling. TL: tunable laser PC: polarization controller MZM: Mach-Zehnder modulator VOA: variable optical attenuator I: input port T: through port

D: drop port

Fig.5.5 shows the proposed silicon-based optical mm-wave signal generator by frequency quadrupling. A CW light at the wavelength of 1552.46 nm generated by a tunable laser (HP 8168F) was tuned exactly to the resonance wavelength of the microring filter. A commercially available MZM was used in the proof-of-principle demonstration. For the future work, the microring filter could be monolithic integrated with the previously proposed silicon-base optical modulator [14] to achieve the mm-wave signal generator by frequency quadrupling. It was applied by a 10-GHz sine wave RF signal generated by a synthesizer at about 1.3 Vπ. In order to produce the optical two-tone for optical mm-wave generation, the DC bias of the

MZM can be set in two states. When the DC bias is set to a minimum transmission, optical carrier suppressed (OCS) optical modulation can be achieved, where the output of the MZM has the first order sidebands, and in principle, without the carrier frequency. The frequency separation between the two first order sidebands is equal to two times of the modulating signal frequency. Hence this only produces frequency doubling. In order to achieve frequency quadrupling, the DC bias can be set to a transmission maximum. In this case, second order sidebands can be generated. And the frequency separation between the two second order sidebands is equal to four times of the modulating signal frequency. An optical notch filter is needed to remove the carrier frequency. In the experiment, the optical signal generated at the output of the MZM was then coupled into the microring resonator through the input port (I). The total input and output coupling loss from fiber to the microring filter was measured to be 9 dB. The optical carrier was removed by the notch filter characteristics of the microring resonator when measured at the drop port (D). The power coupling ratio from the waveguide to the microring was 12.4% (versus a design targeted value of ~12%). For the double waveguide microring resonator, there is a critical coupling only if the ring is lossless. However, the extinction ratio of the notch filter used in this experiment was 30 dB, which is close to critical coupling. The signal was then measured by an optical spectrum analyzer and an RF analyzer, consisting of a 40-GHz PIN photo-detector.

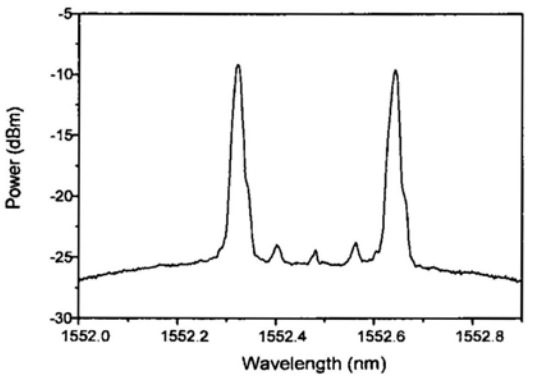

Fig.5.6. optical spectrum at the second order optical sidebands at the output of the microresonator

Fig.5.6 shows the optical carrier and the first order sidebands are 15 dB lower than that of the second order sidebands. The optical spectrum was measured by an optical spectrum analyzer with resolution of 0.01 nm. The wavelength spacing between the two second order modes was 0.318 nm (equal to ~40 GHz). A mm-wave signal that has four times the frequency of the microwave drive signal was thus generated by beating the two second order optical sidebands at a photodetector, which could be located at the antenna site in the ROF system. Including the 9-dB coupling loss (which may be reduced by integrating the filter with modulator), there was a measured 18-dB loss in average RF power using this method of frequency quadrupling.

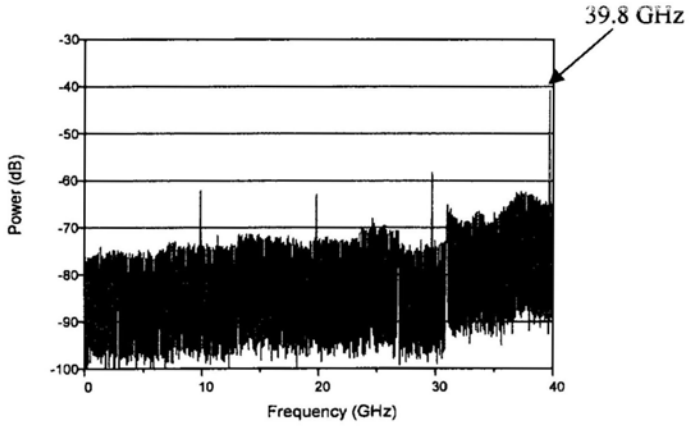

Fig. 5.7 RF spectrum of the generated 39.8 GHz signals

Fig.5.7 shows the RF spectrum of the 40-GHz optical mm-wave signal measured by a 40-GHz PIN photo-detector and HP8564E RF spectrum analyzer (with resolution of 10 MHz). In Fig.5.7, the frequency harmonic components (10, 20 and 30 GHz) also appear in the trace while the 40-GHz harmonic component is about 20 dB higher than the other frequency components.

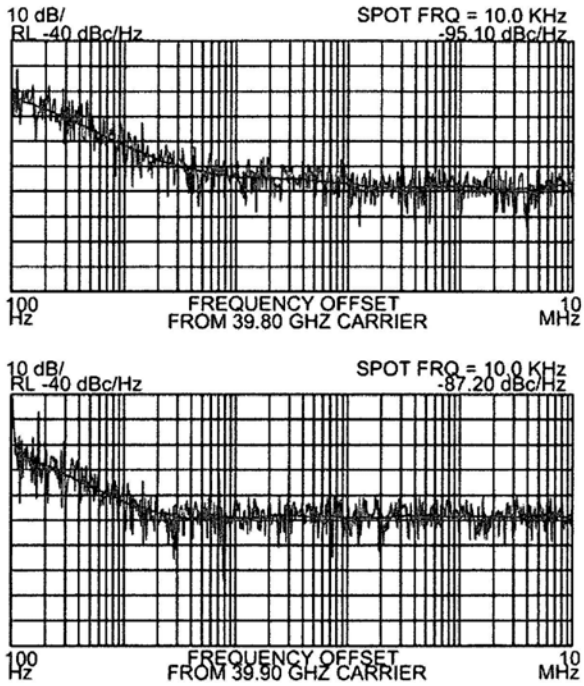

Fig.5.8 Top: Single sideband (SSB) noise spectrum of the RF frequency synthesizer measured at 40-GHz tone. Bottom: SSB noise spectrum of the proposed scheme measured at 40-GHz tone.

Fig.5.8 (bottom) shows the single side band (SSB) noise spectrum of the generated 40-GHz optical mm-wave. The SSB noise spectrum of the 40-GHz signal generated by a RF frequency synthesizer (Agilent E8244A) shown in Fig.5.8 (top) is also given for comparison.

We observed that the SSB noise of the proposed scheme shows similar performance when compared with that of a commercially available frequency synthesizer. The noise increases from -87.20 dBc/Hz to -95.10 dBc/Hz of proposed scheme at spot frequency of 10.0-kHz offset.

We demonstrated a simple technique for frequency quadrupling using a MZM and a microring resonator. 40-GHz optical mm-wave signal was generated from a 10-GHz signal using this technique. The technique relied on the inherent modulation response of a MZM when it is biased at transmission maximum to suppress the odd order optical sidebands; and optical notch filter characteristics of a microring resonator to remove the optical carrier. The scheme has the potential for silicon integration and thus allows lower frequency device such as RF source and optical modulator to generate high frequency optical mm-wave signals, which significantly reduce the cost of the DWDM ROF system.

5.2.2 Using a Phase Modulator

We use a silicon coupled microring resonator to achieve optical frequency quadrupling locally using a PM. Besides the stable characteristic without DC bias, we show that using PM can save ~3-dB power for radio frequency (RF) generation when compared to using AM which become a more efficient approach. The coupled-microring filter functioned as a high performance optical filter removed the optical first order sidebands, so that the two second

order sidebands can then beat with each other in a photodetector at the remote antenna site in the ROF system. The beating of the two optical sidebands generated mm-wave at fourth of the frequency of the phase modulation. The microring resonator can potentially be integrated at the receiver with the photodiode, thus reducing the problem of fading of millimeter wave signals because of dispersion in the transmission optical fiber [20].

The transmission function of a PM is constant while that of AM is sine function. The measured modulation efficiencies are shown in Fig.5.9 in which the AM was biased at transmission minimum and RF power was 1.3 Vπ for frequency doubling case. The modulation efficiency of PM was constant at different driving frequencies. The AM produced 3 dB less efficiency at modulation frequency of 3.5 GHz and 7 dB less at modulation frequency of 15 GHz compared to the PM. This result is consistent with the PM being more efficient in generating the required high frequency harmonics for mm-wave generation.

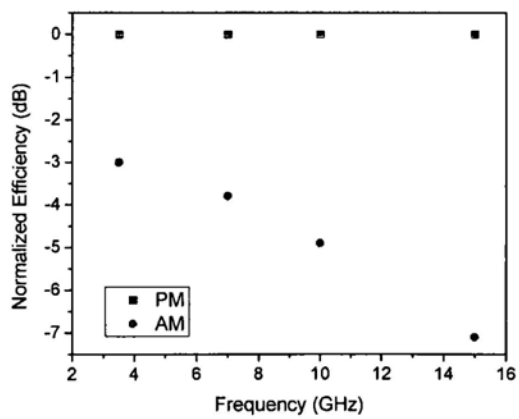

Fig.5.9. Modulation efficiencies of amplitude modulator and phase modulator

For the proof-of-principle demonstration, we used a commercial 10-Gb/s PM instead of a silicon integrated chip. A tunable laser was used as the optical source. A 3.5-GHz electric

sine-wave, generated by a synthesizer, was used to drive the PM. The optical carrier, which was set to match the resonance of the silicon microresonator, was launched to the PM through a PC. The optical carrier was suppressed by properly adjusting the PC as shown in Fig.5.10(a). The first order sidebands were suppressed by transmitting through the microresonator as shown in Fig.5.10(b). The frequency separation between the two second order sidebands was equal to fourth the modulating signal frequency. Hence frequency quadrupling of the electrical drive signal can be simply achieved without needing any DC bias adjustment.

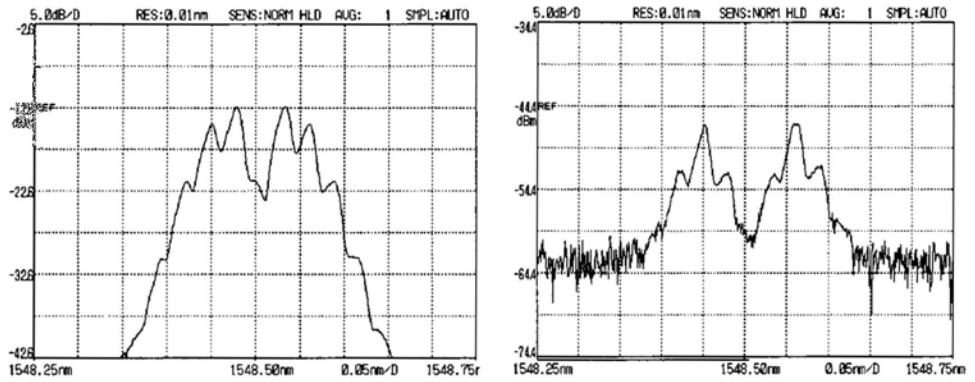

(a) (b)

Fig.5.10. (a) spectrum before microresonator (b) spectrum after microresonator

The RF spectrum of the generated optical signal was measured by a 40-GHz PIN photo-detector and HP8564E spectrum analyzer. As shown in Fig.5.11, 14-GHz component was generated which was 6 dB higher than the 7-GHz harmonic component. Other harmonic components were suppressed. The performance can be further improved by increasing the extinction ratio and Q factor of the microresonator.

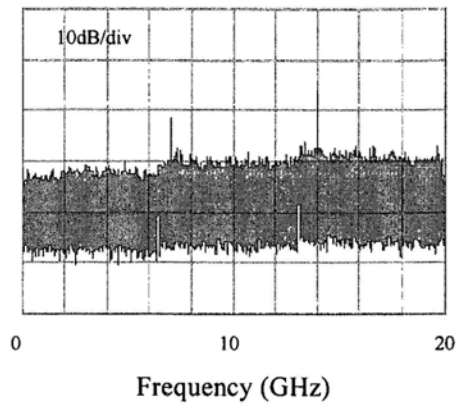

Fig.5.11 RF spectrum at the output of the microresonator

We have demonstrated a simple technique for frequency quadrupling using a PM and a flat-top coupled microresonator. The optical carrier and the first order sidebands were removed while the remaining sidebands produced frequency quadrupling at the photodetector. The scheme has good potential for monolithic integration at the receiver and the capability of multichannel mm-wave signals generation at the receiver can help relax the stringent fiber dispersion requirements for the distribution of millimeter wave signals in optical fiber.

5.3 Millimeter Wave Generation using FWM in Silicon Integrated Chip

Silicon photonic devices have been attractive because of its compact size and can be low cost monolithic integration [21]. The recent explosion in Si photonics is driven mainly by the development of high-volume optoelectronic integrated circuit (OEIC) chips and secondarily by the development of practical photonic ICs (both in SOI) [22]. Four-wave mixing (FWM) in silicon wire waveguides was first demonstrated in [23]. Since FWM is independent of

bit-rate and modulation format, it is a good candidate to implement multichannel frequency up conversion [24, 25].

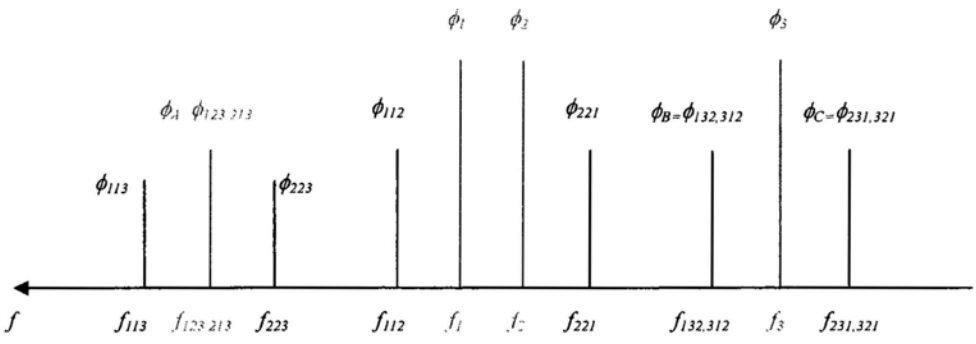

Fig.5.12 Schematic illustration of the FWM

As shown in Fig.5.12, the three FWM participators include pump 1 at frequency f_1, pump 2 at frequency f_2 and idler at frequency f_3. After FWM in a nonlinear medium, new components are generated. Each generated components satisfy a frequency of $f_{xyz}=f_x+f_y-f_z$ (x,y≠z; x,y,z are selected from 1,2,3) and a phase of $\phi_{xyz}=\phi_x+\phi_y-\phi_z$ [26]. The conventional first order FWM refers to f_3, $f_{132,312}$ and $f_{231,321}$. The second order FWM refers to $f_{123,213}$, f_{113} and f_{223}. Since two pumps are generated from the same laser source ($\phi_1=\phi_2$), thus $\phi_{113}=\phi_{223}$.

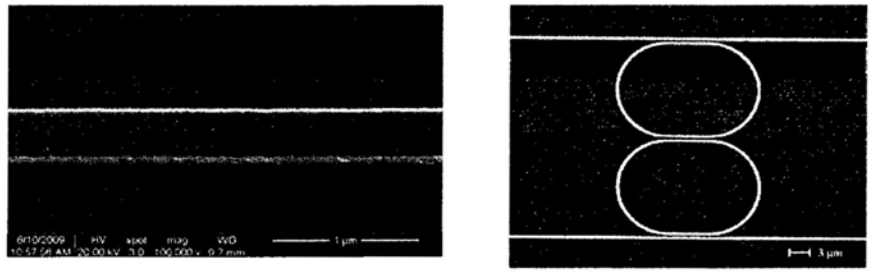

Fig.5.13 Top-view scanning electron micrograph (SEM) of the fabricated waveguide and coupled microring resonator

The silicon nanowire and microring shown in Fig.5.13 were fabricated at IMEC (http://www.imec.be) Belgium on silicon-on-insulator (SOI) wafer same as previous section. The nanowire waveguide is 19-mm long and 480-nm width. Since the microring is not on the same chip with nanowire waveguide, we use a FBG instead for a proof-of-principle demonstration due to experimental limitation. The scanned spectra of microring and FBG shown in Fig.5.14 are almost the same (measured with 0.01-nm resolution) thus the approximation is accurate.

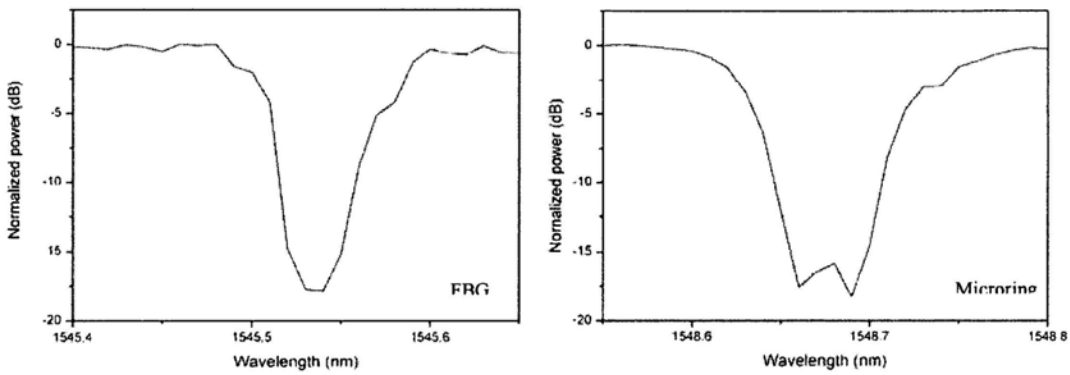

Fig.5.14 Scanned spectrum of (a) FBG and (b) Microring

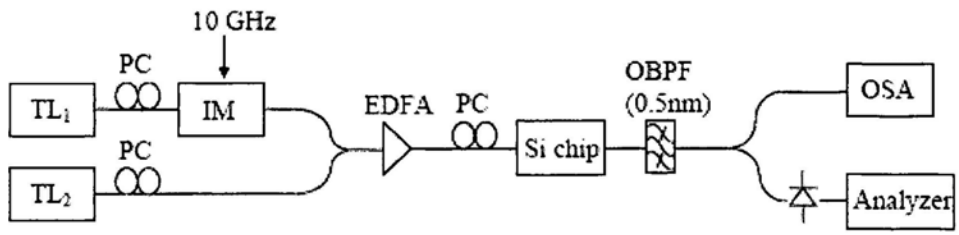

Fig.5.15 Experimental setup. TL: tunable laser; IM: intensity modulator; PC: polarization controller; OBPF: optical band pass filter; OSA: optical spectrum analyzer

The experimental setup is shown in Fig.5.15. A tunable laser at wavelength 1546.84 nm was

sent to an optical intensity modulator. It was then applied by a 10-GHz sine wave RF signals. When DC bias was set to a minimum transmission, DSB carrier suppressed optical modulation can be achieved. Hence pump 1 and pump 2 were generated with the frequency separation of 20 GHz. Another tunable laser at wavelength 1548.25 nm as idler together with the pumps were amplified to 18 dBm before coupling into to waveguide.

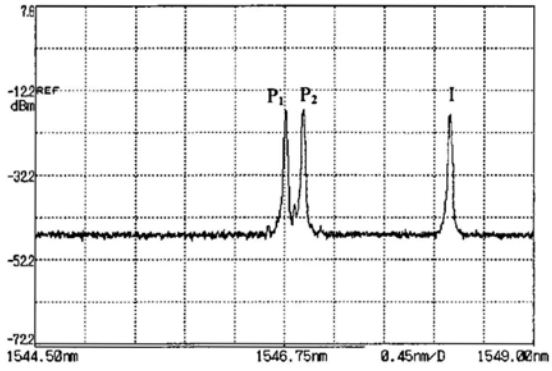

Fig.5.16 Spectrum before the waveguide

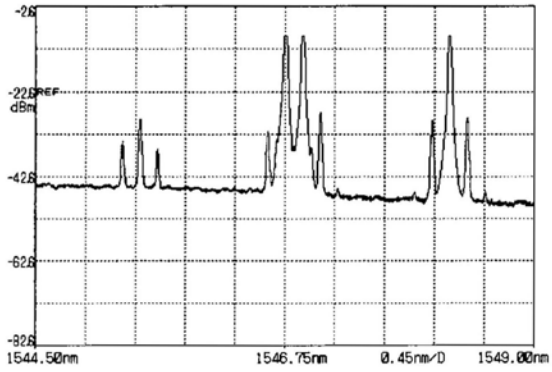

Fig.5.17 Spectrum after the waveguide

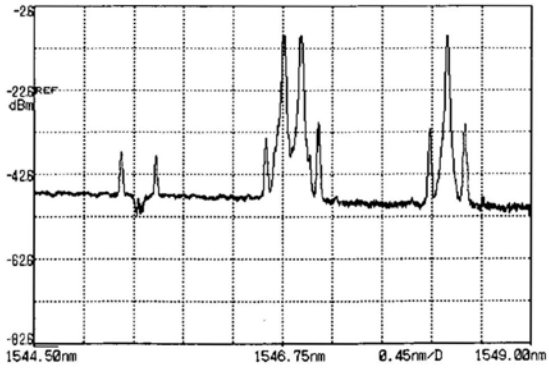

Fig.5.18 Spectrum after the filter

The optical spectra with 0.01-nm resolution before and after the silicon waveguide are shown in Fig.5.16 and Fig.5.17. After the FWM in the waveguide, the DSB with 40-GHz spacing were generated both for first order and second order FWM. For a proof-of-principle demonstration, we used a FBG as filter instead using microring because lack of coupling stage. After the filter, the optical carrier was 11 dB lower than the sidebands shown in Fig.5.18. Finally a 0.5-nm (3-dB bandwidth) filter was used to block the other components. A mm-wave signal that has four times the frequency of the microwave drive signal was generated by beating the two optical sidebands at a photodetector, which could be located at the remote antenna site in the ROF system. Fig.5.19 shows the RF spectrum of the 40-GHz optical mm-wave signal measured by a 40-GHz PIN photo-detector and HP8564E spectrum analyzer (with resolution bandwidth of 300 kHz). In Fig.5.19, the frequency harmonic components (10, 20 and 30 GHz) also appear in the trace while the 40-GHz harmonic component is about 14 to 20 dB higher than the other frequency components.

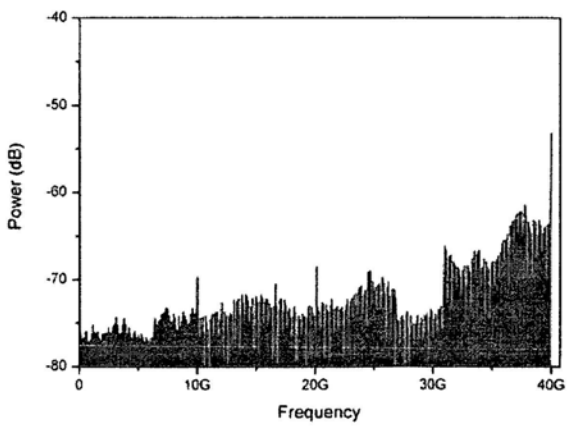

Fig.5.19 RF spectrum of generated signal

We compared the conversion efficiency between first order FWM and second order FWM as shown in Fig.5.20. As the idler was tuned to longer wavelength (25-nm range limited by EDFA bandwidth), the first order FWM has a constant conversion efficiency around -18 dB while the second order FWM had a constant conversion efficiency around -4.5 dB. Since the Q factor and extinction ratio of microring have to be balanced, it is not practical to have high Q (> 6000) and high extinction ratio (> 40 dB) to filter the optical carrier of the first order FWM shown in Fig.5.17. However, the sideband peak power of the second order FWM was only 5 dB lower than that of the first order; it can reduce the stringent requirement for microring filter by 20 dB.

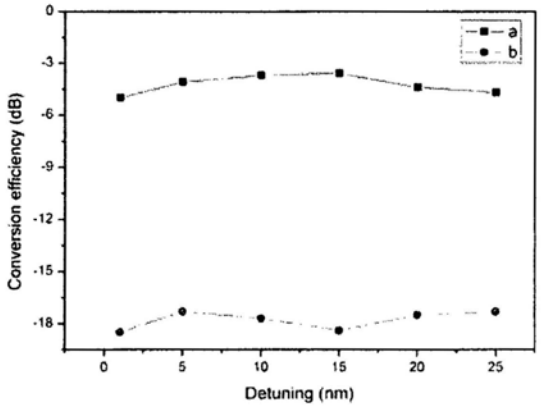

Fig.5.20 Conversion efficiency of first order and second order FWM

We experimentally demonstrated mm-wave generation in a silicon integrated chip using FWM. By filtering the optical carrier of second order FWM, two coherent sidebands beating at photodetector generates 40-GHz RF tone. The dual-pump scheme shows a large bandwidth tuning range. The second order FWM is a good trade-off for mm-wave generation in silicon integrated devices. We analyze the conversion efficiency and bandwidth and show the second

order FWM is suitable for mm-wave generation in silicon integrated devices. The efficiency was significantly limited by the free-carrier absorption effect.

5.4 Long Reach PON with Local Exchange

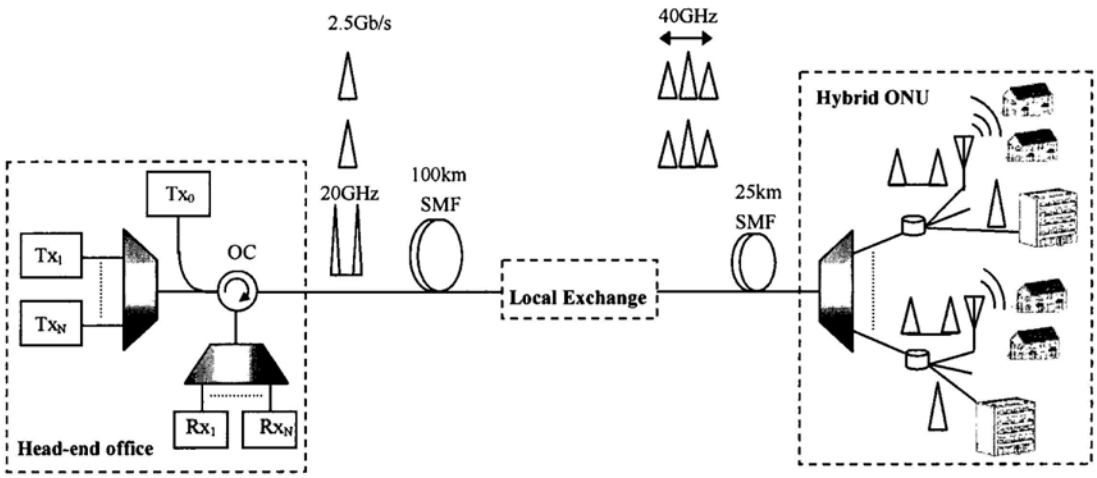

Fig.5.21 Conceptual diagram of the proposed hybrid PONs. Tx: transmitter, OC: optical circulator, SMF: single mode fiber, ONU: optical network unit

Fig.5.21 shows the conceptual diagram of the proposed long reach, high split-ratio wired and wireless hybrid PONs, supporting multicasting 2.5-Gb/s baseband signals and delivering 20 -GHz carrier independently at different wavelengths from the head-end office. They are then mixed at the local exchange (LE) to generate the upconverted signal (optical mm-wave signal) and amplified to compensate the fiber loss. After the LE, two sidebands with 40 GHz spacing are generated which both carry the 2.5-Gb/s data. At ONU, center carrier is filtered for wired

service detection while the remained double sidebands are for wireless service detection. Since a single LE can serve multiple users, the cost can be shared by the users.

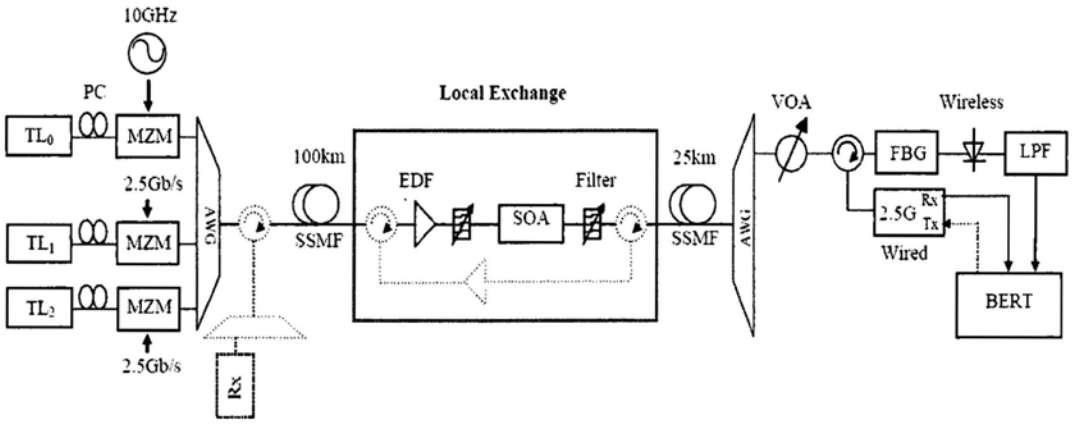

Fig.5.22 Experimental setup of wired and wireless long reach PON. TL: tuneable laser, MZM: Mach-Zehnder modulator, AWG: arrayed waveguide grating, SMF: single mode fiber, Rx: receiver, Tx: transmitter, PC: polarization controller, EDFA: erbium doped fiber amplifier, FBG: fiber bragg grating, SOA: semiconductor optical amplifier, VOA: variable optical attenuator, LPF: low pass filter, BERT: bit-error-rate tester

Fig.5.22 shows the proof-of-concept experiment setup for the long reach wired/wireless hybrid PON employing a remote LE for optical upconversion. At the head-end office, two baseband signals were generated by externally modulated tunable laser 1 (TL_1) at 1546.5 nm and tunable laser 2 (TL_2) at 1548 nm using Mach-Zehnder modulator (MZM) driven with 2.5 Gb/s, pattern length of 2^{31}-1 PRBS. 20-GHz optical carrier was generated by externally modulated tunable laser 0 (TL_0) at 1545.1 nm using MZM driven with 10 GHz sinusoidal

clock. When the dc bias is set to a minimum transmission, OCS or DSB carrier optical modulation can be achieved, and the output of the MZM has the first-order sidebands, and in principle, without the carrier frequency. The frequency separation between the two sidebands is equal to two times the modulating signal frequency. Hence this produces frequency doubling [27]. After that, the three light waves were combined using an AWG and launched into a reel of 100-km SMF. After transmission, three light waves were fed into a LE for remote multi-wavelength upconversion. The LE consists of two optical circulators (OCs), two optical filters, two inline EDFAs for bidirectional power amplification, and a SOA. The three light waves were amplified by an EDFA and then a filter (with 3-dB bandwidth of 8 nm) suppressed ASE noise. The total average optical power launched into the SOA was 3.5 dBm. The SOA (Kamilian) was biased at maximum 250 mA in order to achieve high nonlinear effect.

The 20 GHz clock acted as dual-pump while baseband signals acted as idlers. Sidebands were generated with 20-GHz separation to center carrier after FWM. Then the signal at 1546.5 nm selected by another optical filter (3-dB bandwidth of 0.5 nm) was sent to a reel of 25-km SMF with 10-dBm input power. After transmission, the light was routed to the output port of an AWG depend on its wavelength. A 27-dB attenuation was added using variable optical attenuator to simulate 512 split. A FBG (3-dB bandwidth of 0.1 nm, extinction ratio of 20 dB) transmitted the sidebands for wireless application while reflected the center carrier for wired application. For wireless users, the two sidebands carried with 2.5-Gb/s data beating at photodetector will generate 40-GHz mm-wave. It might be pre-amplified by an electrical

amplifier (EA) to boost the signal before sending to antenna for wireless broadband transmission. For wired users, the reflected center carrier will be directly detected.

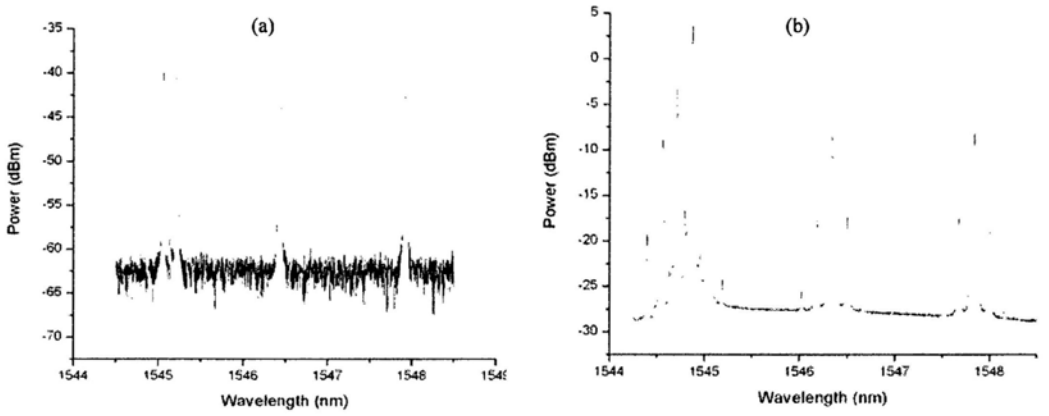

Fig.5.23 Optical spectrum (a) before and (b) after SOA

Fig.5.23(a) shows the optical spectra of the 20-GHz double sideband dual-pump and two 2.5 -Gb/s idlers with center frequency 1.5-nm separation after 100-km transmission. Fig.5.23(b) shows the optical spectra after FWM in SOA at the LE. The baseband signals both generated double sidebands. The separation between one sideband and center carrier is 20 GHz which is equal to the dual-pump separation. Since FWM is data rate independent and capable of performing multi-wavelength generation, the scheme has potential to operate at higher data rate and multiple wavelengths. The FWM conversion efficiency was also investigated as show in Fig.5.24. The idler wavelength was detuned from the center wavelength of dual-pump while the dual-pump was fixed. Inset of Fig. 5.24 shows the conversion efficiency. There is a small fluctuation within 1 dB over 15 nm detuning range. However, for the practical implementation of multi-channel FWM in SOA, the cross talk needs to be

considered. The number of channel depend on the SOA gain bandwidth, channel spacing, signal power and data rate, et al.

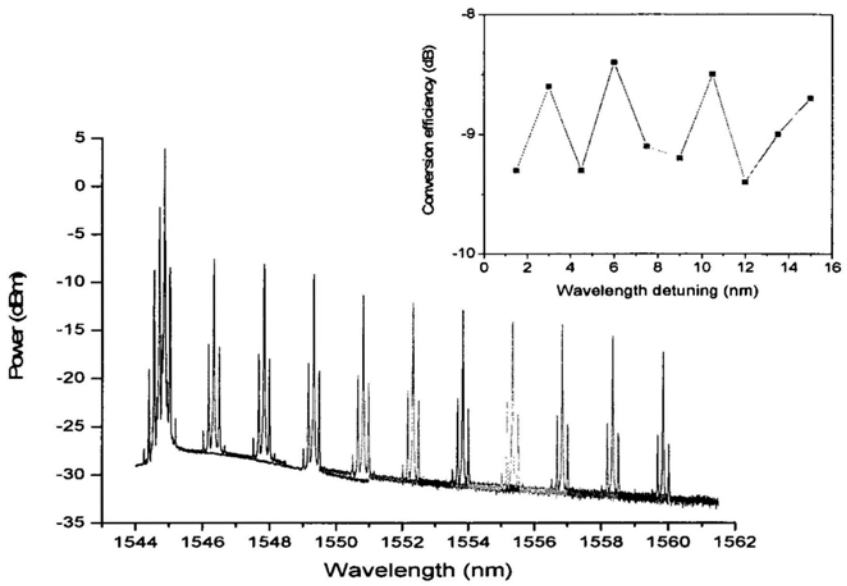

Fig.5.24 FWM conversion efficiency

Since the optical mm-wave was transmitted all-optically from head-end office to remote LE without carrying any data, there is only negligible phase-decorrelation induced amplitude fluctuation after 125-km transmission [28] due to chromatic dispersion. This is mainly induced by the differential propagation delay of the two 40-GHz spaced sidebands [29]. Fig.5.25 shows the transmitted sidebands and reflected center carrier by FBG.

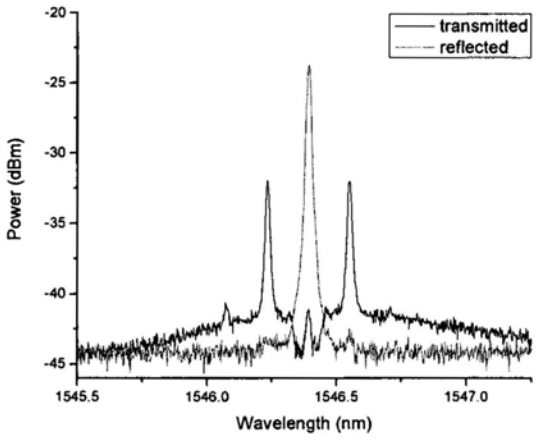

Fig.5.25 Optical spectrum of transmitted and reflected light by FBG

Fig.5.26(a) shows the RF spectrum of 40 GHz carrier generated using two sidebands beating at the photodetector measured with RF spectrum analyzer (HP8168). Its resolution bandwidth was 100 kHz. The carrier to noise ratio of 30 dB was observed in the measurement. The phase noise was also measured to analyze the performance of the measured 40-GHz carrier, as shown in Fig.5.26(b). The purple line indicates the phase noise of 40-GHz signal generated at the source RF signal generator used in the experiment setup. The red line shows the phase noise of a 40 GHz carrier obtained using proposed method. As shown in Fig.5.26(b), the phase noise of 40 GHz carrier from the proposed scheme was ~12 dB higher than that of RF signal generator at the frequency offset of 10 kHz.

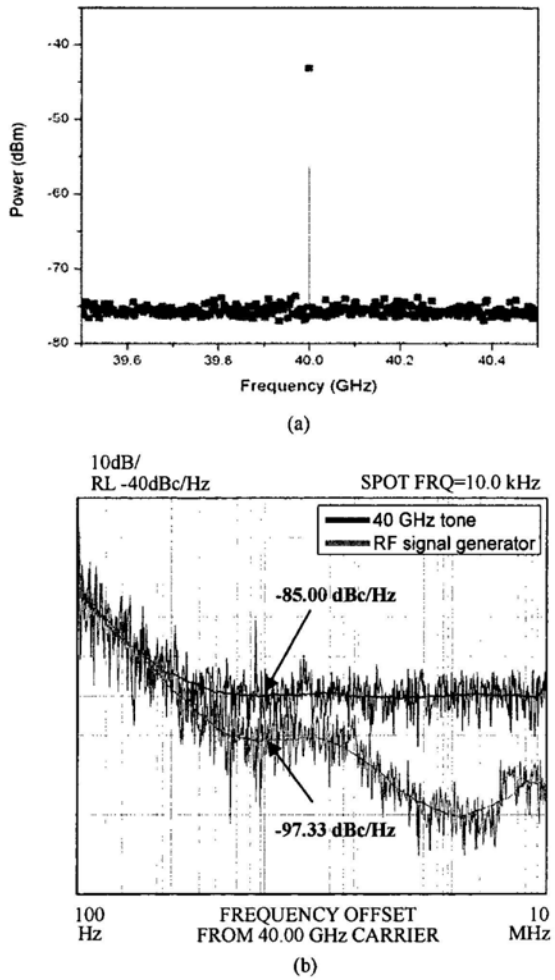

Fig.5.26. 40-GHz (a) RF spectrum and (b) phase noise

The measured eyediagrams after passing a bandwidth of 7.73 GHz low pass filter is shown in Fig.5.27. The high frequency components were blocked and the baseband signal was detected.

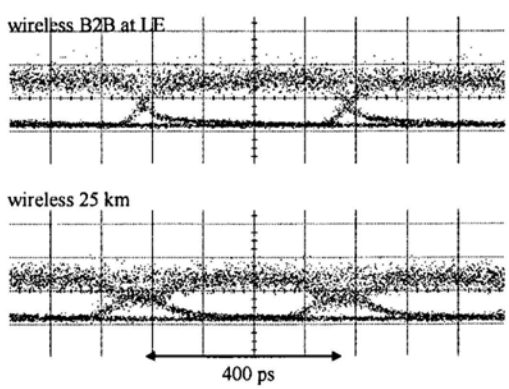

Fig.5.27. Eyediagrams of 2.5-Gb/s signal on 40-GHz carrier measured after a low pass filter. Top: back-to-back case Bottom: after 25-km transmission case

Due to the lack of a 40-GHz RF mixer and RF filter at the laboratory, numerical analysis (using VPI TransmissionMaker V7.5) was performed to evaluate the wireless signal. Fig.5.28 shows the simulated RF spectrum of the optical mm-wave detected after the FBG (Fig.5.22). We can observe that the dominant signal is the 2.5-Gb/s data at the frequency of 40 GHz. An electrical bandpass filter, or a RF antenna with suitable passband, can be used to extract this signal for wireless applications. In the simulation, the wireless signal was extracted by a Bessel bandpass filter (center frequency at 40 GHz and 3-dB bandwidth of 5 GHz) and then RF down-converted to the baseband by using 40 GHz RF sinusoidal signal and RF mixer followed by a Bessel lowpass filter of 2.5 GHz. Inset of Fig. 9 shows the simulated 40-GHz down-converted 2.5-Gb/s eye-diagram with clear eye opening.

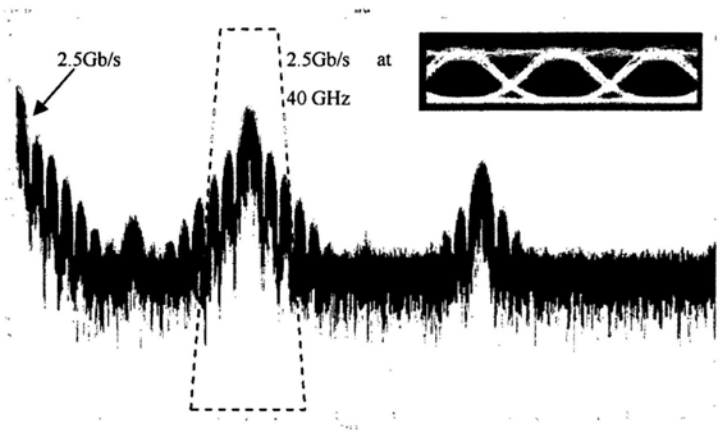

Fig.5.28. RF spectrum of simulation 2.5 Gb/s signal on 40 GHz carrier and respect eyediagram

We can also observe from Fig.5.28 that a baseband 2.5-Gb/s data also appeared due to the self-beating of each sideband of the OCS signal. A Bessel low pass filter was used to detect this signal. Fig.5.29(a) and (b) show the simulated eye-diagrams of the 2.5-Gb/s signals at back-to-back and after the 25-km SMF transmission. We can see that there is a good match in eye-shape with the experimental signals shown in Fig.5.27. We can observe that the 25 km fiber chromatic dispersion causes the reduction in eye-wide, which can be also observed in Fig.5.29(a) and (b). Finally, we also numerical studied the case in which the proposed scheme of optical upconversion at the LE was not deployed, and an optical mm-wave signal (2.5-Gb/s NRZ data carried by optical OCS signal with sideband separation of 40 GHz) was propagating in 125-km SMF. Fig.5.29(c) shows the optical mm-wave signal after 125 km SSMF and the signal can hardly be detected. Resutls show that the proposed scheme can significantly mitigate the fiber chromatic dispersion distorted introduced to the ROF signal.

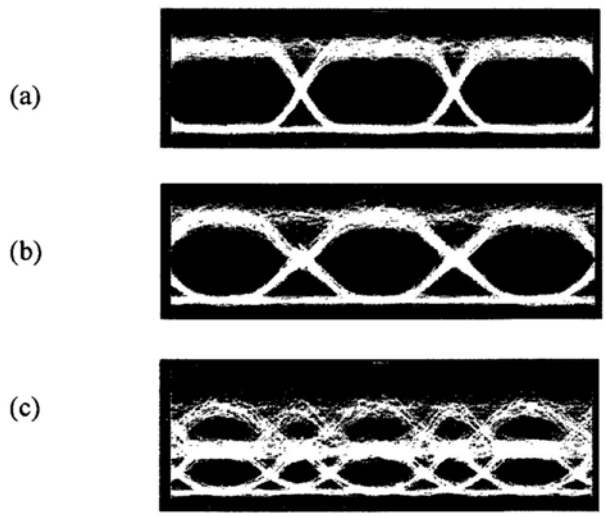

Fig.5.29 Simulated eyediagrams for 2.5-Gb/s signal on 40-GHz carrier (a) back-to back, (b) after 25-km transmission, and (c) after 125-km transmission

Fig.5.30 shows the BER performance and corresponding eyediagrams for wired services. The receiver sensitivity and power penalty without pre-amplification are -17.5 dBm and 2.3 dB at 10^{-9} BER, respectively. The back to back case in the proposed scheme is at head-end office. Moreover, it is scalable to multiple channels at the same cost of one SOA at LE which will have cost advantage on the use of numerous hybrids ONUs.

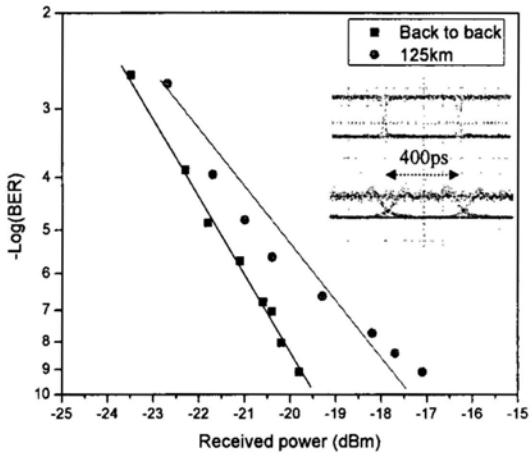

Fig.5.30. Experimental BER and eyediagrams for wired signal

We proposed and experimentally demonstrated a cost efficient hybrid gigabit wired and wireless long-reach and high split-ratio access network based on remote upconversion at the LE. The scheme can deliver 40-GHz mm-wave wireless services supporting wavelength multicast over 125-km SMF. SOA was used as the multi-wavelength broadband optical upconverter and optical power amplifier inside the LE, and a attenuation of 27 dB at remote node shows that a high split-ratio of 512 can be achieved. Wavelength multicast can also be achieved with conversion efficiency variation of within 1 dB over 15 nm wavelength range. The SOA at the LE may support multi-wavelength operation based on FWM for signal upconversion. By optimizing the relative time delay of the multi-channel signal [30], error free multichannel FWM wavelength conversion is possible in the SOA . The experimental

results show that the optical mm-wave signal distortion due to fiber chromatic dispersion can be significantly mitigated by using the proposed scheme.

5.5 Long Reach PON with Hybrid Subcarrier Modulation (SCM)

The hybrid subcarrier modulation (H-SCM) was used for wired/wireless transmission [31], but the dispersion tolerance of the RoF signal has not been studied. In [32], the double sidebands modulation scheme allowed only a low data rate because of dispersion. We propose and demonstrate a cost effective scheme for hybrid wired/wireless access networks based on SCM technique. We generate two sidebands by double sideband with optical carrier suppression and modulate one subcarrier at the head-end station. By beating the two coherent sidebands at a photodetector in the RAU, a 40-GHz mm-wave that carries the 10-Gb/s data is generated for wireless transmission. For the wired connections in PON, the downstream baseband data is obtained by filtering the modulated sideband. The upstream data transmission can use the unmodulated optical sideband. The proposed technique thus supports both a colorless ONU in a PON and a RAU for a hybrid optical wired/wireless network. Analysis using VPI TransmissionMakerV7.1 was performed to confirm the experimental results.

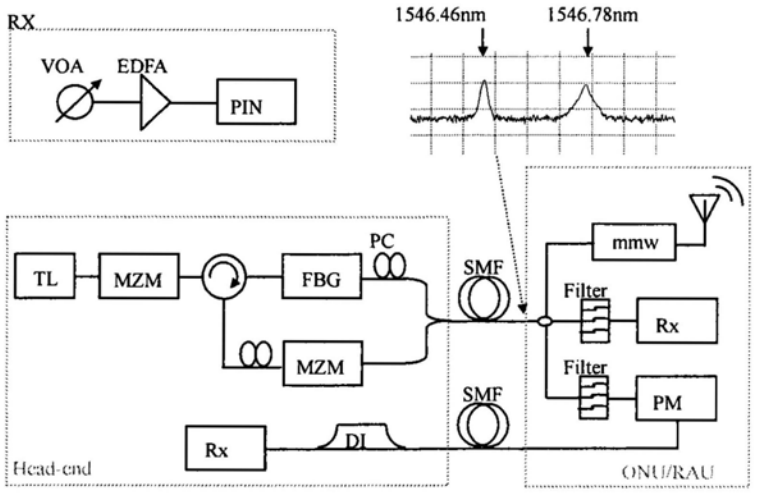

Fig.5.31 Experimental setup of hybrid subcarrier modulation. TL = tunable laser; MZM = Mach Zehnder Modulator; FBG = Fiber Bragg Grating filter; SMF=single mode fiber; MMW= millimeter wave; PM = optical phase modulator; DI= Optical Delay Interferometer

Fig.5.31 shows the experimental setup of the proposed optical wired/wireless network. A CW light at the wavelength of 1546.6 nm generated by a tunable laser (HP 8168F) was launched into a MZM, which was electrical driven at 20-GHz sine wave. By setting the DC bias to minimum transmission of the MZM, the optical carrier was suppressed and two first order sidebands were generated. The frequency separation between the two sidebands was equal to two times the modulation frequency. Hence this produces 40-GHz carrier. A FBG with 3-dB bandwidth of 0.1 nm transmitted one sideband at 1546.46 nm and reflected the other sideband at 1546.78 nm, which was then obtained at the output port of the optical circulator. The reflected sideband was then modulated with 10-Gb/s (2^{31}-1 PRBS) NRZ data via another MZM. After that, the two sidebands were combined through a 3 dB coupler and launched into

a 25 km SMF without dispersion compensation.

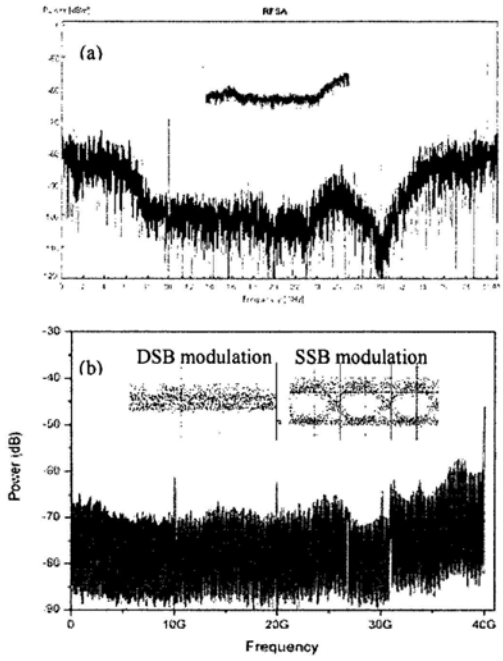

Fig.5.32 (a) simulated and (b) experimental RF spectrum and eyediagrams after 25-km transmission

At the ONU/RAU, part of the signal was tapped out for wireless transmission. The two sidebands beat at the 40-GHz photodetector and generated a 40-GHz mm-wave signal. Numerical analysis using VPI was also performed. Fig.5.32(a) inset shows the simulated RF spectrum when the NRZ data at the head-end station was turned OFF. Only a 40-GHz tone (generated by the coherent beating of the double sideband suppressed carrier signal) is observed. When the NRZ data is turned ON, other RF components around the 40-GHz tone and the 10-GHz, 20-GHz and 30-GHz tones also appear as shown in Fig.5.32 (a). The experimental RF spectrum when the NRZ data is ON is shown in Fig.5.32(b). We can see that

there is a good match between the simulation and the experimental result. Since at the photodetector, we can also observe the self-beating of the 10-Gb/s NRZ signal carried in the RoF signal, a electrical low pass filter with 3-dB bandwidth of 7.5 GHz (Bessel 4^{th} ordered) was connected after the 40-GHz photodetector to obtain the 10-Gb/s NRZ signal. Since only one sideband was modulated (as shown in inset of Fig.5.32(b) inset), the narrow spectrum will have a smaller dispersion than double sideband modulation.

The optical filtered CW sideband was modulated by a PM at the ONU/RAU to produce the 10 -Gb/s, (2^{31}-1 PRBS) DPSK upstream signal. It was then launched towards the head-end Rx. BER and the corresponding eye-diagrams for both downstream NRZ and upstream DPSK were measured as shown in Fig.5.33. Power penalties of downstream and upstream signals after 25-km SMF are 1 and 1.5 dB respectively. We used NRZ for downstream in order to keep the receiver at ONU site simple. DPSK was used for upstream because of its potential improved Rx sensitivity. The DI used for the DPSK demodulation was located at the head-end station. Besides, an AWG can be used between the DI and the Rx, hence, by proper wavelength management, only a single DI can be used to demodulate all the upstream DPSK channels.

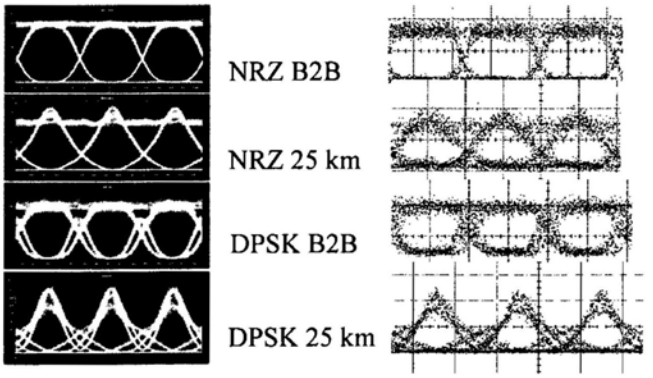

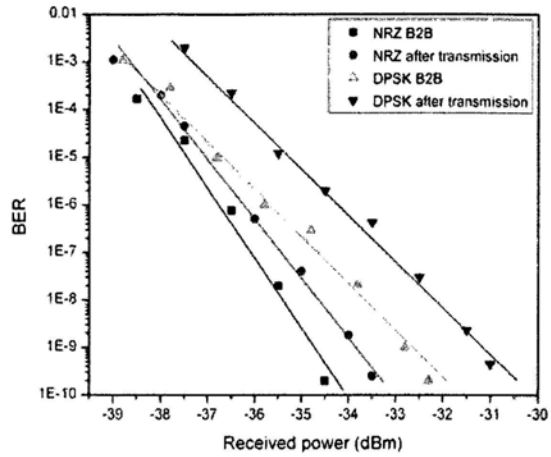

Fig.5.33. Top: Simulated, experimental eyediagrams. Bottom: BER performance for downstream and upstream services versus received optical power.

We successfully demonstrated the generation and transmission of 10-Gb/s wireless signal and 10-Gb/s wireline signal with colorless ONU. Meanwhile, the subcarrier modulation scheme has improved RF fading tolerance. The experiment results and simulation agree quite well. The phase distortion between the two sidebands need to be carefully considered when using AWG or transmitting in long length fiber.

5.6 Mitigation of Signal Distortions using Reference Signal Distribution

As mentioned before, due to a large number of RAUs is required for the mm-wave ROF system, colorless RAU with optical carrier generated and distributed from the HE is employed. This can reduce the inventory cost, since wavelength specific or wavelength tunable light source is not required at the RAU. Centralized wavelength control is used at the

HE. In the experience, reflective semiconductor optical amplifier (RSOA) is used as the colorless modulator inside the RAU. RSOA is generally considered as a potential low-cost and relatively high data rate device. It has low polarization dependent gain. Recently, 10 Gb/s RSOA has been implemented [33]. In the proposed scheme, the upstream data is modulated onto the downstream data by wavelength reuse [34-36]. Transmission comparison with the DSB, OCS and SSB optical mm-wave signals is performed by means of numerical simulations, showing the proposed system with reference signal distribution may mitigate signal fading and code time-shifting.

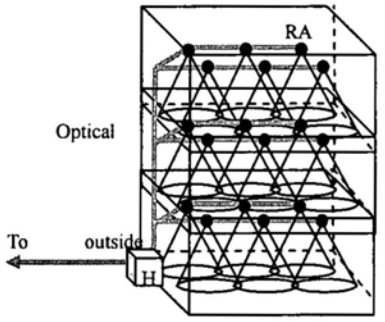

Fig.5.34. Schematic ROF architecture inside a building. HE: head-end, RAU: remote antenna units.

Fig.5.34 shows the schematic of a typical picocellular system inside a building. The fiber infrastructure connects many RAUs to the HE. The RAU merely consists of a simple electronic control circuit and a pair of O/E and E/O converter. For the downstream communication, the electrical data will be first converted to optical signal by the E/O converter at the HE. The optical data will then be transmitted to the RAU, where the O/E module will convert the optical data to electrical data, which will then be emitted by the antenna to the mobile station (MS). For the upstream traffic, the E/O converter at the RAU

will convert the received RF signal from the antenna to optical signal. The signal will be detected by the O/E converter at the HE. In order to further reduce the cost of the RAU, a single antenna with a switch (SW) can be used for both upstream and downstream communications by using the time division duplex (TDD) mode (Fig.5.35).

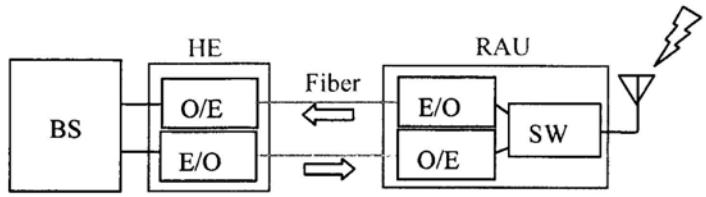

Fig.5.35. Schematic of the ROF system. BS: base station. HE: head-end, RAU: remote antenna unit, SW: electrical switch.

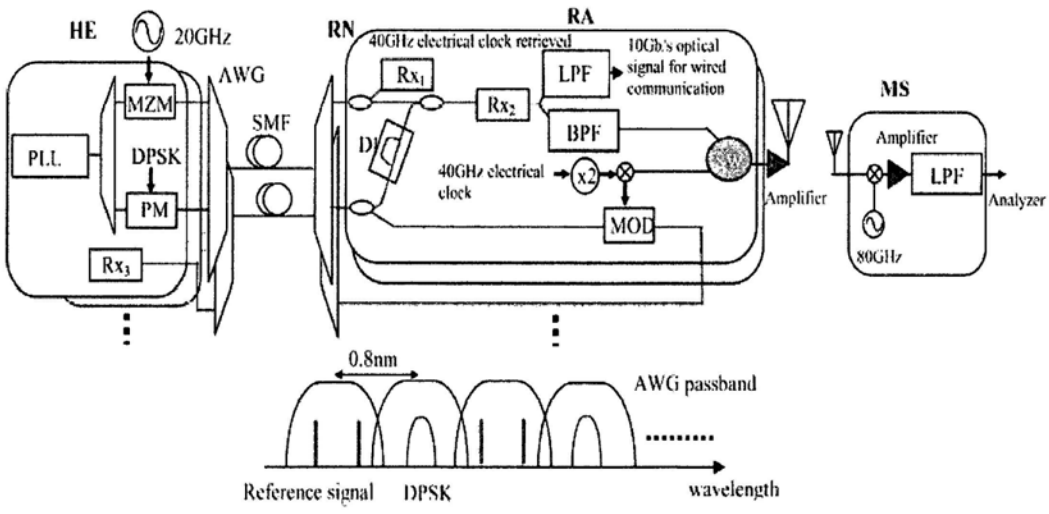

Fig.5.36. Proposed ROF system using reference signal distribution. MZM: Mach-Zehnder modulator, PM: phase modulator, AWG: arrayed waveguide grating, SMF: single mode fiber,

DI: delayed interferometer, Rx: optical pre-amplified receiver, MOD: modulator, MS: mobile station, PLL: phase locked laser. Inset: schematic of optical spectra of optical clock and DPSK signals.

Fig.5.36 shows the proposed architecture of the ROF system using reference signal distribution. For the downstream link, the optical reference signal is generated by modulating the continuous wave (CW) via a MZM at the HE. In order to produce the optical two-tone for optical mm-wave generation, the DC bias of the MZM is set to a minimum transmission and driven by a 20-GHz sinusoidal signal. Hence, double sideband with suppressed carrier optical modulation is achieved, and the first order sidebands with frequency separation equal to twice the modulating signal frequency is observed at the output of the MZM. The downstream data is encoded using DPSK modulation via a PM. The downstream data can be used for both wireless and wired optical communication. It is transmitted at another wavelength, which is 100 GHz away from the wavelength of the reference signal. To improve the coherence of the laser sources, dual-wavelength laser [37] or phase-locked laser (PLL) with mode spacing of 100 GHz can be used. Both the optical reference signal and the downstream signal are wavelength multiplexed by a standard AWG (Gaussian-shaped, 100 GHz channel spacing with 3-dB width of 50 GHz). In this scheme, multiple ROF channels can by supported by using alternative reference and DPSK data channels aligning with the AWG passband as shown in the inset of Fig.5.36.

The downstream data signal and the optical reference signal are then transmitted through a SMF to the remote node (RN), which then distribute the data to different RAUs. The optical

reference and the downstream signals are wavelength de-multiplexed at the RN. The optical reference signal can be power divided via a passive fiber splitter to an optical Rx_1 with BW of 40-GHz at the RAU to retrieve the 40-GHz electrical clock source, which could be used for the upstream data down-conversion from RF to baseband.

At the RAU, a high BW (> 80 GHz) optical Rx_2 is used to obtain the electrical mm-wave signal for the antenna. The electrical mm-wave is produced by beating the optical reference signal and the downstream demodulated DPSK signal inside the optical Rx_2. For the wireless communication, a bandpass filter (BPF) with center frequency at 80 GHz (BW of 20 GHz) is used after the Rx_2 to retrieve the mm-wave signal. A low pass filter (LPF) with 3-dB bandwidth of 10 GHz can be used to retrieve the 10 Gb/s optical data for wired communication. As shown in Fig. 5.36, the downstream DPSK signal is power divided into 2 equal parts. One part is launched into a DI with 100 ps delay for demodulating the 10-Gb/s DPSK signal into intensity modulated signal. The other half of the downstream signal is then launched into an intensity modulator, which is driven by a baseband NRZ upstream data for signal remodulation. The upstream NRZ OOK signal will then be transmitted back to the Rx_3 at the HE. The baseband NRZ data can be obtained by mixing the clock signal (retrieved from the optical reference signal as described before) and the received upstream signal from the antenna. A single antenna with an electrical SW is used for both upstream and downstream communications in TDD mode.

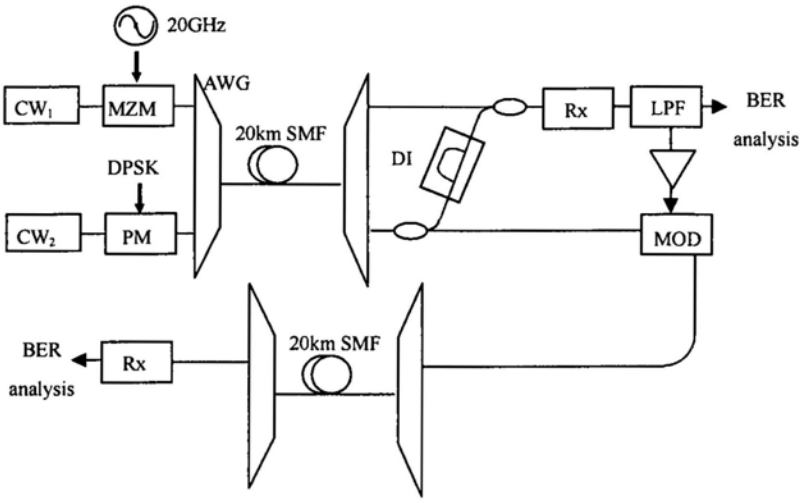

Fig.5.37. Experimental setup of ROF system using a separate optical clock distribution. MZM: Mach-Zehnder modulator, PM: phase modulator, AWG: arrayed waveguide grating, SMF: single mode fiber, DI: delayed interferometer, Rx: optical pre-amplified receiver, MOD: modulator.

Fig.5.37 shows the experimental setup of the ROF system. The downstream DPSK signal was modulated at 10 Gb/s, PRBS, 2^{23}-1 at one wavelength which is 100 GHz away from the wavelength of the optical reference signal. Both the optical reference and the DPSK signals were then transmitted through 20-km SMF without dispersion compensation. At the RAU, a 100 GHz channel spacing, Gaussian shaped AWG was used to wavelength de-multiplexed the optical reference and the DPSK signals. The DPSK signal was power divided by a 3-dB fiber splitter. One part was demodulated by the DI of 100 ps. The demodulated DPSK signal was then combined with the optical reference signal and launched into the optical Rx. An optical Rx with LPF bandwidth of 10 GHz was used to obtain the 10-Gb/s demodulated DPSK data for wired communication. Due to the unavailability of > 80 GHz optical Rx and the 80 GHz electrical BPF, numerical simulation was used for the characterization.

The other part of the un-demodulated DPSK signal was launched into the MOD, which was a MZM used to produce the 10-Gb/s upstream optical OOK data. We also considered the case of asymmetric downstream and upstream transmissions. In this case, the downstream optical signal was then launched into a RSOA, which was driven by a baseband 2.5-Gb/s NRZ upstream data for signal remodulation. The upstream OOK signal was then transmitted back to the Rx at HE.

Fig.5.38 shows the BER measurements of the downstream and upstream signals at back-to-back and after 20-km transmission without dispersion compensation. Fig.5.38(a), (b) and (c) show the experimental eye diagrams of 10-Gb/s downstream demodulated DPSK signal (using the 10-GHz electrical BPF to remove the high frequency components detected by the Rx at RAU), upstream remodulated 10-Gb/s OOK signal and upstream remodulated 2.5-Gb/s OOK signal using RSOA. We observed about 1.7-dB power penalty in the downstream demodulated DPSK signal. As described before, half of the downstream signal was launched into the RSOA for signal remodulation to produce the upstream signal. Due to the constant intensity of the downstream DPSK signal, only a small power penalty of 0.5 dB was observed in the upstream OOK signal after the 20-km transmission. The target 10-Gb/s signal carried by mm-wave at 80 GHz frequency band could be obtained by using a electrical BPF with center frequency of 80 GHz and BW of 20 GHz connected to a high speed optical Rx. Numerical simulation will be described in next Section.

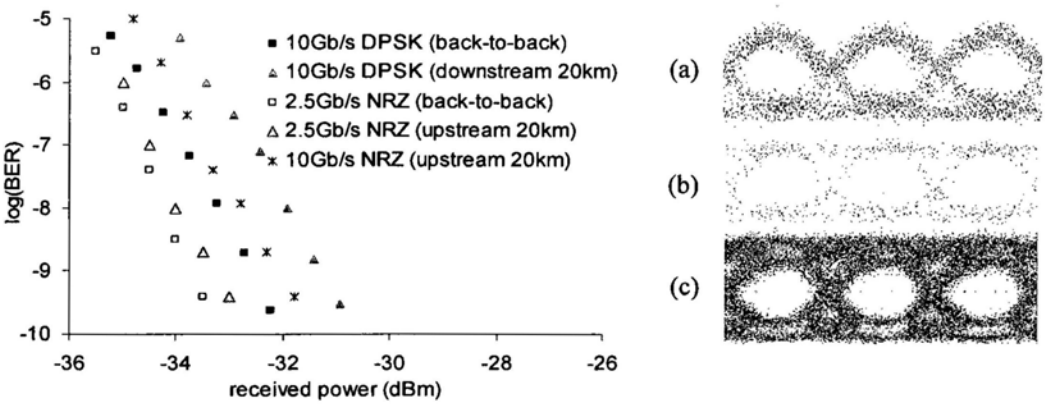

Fig.5.38. BER of the 10-Gb/s downlink DPSK, 10-Gb/s and 2.5-Gb/s NRZ remodulated signals. Experimental eye diagrams: (a) demodulated DPSK signal received at RAU, (b) remodulated 10-Gb/s uplink NRZ signal received at HE and (c) remodulated 2.5-Gb/s uplink NRZ signal received at HE.

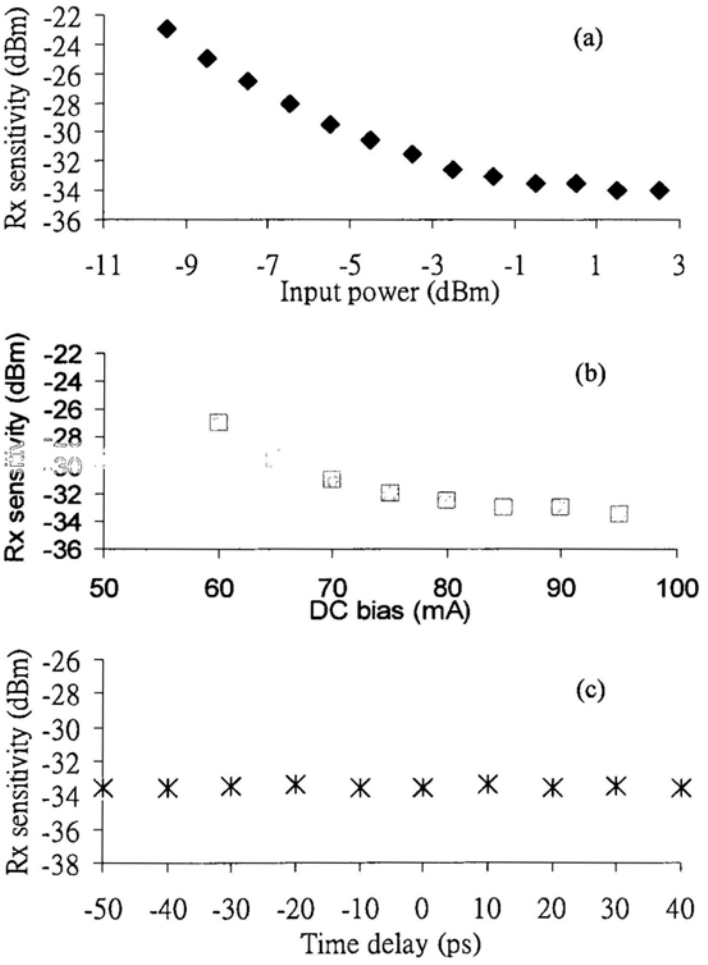

Fig.5.39. Rx sensitivities of the upstream remodulated OOK signal (a) under different injected powers when the RSOA was dc biased at 95 mA, (b) under different dc biases, when the input downstream signal to the RSOA is at ~ 0 dBm, (c) under different delays of the downstream DPSK signals.

We also studied the different operation conditions of the RSOA used at the RAU. Fig.5.39(a) shows the Rx sensitivities of the upstream OOK signal under different launched powers when the RSOA was dc biased at 95 mA. We can observe that the Rx sensitivity is minimum, and starts to saturate at launched power of -2 dBm. Rx sensitivity of -23 dBm was measured when the input power to the RSOA is about -10 dBm. Fig.5.39(b) shows the Rx sensitivities of the upstream OOK signal under different dc biases, when the input downstream signal to the RSOA is at ~ 0 dBm. We can also see that the optimum DC driving current to the RSOA is ≥ 85 mA. It is also worth to mention that synchronization between the downstream and remodulation upstream signals is not required. Fig.5.39(c) shows the measured Rx sensitivities of the upstream OOK signal under different delays of the downstream DPSK signal when the RSOA was dc based at 95 mA and the input optical power was about 0 dBm.

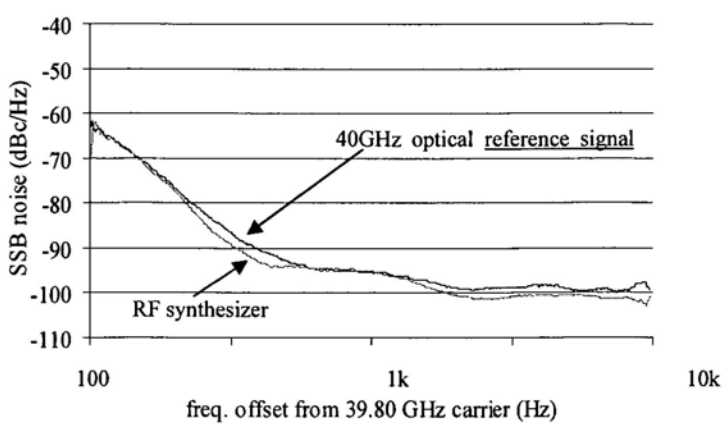

Fig.5.40. Single sideband (SSB) noise spectrum of the RF frequency synthesizer measured at 40 -GHz tone and the 40 GHz optical reference signal.

We also experimentally characterized our 40-GHz optical reference signal (clock signal) by studying the single sideband (SSB) noise spectrum (Fig.5.40). In this measure, the optical Rx was a 40-GHz PIN photodiode connected to a RF spectrum analyzer (HP8564E). The SSB noise spectrum of an electrical 40-GHz signal generated by a RF frequency synthesizer (Agilent E8244A) was also given for comparison. We observed that the SSB noise of the 40 -GHz signal generated by the optical means shows similar performance when compared with the frequency synthesizer. It is about -95 dBc/Hz at the spot frequency of 10-kHz offset.

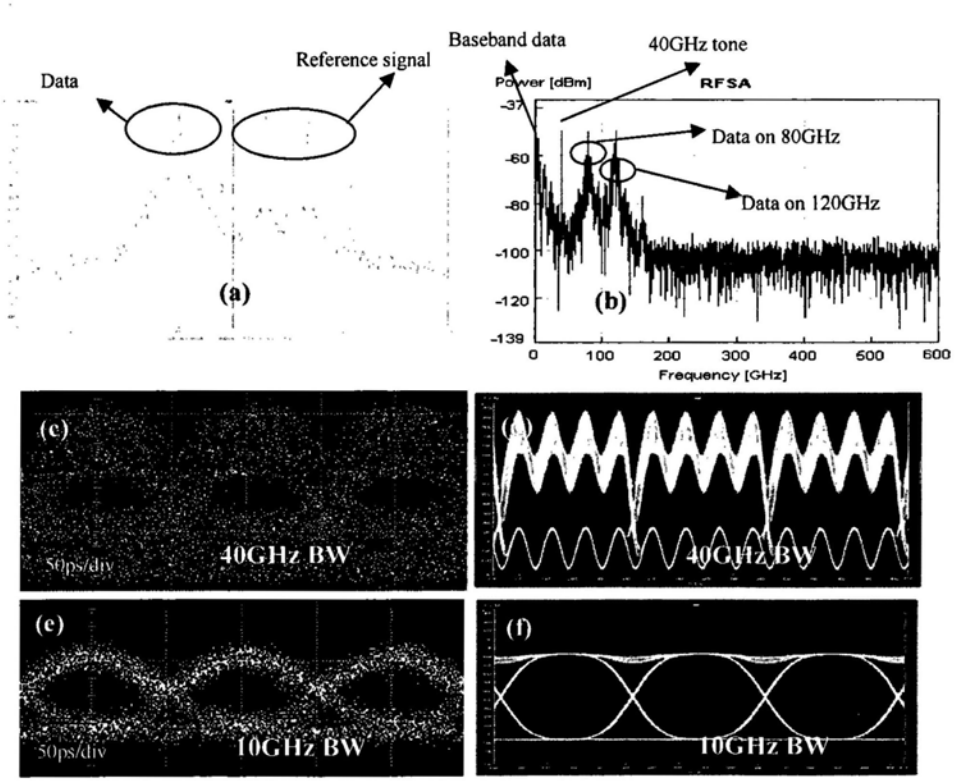

Fig.5.41. (a) Simulated optical spectra of the DPSK and reference signals, (b) simulated RF spectra of different electrical components detected at the downstream Rx inside the RAU. Eye

diagrams: (c) experimental and (d) simulated downlink signal measured by Rx with a 40-GHz LPF; (e) experimental and (f) simulated downlink signal measured by Rx with 10-GHz LPF.

Numerical simulations were performed using VPI Transmission Maker V7.5. For our proposed scheme, we used a dual-wavelength PLL with frequency separation of 100 GHz. The laser linewidth is 10 MHz. 10-Gb/s DPSK signal was encoded at one wavelength. On the other wavelength, the optical reference signal was generated by biasing a MZM at transmission minimum and driven by a 20-GHz sinusoidal signal. Hence, double sideband with suppressed carrier optical modulation was achieved. Both the signals are wavelength multiplexed by an AWG (Gaussian-shaped, 100-GHz channel spacing with 3-dB width of 50 GHz). They were then transmitted through 20-km SMF (dispersion parameter = 17 ps/nm/km). They were wavelength demultiplexed by another AWG. Half power of the DPSK signal was demodulated by the DI of 100 ps. The demodulated DPSK signal was then combined using fiber coupler with the optical reference signal, and launched into the optical Rx. Fig.5.41(a) shows the simulated optical spectra of the data and reference signals and Fig.5.41(b) shows the simulated RF spectra of different electrical components detected at the downstream Rx inside the RAU. In Fig.5.41(b), we can observe the baseband 10-Gb/s data, a 40-GHz tone (generated by the reference signal itself), a 10-Gb/s data on 80-GHz carrier (generated by the coherent beating between the DPSK and the lower sideband of the reference signal), a 10-Gb/s data on 120-GHz carrier (generated by the coherent beating between the DPSK and the upper sideband of the reference signal). Our targets are the baseband 10-Gb/s data (could be obtained by a 10-GHz LPF) and the 10 Gb/s on 80 GHz (could be obtained by a RF BPF with center frequency at 80

GHz and BW of 20 GHz). Due to the unavailability of the 80-GHz optical Rx and the 80-GHz electrical BPF in the laboratory, we used a 40-GHz bandwidth optical Rx in the experiment to confirm the photo-mixing processing. Fig.5.41(c) and (d) show the experimental and simulated eye diagrams of the optical mm-wave signal detected at the RAU (Fig.5.36) by using Rx with an LPF bandwidth of 40 GHz. We observed a good match in eye-shape between them. Since the BER tester and the RF synthesizer were not synchronized, we cannot observe the 40-GHz sinusoidal signal at the top and bottom of the experimental eye in Fig.5.41(c). Then, by inserting an electrical LPF with BW of 10 GHz after the optical Rx, the baseband 10-Gb/s intensity modulated signal can be clearly observed by removing the high frequency components. Fig.5.41(e) and (f) show the experimental and simulated eye diagrams of the baseband 10-Gb/s signal respectively.

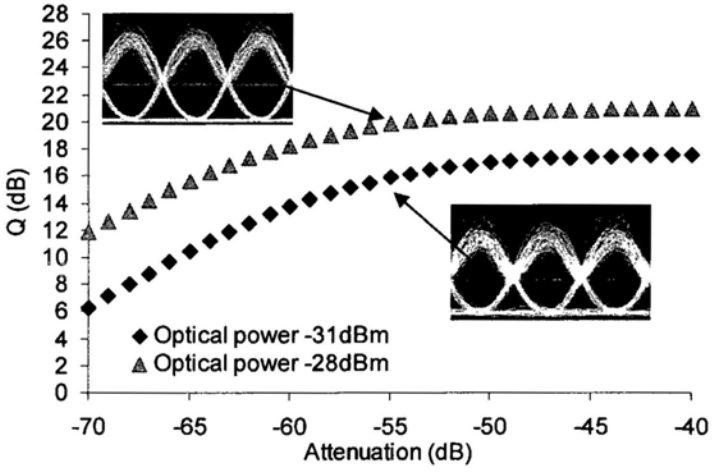

Fig.5.42. Simulated Q (dB) of the down-converted OOK signal at the MS under different attenuations between the RAU and the MS. Insets: simulated eyes of demodulated OOK at MS when attenuation was -55 dB.

Then, simulations were performed for the RF signal (10-Gb/s data on 80-GHz carrier) analysis. Two different optical launched powers to the Rx_2 inside the RAU in Fig.5.36 (-31 dBm and -28 dBm) were studied. -31 dBm launched power was chosen due to the error-free demodulated DPSK condition as shown in Fig.5.38 RF amplifiers (20-dB gain, noise figure 3 dB) were used in the RAU and the MS respectively. Fig.5.42 shows the simulated Q (dB) values of the down-converted OOK signal at the MS under different atmospheric attenuations between the RAU and the MS, showing the atmospheric attenuation can up to 55 dB for the optical input power of -31 dBm to the RAU, in order to achieve error-free down-converted signal at the MS.

5.6.1 Comparison with DSB, OCS and SSB Schemes

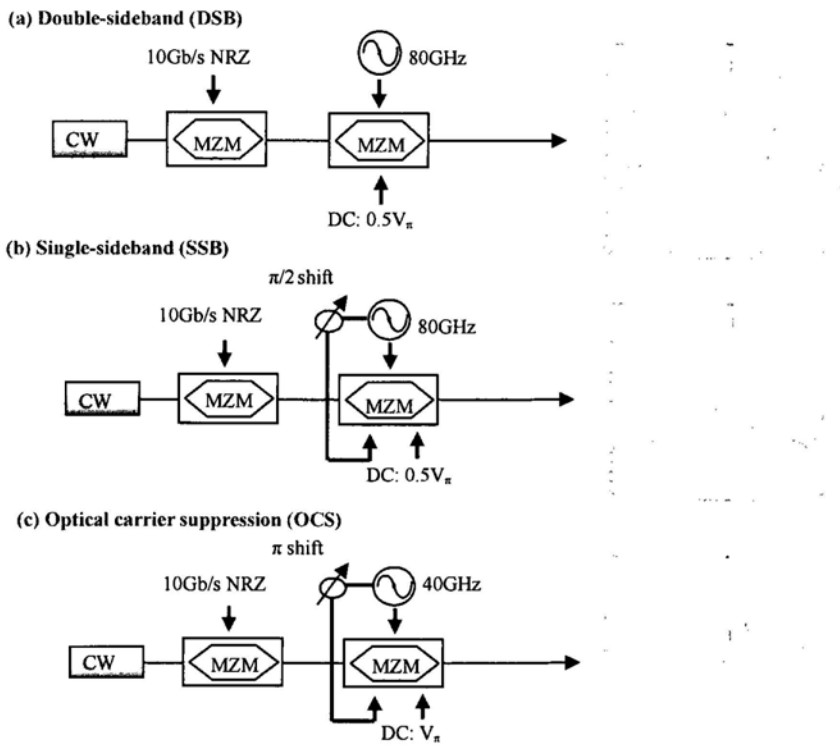

Fig.5.43. Up-conversion setups of the DSB, SSB, OCS [38].

In this section, we compared the proposed scheme with the DSB, OCS and SSB optical mm-wave schemes by using VPI Transmission Maker V7.5. To simplify the comparison, 10 -Gb/s NRZ baseband data modulated on 80-GHz carrier was used in all cases. The simulation parameters of the proposed scheme were described in Section IV. Since the performances of the optical mm-wave signals depend on the optical generation methods, we arbitrary divided the generation methods into two categories. Fig.5.43 shows the first category of optical mm-wave generation using DSB, SSB and OCS as described in ref. [38], with the corresponding simulated output optical spectra (resolution 0.01 nm). Baseband data signal was generated by the first MZM driven by a 10-Gb/s electrical NRZ signal. For the DSB modulation scheme, the second MZM was biased at 0.5 V_{π}, and the frequency of the driving RF signal was 80 GHz. A dual-arm MZM was used to achieve the SSB modulation, as shown in Fig.5.43(b). The two electrical RF signals to drive the dual-arm MZM had a $\pi/2$ phase shift, and was dc biased at 0.5 V_{π}. When the phase difference of the two electrical RF signals to drive the dual-arm MZM was π, and the dc bias was at V_{π}, OCS modulation is achieved, as shown in Fig.5.43(c). All the signals were detected by using optical Rx with Bessel third order BPF at center frequency of 80 GHz and BW of 20 GHz.

As shown in Fig.5.43(a), for the DSB optical mm-wave, the electrical current in the Rx is generated by three lightwaves at ω_c-ω_m, ω_c, ω_c+ω_m, where the ω_c and ω_m are the frequencies of the optical carrier and the modulation respectively. Hence, it suffers from both fading and the code time-shifting (Fig.5.44(a)). In this category of generation methods, we can observe form Fig.5.43 that the optical spectra of the SSB and OCS are similar. There are two dominant tones

in each signal (ω_c-ω_m and ω_c, in the SSB modulation; and ω_c-$\omega_m/2$ and ω_c+$\omega_m/2$ in the OCS modulation). The transmission distance of the SSB and OCS are limited due to the code time-shifting by the two dominant tones, as shown in Fig.5.44(b) and (c). For the proposed approach as shown in Fig.5.44(d), we can observe that the envelope of the signal can maintain the shape.

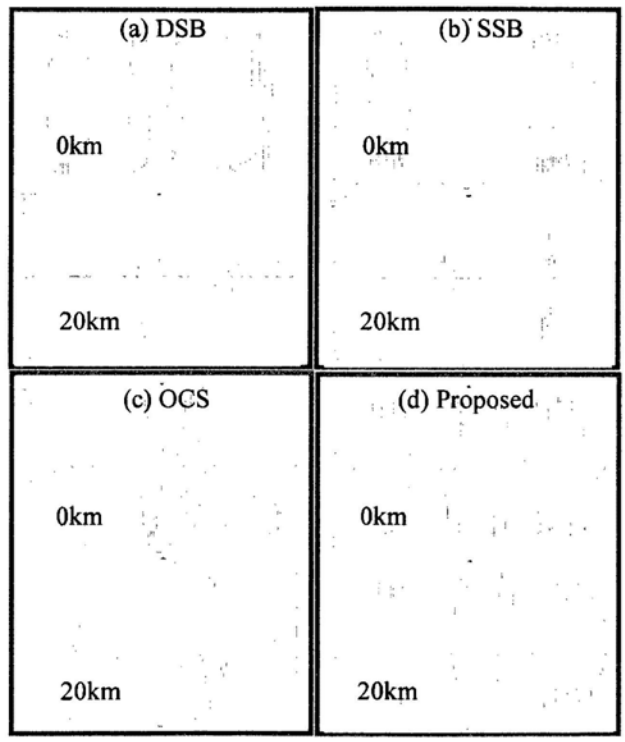

Fig.5.44. Simulated time traces (first category) of 10-Gb/s NRZ mm-wave signal modulated by 80 GHz carrier using (a) DSB, (b) SSB, (c) OCS and (d) the proposed scheme. They are detected at back-to-back, after propagating of 20-km SMF.

Then, we studied the second category of mm-wave generation, as shown in Fig.5.45. The DSB signal was generated via an MZM which was driven by an electrical mixed signal of the baseband 10-Gb/s NRZ and the 80-GHz clock, as shown in Fig.5.45(a). The SSB signal was generated by using an offset OBF (Gaussian shaped, 20-GHz 3-dB bandwidth, offset by 120 GHz) to suppress one sideband (> 20 dB) of the optical DSB signal, as shown in Fig.5.45(b). Fig.5.46 shows the simulated time traces of the optical mm-wave signal generated in the second category using RF mixer. We can observe that the DSB signal (Fig.5.46(a)) also suffers from both fading and the code time-shifting. However, the SSB signal generated by using a RF mixer and an offset OBF (Fig.5.46(b)) performs much better than that in the first category (using cascaded MZMs) (Fig.5.43(b)). And the SSB generated using an RF mixer and offset OBF performs as well as the proposed scheme. By studying the optical spectrum of the SSB signal generated in the second category, we can observe that the center wavelength is mainly dc component (Fig.5.45(b)). It is different from the case of SSB generated by using cascaded MZMs (Fig.5.43(b)), which hence suffers form code time-shifting.

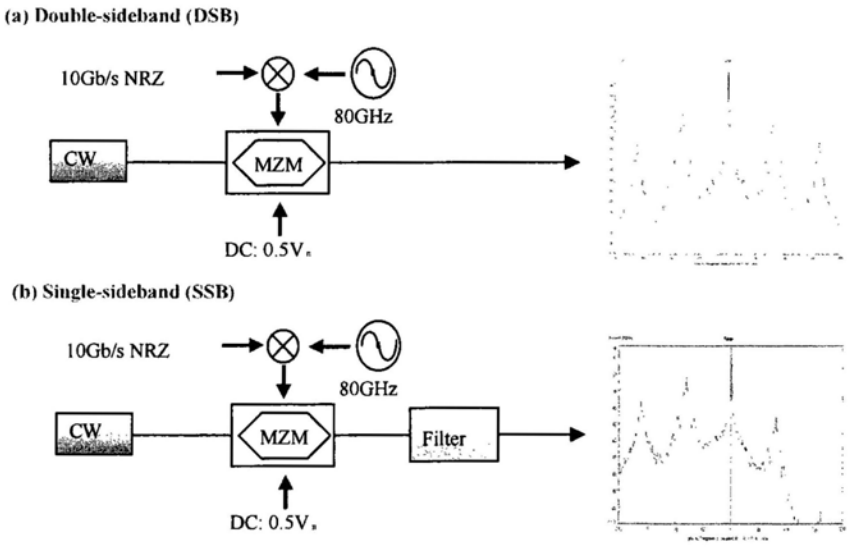

Fig.5.45. Up-conversions of the DSB and SSB using RF mixer.

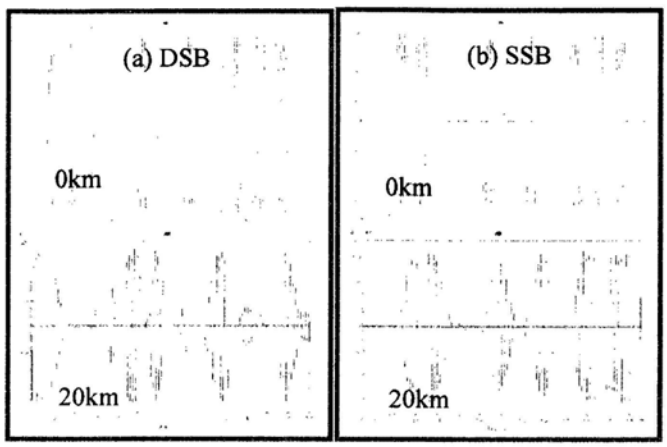

Fig.5.46. Simulated time traces (second category) of 10-Gb/s NRZ mm-wave signal modulated by 80-GHz carrier using (a) DSB, (b) SSB. They are detected at back-to-back, after propagating of 20-km SMF.

Colorless RAU with optical carrier generated and distributed from the HE is an attractive network architecture. We proposed and demonstrated a novel bidirectional ROF system using a reference signal distribution to mitigate signal fading and code time-shifting. Experimental characterization of the RSOA based remodulation unit and the 40 GHz optical reference signal is also performed. A signal remodulation scheme using downstream DPSK and upstream OOK was demonstrated in a 20-km reach ROF system. Numerical simulations were performed to compare the proposed scheme with DSB, OCS and SSB. Simulation results show that the SSB generated using an RF mixer and offset OBF performs as well as the proposed scheme. The proposed scheme requires dual-wavelength laser or other phase-locked laser, and this may

increase the complexity and the cost of the system. We believe that the proposed scheme using separate data and reference signals could be an alternative to mitigate fiber chromatic dispersion, particularly when the mm-wave frequency is becoming higher and higher, and the cost of the high frequency RF mixer will be much higher than the cost of the phase-locked laser.

REFERENCES

[1] Zhensheng Jia Jianjun Yu, G. Ellinas, Gee-Kung Chang, "Key enabling technologies for optical-wireless networks: Optical millimeter-wave generation wavelength reuse, and architecture", J Lightwave Technol., Vol. 25, No. 11, pp. 3452-3471, 2007

[2] J. J. Vegas Olmos, T. Kuri, and K.-I. Kitayama, "Dynamic reconfigurable WDM 60 GHz millimeter-wave-band radio-over-fiber access network: Architectural considerations and experiment," J. Lightw. Technol., vol. 25, no. 11, pp. 3374 3380, Nov. 2007.

[3] M. Huchard, M. Weiss, A. Pizzinat, S. Meyer, P. Guignard, and B. Charbonnier, "Ultra-broadband wireless home network based on 60-GHz WPAN cells interconnected via RoF," J. Lightw. Technol., vol. 26, no. 15, pp. 2364 2372, Aug. 2008.

[4] J. Kim, Y.-D. Chung, K.-S. Choi, D.-S. Shin, J.-S. Sim, and H.-K. Yu, "60-GHz system-on-packaging transmitter for radio-over-fiber applications," J. Lightw. Technol., vol. 26, no. 15, pp. 2379 2387, Aug. 2008.

[5] M.Weiß, M. Huchard, A. Stöhr, B. Charbonnier, S. Fedderwitz, and D. S. Jäger, "60-GHz photonic millimeter-wave link for short- to mediumrange wireless transmission up to 12.5 Gb/s," J. Lightw. Technol., vol. 26, no. 15, pp. 2424 2429, Aug. 2008.

[6] J. J. V. Olmos, T. Kuri, and K.-I. Kitayama, "Dynamic reconfigurable WDM 60 GHz millimeter-wave-band radio-over-fiber access network: architectural considerations and experiment," J. Lightw. Technol., vol. 25, no. 11, pp. 3374 3380, Nov. 2007.

[7] J. J. V. Olmos, T. Kuri, T. Sono, K. Tamura, H. Toda, and K.-I. Kitayama, "Reconfigurable 2.5-Gb/s baseband and 60-GHz (155-Mb/s) millimeter-waveband radio-over-fiber (interleaving) access network," J. Lightw. Technol., vol. 26, no. 15, pp. 2506 2512, Aug.

2008.

[8] A. Hirata, H. Takahashi, R. Yamaguchi, T. Kosugi, K. Murata, T. Nagatsuma, N. Kukutsu, and Y. Kado, "Transmission characteristics of 120-GHz-band wireless link using radio-on-fiber technologies," J. Lightw. Technol., vol. 26, no. 15, pp. 2338 2344, Aug. 2008.

[9] G. Qi, J. Yao, J. Seregelyi, S. Paquet, and C. Bélisle, "Optical generation and distribution of continuously tunable millimeter-wave signals using an optical phase modulator," J. Lightw. Technol., vol. 23, no. 9, pp. 2687-2695, Sep. 2005.

[10] J. Yu, Z. Jia, L. Xu, L. Chen, T. Wang, and G. K. Chang, "DWDM optical millimeter-wave generation for radio-over-fiber using an optical phase modulator and an optical interleaver," IEEE Photon. Technol. Lett., vol.18, no.13, pp. 1734-1736, Jul. 2006.

[11]L. Xu, C. Li, C. Y. Wong, and H. K. Tsang, "Optical differential phase shift keying demodulation using a silicon microring resonator", IEEE Photon Technol Lett., vol. 21, no. 5, pp. 295-297, 2009

[12]L. Xu, C. Li, C. W. Chow, and H. K. Tsang, "Optical mm-wave signal generation by frequency quadrupling using an optical modulator and a silicon microresonator filter", IEEE Photon Technol Lett., vol. 21 no. 4, pp. 209-211, 2009

[13] D. Taillaert, P. Bienstman, and R. Baets, "Compact efficient broadband grating coupler for silicon-on-insulator waveguides," Opt. Lett., Vol.29, No. 23, pp.2749-2751, 2004.

[14] L. Liao, D. Samara-Rubio, M. Morse, A. Liu, D. Hodge, D. Rubin, U. Keil, and T. Franck, "High speed silicon Mach-Zehnder modulator," Opt. Express vol. 13, no. 8, pp. 3129-3135, 2005.

[15] M. Attygalle, C. Lim, and A. Nirmalathas, "Extending optical transmission distance in

fiber wireless links using passive filtering in conjunction with optimized modulation", J Lightwave Technol., Vol. 24, No. 4, pp. 1703 1709, 2006

[16] T. Kuri and K. Kitayama, "Optical heterodyne detection technique for densely multiplexed millimeter-wave-band radio-on-fiber systems", IEEE Photon Technol Lett, Vol. 21, No. 12, pp. 3167 3169, 2003

[17] X. Zhang, B. Liu, J. Yao, K. Wu and R. Kashap, "A novel millimeter-wave-band radio-over-fiber system with dense wavelength-division multiplexing bus architecture", IEEE Trans Microwave Tech, vol. 54, no. 2, pp.929 937, 2006

[18] L. Chen, X. Y. Lei, S. C. Wen and J. G. Yu, "A novel radio over fiber system with DWDM mm-wave generation and wavelength reuse for upstream data connection", Opt. Express, vol. 15, no. 9, pp. 5893 5897, 2007

[19] G. H. Qi, J. P. Yao, J. Seregelyi, S. Paquet, C. Belisle, "Generation and Distribution of a Wide-Band Continuously Tunable Millimeter-Wave Signal with an Optical External Modulation Technique" IEEE Transactions on Microwave Theory and Techniques, vol. 53, no. 10, pp. 3090-3097, 2005

[20] C. W. Chow, L.Xu, C. H. Yeh, C. H. Wang, F. Y. Shih, H. K. Tsang, C. .L. Pan, and S. Chi, "Mitigation of Signal Distortions Using Reference Signal Distribution With Colorless Remote Antenna Units for Radio-Over-Fiber Applications", J. Lightw. Technol, vol. 27, no. 21, pp. 4773-4780, 2009

[21] B. Jalali, S. Fathpour, "Silicon photonics", J. Lightw. Technol., vol. 24, no. 12, pp. 4600-4615, 2006

[22] R. Soref, "The Past, Present, and Future of Silicon Photonics" IEEE J. Selected Topics in

Quantum Electronics, vol. 12, no. 6, pp. 1678-1687, 2006

[23] K. Yamada, H. Fukuda, T. Tsuchizawa, T. Watanabe, T. Shoji, and S. Itabashi, "Four-wave mixing in silicon wire waveguides", Optics Express, vol. 13, no. 12, pp. 4629-4637, 2005

[24] J. X. Ma, J. J. Yu, C. X. Yu, Z. S. Jia, X. Z. Sang, Z. Zhou, T. Wang, and G. K. Chang, "Wavelength Conversion Based on Four-Wave Mixing in High-Nonlinear Dispersion Shifted Fiber Using a Dual-Pump Configuration", J. Lightw. Technol., vol. 24, no. 7, pp. 2851- 2858, 2006

[25] J. J. Ju, M. F. Huang, Z. S. Jia; L. Chen; J. G. Yu, G. K. Chang; "Polarization-Insensitive All-Optical Upconversion for Seamless Integration Optical Core/Metro/Access Networks With ROF Systems Based on a Dual-Pump FWM Scheme", J. Lightw. Technol., vol. 27, no. 14, pp. 2605 – 2611, 2009

[26] N. Shibata, R. P. Braun, R. G. Waarts, "Phase-mismatch dependence of efficiency of wave generation through four-wave mixing in a single-mode optical fiber," IEEE J. Quant. Electron., vol. 23, no. 7, pp. 1205-1210, 1987.

[27] L. Xu, C. Li, C. W. Chow, and H. K. Tsang, "Optical mm-Wave Signal Generation by Frequency Quadrupling Using an Optical Modulator and a Silicon Microresonator Filter " IEEE Photon. Technol. Lett., vol. 21, no. 4, pp. 209-211, 2009

[28] H. C. Chien, A. Chowdhury, Z. Jia, Y. T. Hsueh, G. K. Chang, "60 GHz millimeter-wave gigabit wireless services over long-reach passive optical network using remote signal regeneration and upconversion", OPTICS EXPRESS, vol. 17 no. 5 pp. 3036-3041, 2009

[29] U. Gliese, S. Norskov, and T. N. Nielsen, "Chromatic Dispersion in Fiber-Optic Microwave and Millimeter-Wave Links", IEEE, Trans. Microwave Theory Technol. 44, 1716-1724, 1996

[30] H. Wen, H. Jiang, X. P. Zheng, H. Y. Zhang, and Y. L. Guo, "Performance Enhancement of Multiwavelength Conversion of RZ-DPSK Based on Four-Wave Mixing in Semiconductor Optical Amplifier", IEEE Photon. Technol. Lett., vol. 19, no. 18, pp. 1377-1379, 2007

[31] S. H. Fan, H. C. Chien, Y. T. Hsueh, A. Chowdhury, J. J. Yu, G. K. Chang, "Simultaneous Transmission of Wireless and Wireline Services Using a Single 60-GHz Radio-Over-Fiber Channel by Coherent Subcarrier Modulation", IEEE Photon. Technol. Lett., vol. 21, no. 16, pp. 1127-1129, 2009

[32] J. J. Yu, Z. S. Jia, T. Wang, G. K. Chang, "A Novel Radio-Over-Fiber Configuration Using Optical Phase Modulator to Generate an Optical mm-Wave and Centralized Lightwave for Uplink Connection", IEEE Photon. Technol. Lett.,, vol. 19, no. 3, pp. 140-142, 2007

[33] K. Y. Cho, Y. Takushima, and Y. C. Chung, "10-Gb/s operation of RSOA for WDM PON," IEEE Photon. Technol. Lett., vol. 20, no. 18, pp. 1533 1535, 2008.

[34] L. Chen, Y. Shao, X. Lei, H. Wen, and S. Wen, "A novel radio-over-fiber system with wavelength reuse for upstream data connection," IEEE Photon. Technol. Letts., vol. 19, no. 6, pp. 387 389, 2007.

[35] J. Yu, M. F. Huang, D. Qian, L. Chen, and G. K. Chang, "Centralized lightwave WDM-PON employing 16-QAM intensity modulated OFDM downstream and OOK modulated upstream signals," IEEE Photon. Technol. Lett., vol. 20, no. 18, pp. 1545 1547, 2008.

[36] C. W. Chow, "Wavelength remodulation using DPSK down-and-upstream with high extinction ratio for 10-Gb/s DWDM-passive optical networks," IEEE Photon. Technol. Lett., vol. 20, no. 1, pp. 12 14, 2008.

[37] C. H. Yeh, C. W. Chow, F. Y. Shih, C. H. Wang, Y. F. Wu, and S. Chi, "Tunable dual-wavelength fiber laser using optical-injection Fabry-Perot laser," IEEE Photon. Technol. Lett., vol. 20, no. 24, pp. 2093 2095, 2008.

[38] Z. Jia, J. Yu, G. Ellinas, and G. K. Chang, "Key enabling technologies for optical-wireless networks: Optical millimeter-wave generation, wavelength reuse, and architecture," J. Lightw. Technol., vol. 25, no. 11, pp. 3452 3471, 2007.

Chapter 6

Conclusions and Future Work

6.1 Summary and Conclusions

This thesis focuses on the novel photonics components and subsystem for use in future access networks. In Chapter 1, we overviewed the access networks and analyzed the development trend to WDM-PON. Research challenges of access networks are mainly on the development of low cost transceivers, colorless ONU structure and mm-wave signal generation/distribution.

In Chapter 2, we applied advanced modulation formats to access networks in order to achieve colorless ONU. We evaluated DPSK remodulation of DRZ downstream channel for upstream transmission. We showed that DRZ is particularly suitable for orthogonal modulation due to its feature of carrying power in both "one" and "zero" bits which can help realize multibit per symbol function. However, the generation of DRZ is still difficult. We also showed that silicon microring filters may be used for DPSK and DQPSK demodulation. Compared to the conventional MZDI, the microring resonator was found to have advantages of compact size, easy integration and operation over a wider range of bit rates.

In Chapter 3, we proposed a novel nonreciprocal optical modulation structure for integrated ONU and compared the performances of different modulation formats. The ASK downstream/DPSK upstream case require a low ER of ASK and consequent limited reach. In the other scenario, the DPSK downstream/ASK upstream case has the disadvantage that each ONU will need a DI for downstream DPSK signal demodulation. We think that the DPSK downstream and ASK

uptstream remodulation has a good potential for use in future WDM PON, however, practical implementation of this scheme depends on a robust low cost DPSK demodulation scheme such as cost effective athermal DPSK demodulators can be developed for use at the ONU.

In Chapter 4, characteristic of long wavelength, high speed VCSEL was investigated and its applications in advanced modulation format generation and WDM-PON were presented. VCSELs can be used as cost effective high speed transmitters in access networks, however, the large chirp of direct modulation will limit the transmission length.

In Chapter 5, we demonstrated several approaches for RF generation and novel architectures for long reach, high split ratio hybrid PON. The convergence of mm-wave wireless and wired PONs in an integrated platform can be a promising technique in future access networks for providing broadband wired and wireless access services with increased mobility and reduced cost. Frequency up conversion may generate high frequency mm-wave optical signal using low frequency electric component which simplifies complexity and reduces cost. Besides mm-wave generation, the transmission of optical mm-wave is also crucial in ROF systems because chromatic dispersion can cause signal distortions. To address the problems, we proposed and demonstrated remote up conversion at local exchange, hybrid subcarrier modulation (SCM) and reference signal distribution methods.

6.2 Future Work

Today's commercial high-speed optical modulators at >>10 Gb/s are based on electro-optic materials such as lithium niobate [1] and III-V semiconductors [2]. They typically rely on large (few cm in length) lithium niobate based electro-optic crystals, but their size means that not many modulators may be made per wafer. Thus existing linear lithium niobate optical modulators are

expensive, and although their cost can be justified for the head-end of a distribution network serving hundreds of end users, that same cost makes them unviable for use in ONU/RAU that perhaps serves only one end customer [3]. Silicon photonics has been attracting intense interest as it offers an opportunity for low cost optoelectronic solutions for applications ranging from telecommunications down to chip-to-chip interconnects. Performing photonic functions in SOI optical waveguides has emerged in the last decade as a hot research field because it provides a promising alternative to the use of the more costly conventional materials such as lithium niobate or III-V semiconductors. The main advantages of using silicon lies in its shared fabrication technology base with mainstream CMOS microelectronics which allows scaling of photonic devices to sub-micron width waveguides and also allows high-yield fabrication of the sub-micron sized components. Thus silicon photonics is a potentially low cost technology leveraging on standard microelectronic fabrication technologies to yield thousands of devices on a single silicon wafer. High speed silicon based Mach-Zehnder modulator has recently been demonstrated in [4, 5] but the integration of high speed silicon modulators with the other components for colorless ONU and low cost OLT transmitter arrays is an area for future development. Bringing silicon photonics to optical access networks may dramatically reduce the cost and finally realize broadband connection affordable.

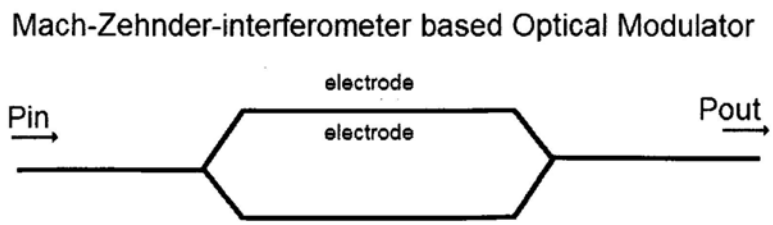

Fig.6.1 Schematic diagram of Mach-Zehnder interferometer silicon modulator containing two pn junctions.

The proposed high speed silicon modulator is based on Mach-Zehnder interferometer type with reversed biased pn diode embedded in both arms as shown in Fig.6.1. The refractive index of silicon may be electrically modulated by changing the density of electrons and holes in the silicon conduction and valence bands respectively. The optical power at the output of an integrated silicon Mach Zehnder interferometer may thus be modulated by simply applying a voltage to a silicon diode which is formed within the region where light is confined by the optical waveguide. Unlike conventional lithium niobate modulators, the modulation of refractive index of silicon is a nonlinear function of the applied voltage. Thus the first step in the design of a linear modulator must be to develop a good model of how the free carrier density in the waveguide varies with applied voltage and thus allow the effective index change in the waveguide, and hence the modulator electro-optical transfer functions to be derived.

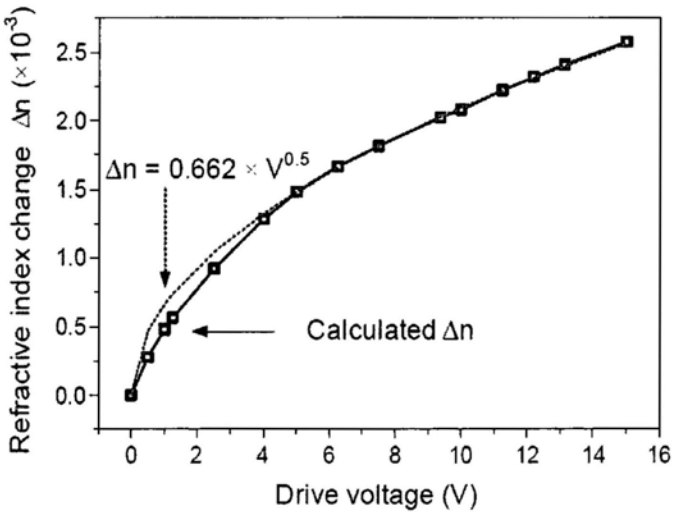

Fig.6.2 Calculated effective refractive index change (blue solid line) as a function of drive voltage and an approximate.

The initial simulation results shown in Fig.6.2 suggest that the effective index varies approximately as the square root of the applied voltage. The magnitude of the calculated refractive index modulation suggest that it may be possible to use waveguides of about 500nm

width and lengths of a few millimeters to achieve pi phase shift using a reverse biased diode.

Impedance matching is the electronics design practice of setting the input impedance of an electrical load equal to the fixed output impedance of the signal source to which it is ultimately connected, usually in order to maximize the power transfer and minimize reflections from the load. In the real optic communication system, the output impedance is 50 Ohm; the input impedance of the modulator is designed close to 50 Ohm in order to improve the modulation efficiency.

A well-established approach to very wide electrical bandwidth modulators with low drive voltage is the so-called traveling-wave design. It allows high electric fields overlapping very well with the optical mode. To maximize the bandwidth, microwave and optical velocities should be matched. In traveling-wave modulators based on silicon, velocity matching requires slowing the microwave signal. Velocity slowing can be achieved using capacitively loaded slow-wave electrodes. In such a design, the electrode is designed as a transmission line. Therefore, electrode capacitance is distributed and does not create an *RC* limit on the modulator speed [6].

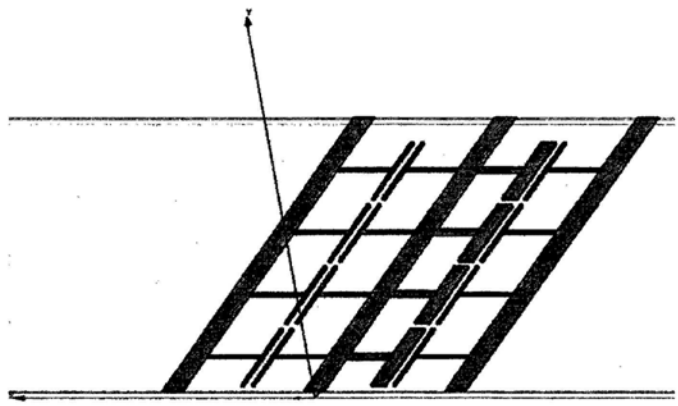

Fig.6.3 Sketch of T-rail structure

The electrode is a ground–signal–ground (G–S–G) coplanar waveguides shown in Fig.6.3. The two waveguides form the arms of a Mach–Zehnder-type modulator. T-rails stem from either side of the centre conductor and from the inner side of both ground planes. In the gap between the two T-rails, a small capacitor is formed. These capacitors periodically load the line and slow the microwave phase velocity by increasing the capacitance per unit length of the line. Charge is pumped in and out of these capacitors in the form of displacement current, the axial transmission line currents experiencing the conductor loss do not flow through them. The axial currents flow along the centre conductor and ground planes of the unperturbed geometry. Since the gap between the centre conductor and the ground planes can be quite large, current crowding effects which increase microwave loss are minimized. However, since there is no axial transmission line current flowing along the narrow rails that form the capacitor plates, the gap between the rails can be made very small with minimal increase in microwave loss. This results in a very large electric field between the capacitor rails. By positioning the optical guides under or between the rails, it is possible to obtain large electric fields overlapping quite well with the optical modes [7]. We use high frequency structural simulator (HFSS 8.0), which is a commercial finite element method solver for electromagnetic structures, to simulate the impedance and velocity matching conditions. The simulation model is set as follows. Fig.6.4 is the cross section view. The silicon substrate is 700-μm thick. Above the silicon substrate, there is a 2-μm thick SiO_2 substrate. On the top, there is a 0.75-μm thick silicon substrate. The metal (Aluminum) on top of the silicon is 0.5 μm thick. The sample is surrounded by air. Fig.6.5 is the top view of one period. The parameters shown have been optimized already.

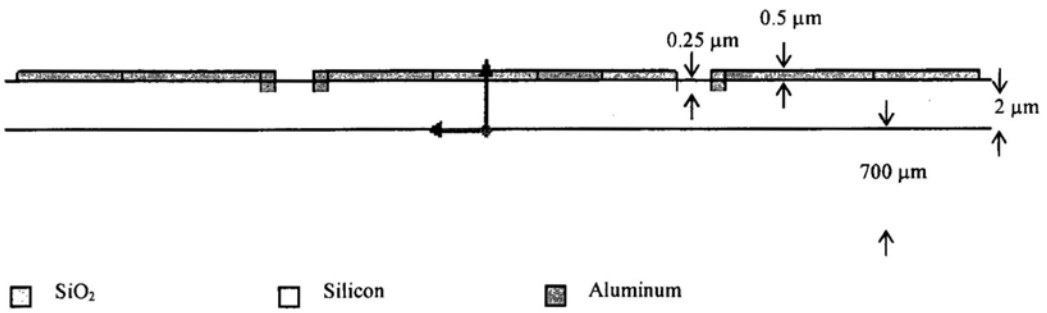

Fig.6.4 Cross section view of the T-rail structure

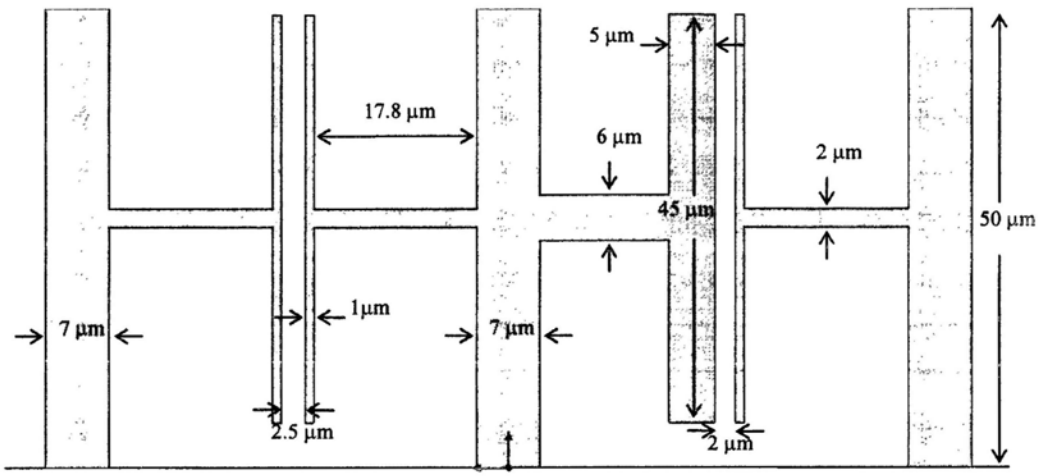

Fig.6.5 Top view: one period of T-rail structure

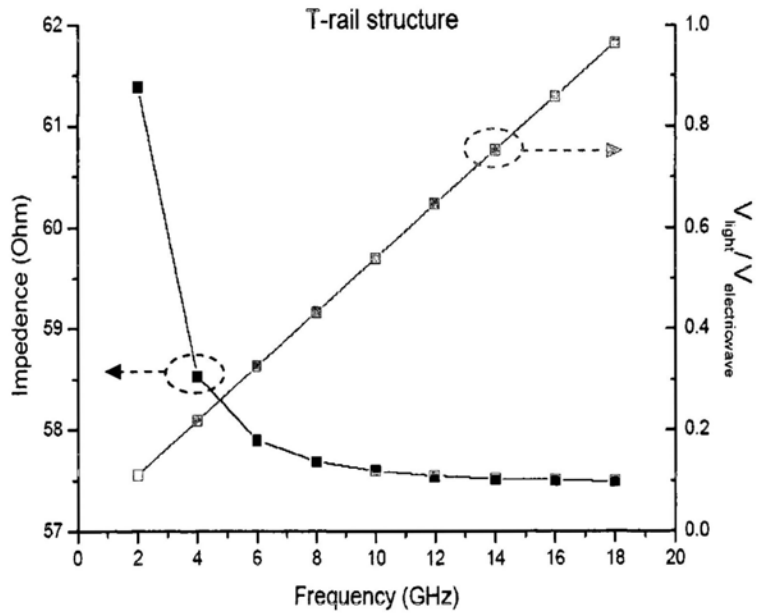

Fig.6.6 Simulated impedance and velocity ratio curve against frequency

The ratio of velocity of light over velocity of electricwave against frequency and impedance against frequency are both plotted in Fig.6.6. The simulated results show that the impedance tends to 57 Ohm at frequencies above 10 GHz. Meanwhile, the ratio of velocity of light over that of electric wave is linearly increased with frequency and they are equal at 19 GHz. This shows the designed structure has the best performance at 19 GHz and has an optimized performance at target 10 GHz. The Cadence mask is shown in Fig.6.7.

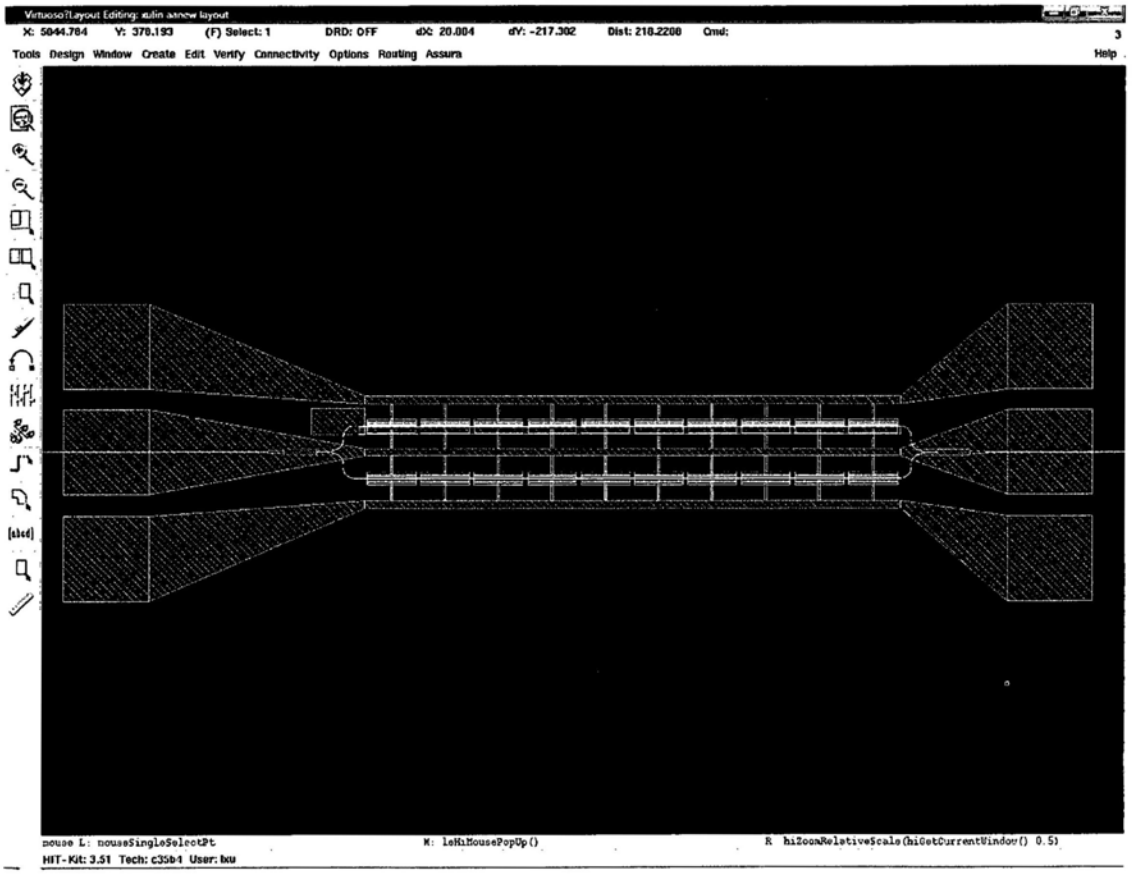

Fig.6.7 Layout of Cadence mask

For the next phrase, we will carry out extensive testing of the modulators. The tests will include measurement of the photonic response including the insertion loss, modulation efficiency, modulation bandwidth.

REFERENCES

[1] K. Noguchi, O. Mitomi, H. Miyazawa, "Millimeter-wave Ti: LiNbO3 optical modulators," J. Lightwave Technol., vol. 16, no. 4, pp. 615-619, 1998

[2] K. Tsuzuki, T. Ishibashi, T. Ito, S. Oku, Y. Shibata, T. Ito, R. Iga, Y. Kondo, Y. Tohmori, "A 40-Gb/s InGaAlAs-InAlAs MQW n-i-n Mach-Zehnder modulator with a drive voltage of 2.3 V," IEEE Photon. Technol. Lett., vol. 17, no. 1, pp. 46-48, 2005

[3] M. Huchard et al."Ultra-Broadband Wireless Home Network Based on 60-GHz WPAN Cells Interconnected via RoF," Journal of Lightwave Technology, vol. 26 no. 15, pp.2364-2371, 2008

[4] A. S. Liu, L. Liao, D. Rubin, H. Nguyen, B. Ciftcioglu, Y. Chetrit, N. Izhaky, and M. Paniccia, "High-speed optical modulation based on carrier depletion in a silicon waveguide" OPTICS EXPRESS, vol. 15, no. 2, pp. 660-668, 2007

[5] William M. J. Green, Michael J. Rooks, Lidija Sekaric, and Yurii A. Vlasov, "Ultra-compact, low RF power, 10 Gb/s silicon Mach-Zehnder modulator", Optics Express, vol. 15, no. 25, pp. 17106-17113, 2007

[6] JaeHyuk Shin, C. Ozturk, S. R. Sakamoto, Y. J. Chiu, and Nadir Dagli, "Novel T-Rail Electrodes for Substrate Removed Low-Voltage High-Speed GaAs/AlGaAs Electrooptic Modulators" IEEE TRANSACTIONS ON MICROWAVE THEORY AND TECHNIQUES, vol. 53, no. 2, pp. 636-643, 2005

[7] S. R. Sakamoto, R. Spickermann, N. Dagli, "Narrow-Gap Coplanar Slow-Wave Electrode for Traveling-Wave Electrooptic Modulators", ELECTRONICS LETTERS, vol. 31, no. 14, pp. 1183-1185, 1995

Appendix A

List of abbreviations:

AM: amplitude modulator

ASK amplitude shift keying

AWG: arrayed waveguide grating

AMI: alternate mark inversion

ASE: amplified spontaneous emission

ATM: asynchronous-transfer-mode

APD: Avalanche photodiode

BS: base station

BW: bandwidth

BER: bit error rate

BFL: birefringent fiber loop

BOX: buried oxide

BERT: bit-error-rate tester

BPON: broadband PON

BFL: birefringent fiber loop

B2B: back to back

CO: central office

CW: continuous wave

CD: chromatic dispersion

DFB: distributed fiber bragg laser

DCF: dispersion compensating fiber

DGD: differential group delay

DSF: dispersion shift fiber

DI: delay interferometer

DRZ: dark return-to-zero

DQPSK: differential quadrature phase-shift keying

DWDM: dense wavelength division multiplexed

DSB: double sideband

DPSK differential-phase-shift-keying

ER extinction ratio

EOM: electro-optic modulator

EDFA: erbium doped fiber amplifier

EA: electrical amplifier

EPON: Ethernet PON

FPLD Fabry-Perot laser diode

FWHM: full-width- half-maximum

FWM: four-wave mixing

FBG: fiber Bragg gratings

FSAN: full service access network

GPON: gigabit PON

HBDDRZ: half-bit-delayed dark return-to-zero

HDP: high density plasma

HE: head-end

IC: integrated circuit

LPF: low pass filter

LE: local exchange

LO: local oscillator

LD: laser diode

LAN: local area networks

MOD: modulator

MM-wave: millimeter wave

MZM: Mach-Zehnder modulator

MS: mobile station

MZDI: Mach-Zehnder delay interferometer

NRZ: non return-to-zero

NZ-DSF: non-zero dispersion-shift-fiber

ONU: optical network unit

OLT: optical line terminal

OOK: on-off keying

OSA: optical spectrum analyzer

OEIC: optoelectronic integrated circuit

OC: optical circulator

OCS: optical carrier suppress

OBF: optical bandpass filter

PON: passive optical network

PM: phase modulator

PC: polarization controller

PRBS: pseudo-random binary sequence

PD: photodiode

PIN: Pin diode

PLL: phase locked laser.

Q factor: quality factor

QoS: quality of service

RF radio frequency

RZ: return-to-zero

ROF: Radio-over-fiber

RAU: remote antenna unit

RN: remote node

Rx: receiver

RSOA: reflective semiconductor optical amplifier

VCSEL: vertical surface emitting laser

SMF: single mode fiber

SOA: semiconductor optical amplifier

SOI: silicon-on-insulator

SEM: scanning electron microscope

SSB: single sideband

SCM: subcarrier modulation

SW: switch

TL: tunable laser

TEC: temperature electric control

Tx: transmitter

TDD: time division duplex

TDM: time-division multiplexing

UV: ultraviolet

VOA: variable optical attenuator

VCSEL: vertical cavity surface emitting laser

WDM: wavelength division multiplexing

Appendix B

List of figures:

Appendix C

BER Measurement: Optically Preamplified Receiver

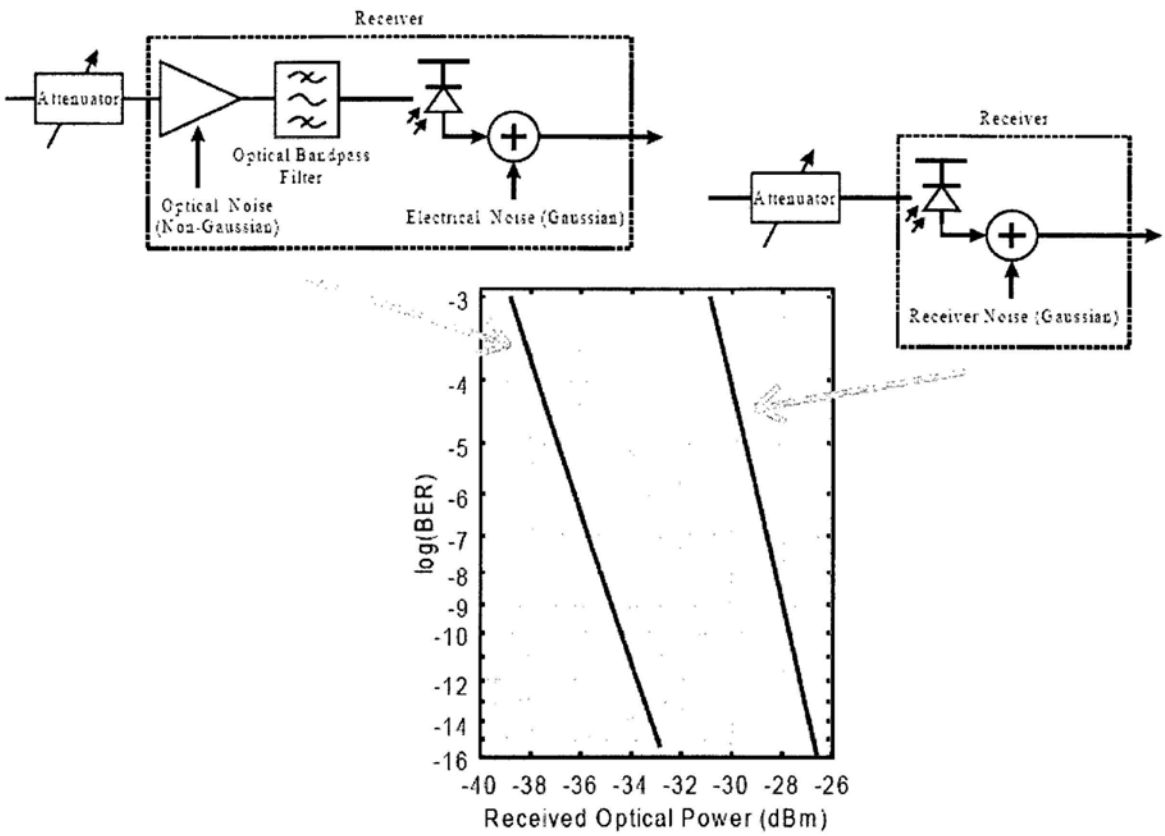

The gradient of the two curves is different

- due to signal-dependent (signal-spontaneous beat) noise in the preamplified receiver

Non-Gaussian noise produces a straight line

- optimum decision threshold is different, though similar effects observed with APD receivers

Ref: "Minding Your BER's and Q's Bit-Error-Rate and Q Factor Measurement: Theory and Practice", Mark Summerfield, Thursday November 4, 1999

Appendix D

List of publications:

Journal Papers

1. **L. Xu**, C. W. Chow, and H. K. Tsang, "Multicast, long reach, high split ratio wired and wireless hybrid PON", submitted to 2010 T-MTT JLT Microwave Photonics
2. **L. Xu** and H. K. Tsang, "Non-Reciprocal Optical Modulation for Integrated Optical Transceivers in Passive Optical Networks", J. OPT. COMMUN. NETW., vol. 2, no. 3, pp. 131-136, 2010
3. C. W. Chow, **L. Xu**, et al, "40 Gb/s Upstream Transmitters using Directly-Modulated 1.55 μm VCSEL array for High-Split-Ratio PONs", Photonics Technology Letters, vol. 22, no. 5, pp. 347-349, 2010
4. C. W. Chow, C. H. Yeh, **L. Xu**, et al, "Rayleigh Backscattering Mitigation Using Wavelength Splitting for Heterogeneous Optical Wired and Wireless Access Networks", submitted to Photonics Technology Letters
5. C. W. Chow, **L. Xu**, et al, "Mitigation of Signal Distortions Using Reference Signal Distribution With Colorless Remote Antenna Units for Radio-Over-Fiber Applications", Journal of Lightwave Technology, , vol. 27, no. 21, pp. 4773-4780, 2009
6. **L. Xu**, C. Li, et al, "Optical frequency doubling for multichannel radio-over-fiber system based on integrated phase modulator and silicon coupled-microring notch filter", Electronics Letters, vol. 45, no. 13, pp. 697-698, 2009
7. **L. Xu**, C. Li, et al, "Optical frequency doubling for multichannel radio-over-fiber system based on integrated phase modulator and silicon coupled-microring notch filter", Electronics Letters, Special Issue, pp. 33-34, 2009

8. **L. Xu**, C. Li, C. W. Chow and H. K. Tsang, "Optical mm-wave signal generation by frequency quadrupling using an optical modulator and a silicon microresonator filter", Photonics Technology Letters, vol. 21, no. 4, pp. 209-211, 2009
9. **L. Xu**, C. Li, C. Y. Wong and H. K. Tsang, "Optical Differential Phase Shift Keying Demodulation Using a Silicon Microring Resonator", Photonics Technology Letters, vol. 21, no. 5, pp. 295-297, 2009
10. **L. Xu** and H. K. Tsang, "Colorless WDM-PON Optical Network Unit (ONU) Based on Integrated Nonreciprocal Optical Phase Modulator and Optical Loop Mirror", Photonics Technology Letters, , vol. 20, no. 10, pp. 863-865, 2008
11. **L. Xu** and H. K. Tsang, "WDM-PON Using Differential-Phase-Shift-Keying Remodulation of Dark Return-to-Zero Downstream Channel for Upstream", Photonics Technology Letters, vol. 20, no. 10, pp. 833-835, 2008

Conference Papers

1. **L. Xu,** C.Li, X. Chen, and H.K.Tsang, "DQPSK Demodulation Using Integrated Silicon Resonators" accepted by ECIO 2010, Cambridge, UK
2. H.K.Tsang, X. Chen, **L. Xu** and C.Li, "Some Recent Developments in Silicon Photonics Enabled by EpixFab", invited talk, ECIO 2010, Cambridge, UK
3. C. W. Chow, **L. Xu**, et al, "Using Wavelength Splitting at the Remote Node to Mitigate Rayleigh Backscattering for Optical Wired and Wireless Access Networks", OWQ4, OFC/NFOEC 2010, San Diego, California, USA
4. X. Chen, C. Li, Y. Gao, **L. Xu**, et al, "Characterization of Integrated Polarization-Diversity DPSK Demodulator with Two-Dimensional Chirped Grating

Couplers and Ring Resonators", JWA26, OFC/NFOEC 2010, San Diego, California, USA

5. L. Xu, W. Hofmann, et al, "Multilevel Amplitude Modulation of 1.55-um VCSELs", 10th IEEE Photonics Society Hong Kong Chapter Postgraduate Conference, 2009
6. **L. Xu**, W. Hofmann, et al, "1.55-□m VCSEL Transmission Performance up to 20 Gb/s for Access Networks", post-deadline paper, OECC, 2009, Hong Kong
7. **L. Xu**, H. K. Tsang, W. Hofmann, M. C. Amann, "10-Gb/s Colorless Re-modulation of Signal from 1550nm Vertical Cavity Surface Emitting Laser Array in WDM PON", CI3.4, CLEO/Europe-EQEC, June 2009, Munich, Germany
8. **L. Xu**, C.Y. Wong, C. Li, C. W. Chow and H. K. Tsang, "Multi-channel mm-wave generation by frequency quadrupling using an optical modulator and a cascaded silicon microring filter" CI.P.3, CLEO/Europe-EQEC, June 2009, Munich, Germany
9. C. W. Chow, **L. Xu**, et al, "Bidirectional ROF Transmission and Signal Remodulation Using Separate Optical Clock Distribution to Mitigate Signal Distortions" OWP3, OFC/NFOEC 2009, San Diego, California, USA
10. X. Chen, C. Li, **L. Xu**, H. K. Tsang "DPSK Demodulation Using Mach-Zehnder Delay-Interferometer on Silicon-on-Insulator Integrated with Diffractive Grating Structure ", SuF3, AOE, 30 October-2 November, 2008, Shanghai, China
11. **L. Xu**, C. Li and H. K. Tsang, "Silicon Microring Resonator Optical DPSK Demodulator", post-deadline paper, Photonics in Switching Conference (PS2008), 2008, Hokkaido, Japan
12. **L. Xu** and H. K. Tsang, "Asynchronous Orthogonal Modulation of Intensity and Phase for Label-Switched Optical Packets", IA4, ICO-21 2008 Congress, Sydney, Australia
13. **L. Xu** and H. K. Tsang, "Non-Reciprocal Optical Phase Modulation for Integrated NRZ/DPSK Data Re-Modulation in Optical Access Networks",CTuLL2, CLEO/QELS 2008, San Jose, California, USA

14. **L. Xu** and H. K. Tsang, "Differential Phase Shift Keying for Asynchronous Upstream Remodulation of Dark Return-to-Zero Downstream Channel", OWH6, OFC/NFOEC 2008, San Diego, California, USA

15. **L. Xu**, P. S. Chan, Y. Liu, and H. K. Tsang, "40 Gb/s OTDM to 4X10Gb/s WDM conversion via birefringence switching", 13B1-4, OECC/IOOC 2007, Pacifico Yokohama, Japan

16. **L. Xu** and H. K. Tsang, "Generation of ultrafast dark RZ using detuned filter after a SOA", 7th IEEE Hong Kong LEOS Postgraduate Conference, 2006